



POLITECHNIKA POZNAŃSKA



Poznan University of Technology

Faculty of Chemical Technology

Institute of Chemistry and Technical Electrochemistry

Field of Study: Chemical Sciences

Xuexue Pan

**Strategies for designing high performance
sodium-ion capacitors**

Strategie projektowania kondensatorów sodowo-jonowych o wysokiej
wydajności

DOCTORAL DISSERTATION

Promoter:

Prof. François Béguin

Co-promoter:

Dr. Agnieszka Chojnacka

Poznań, 2021



This thesis research was carried out within the frame of the TEAM-TECH project no. POIR.04.04.00-00-3D6F/16-00 of the Foundation for Polish Science co-financed by the European Union from the European Regional Development Fund under the Intelligent Development Operational Program.

Project leader: Professor **François Béguin**

Badania do niniejszej pracy prowadzone były w ramach projektu TEAM-TECH nr POIR.04.04.00-00-3D6F/16-00 Fundacji na rzecz Nauki Polskiej współfinansowanego przez Unię Europejską z Europejskiego Funduszu Rozwoju Regionalnego w ramach Programu Operacyjnego Inteligentny Rozwój.

Kierownik projektu: Profesor **François Béguin**

Acknowledgments

I am grateful to the scientific promoter of this thesis, **Prof. François Béguin**, for all his time and efforts put into this work. During my PhD studies, my promoter has placed strict demands on me, guided me carefully, encouraged me continuously and spurred me constantly. He gave me a platform to develop my strengths and increase my abilities. Moreover, he taught me rigorous and realistic scientific research ideas, scholarly methods and problem-solving thinking, and led me to the palace of science. His profound knowledge, striving for excellence, keen academic vision and profound insight gave me a lifetime of inexhaustible treasure. My promoter has devoted a lot of time and effort to the research tasks from the selection of materials, the detail of experiments and discussion of results. When I was confused about the selection of materials and thinking of the experiments, it was my promoter who gave me timely guidance and encouragement, which opened my mind and made me full of confidence.

I still solemnly thank my co-promoter **Dr. Agnieszka Chojnacka**. Without her help, I would not even have the courage to start this unforgettable voyage, let alone overcome numerous difficulties, successfully complete the thesis, and go to the end.

Last but not least, I would also like to mention all the persons who helped me during the preparation of this thesis: Paweł Jeżowski, Barbara Górka, Adam Ślesięński, Emmanuel Pameté Yambou, Seyed Esmaeil Mohammadi Pourhosseini and Zhuanpei Wang, as well as all the present and former members of the Power Sources Group in Poznan University of Technology.

Table of Content

General introduction	6
Chapter I.....	14
<i>Literature review</i>	
1. Electrical double-layer capacitors (EDLCs).....	15
1.1 Principle and properties of EDLCs	15
1.2 Carbon materials for EDLCs	19
1.3 Electrolytes for EDLCs.....	22
2. Na-ion batteries (NIBs)	25
2.1 Principles of NIB operation	25
2.2 Organic electrolytes for NIBs	26
2.3 Anodic materials for NIBs	29
2.4 Solid electrolyte interphase formation on negative electrodes	41
3. Na-ion capacitors (NICs).....	45
4. Presodiation of anodic materials	49
4.1 Presodiation from a metallic sodium auxiliary electrode	49
4.2 Sacrificial materials in positive electrodes	49
5. Conclusion.....	53
Chapter II	55
<i>High performance hybrid sodium-ion capacitor with tin phosphide used as battery-type negative electrode</i>	
1. Summary of the publication	56
Chapter III.....	59
<i>Na₂S sacrificial cathodic material for high performance sodium-ion capacitors</i>	

Strategies for designing high performance sodium-ion capacitors

1. Summary of the publication	60
Chapter IV.....	63
<i>Advantageous carbon deposition during the irreversible electrochemical oxidation of Na₂C₄O₄ used as a presodiation source for the anode of sodium-ion systems</i>	
1. Summary of the publication	64
Chapter V	67
<i>A strategy for designing more durable sodium-ion capacitors with optimized output energy</i>	
1. Summary of the publication	68
General conclusion.....	70
References.....	73
Scientific achievements	85
Abstract.....	88
Streszczenie.....	93

General introduction

Energy plays a significant role in people's lives, especially in the modern society. Until now, many public concerns are focusing on the massive consumption of fossil fuels and the production of greenhouse gases. The replacement of fossil energy with a clean and renewable energy resource becomes a top research direction, focusing people's wide attention. Although the current natural energy sources, including solar energy, wind energy, tidal energy and hydropower, have significantly been developed, considering their disadvantages, *e.g.*, continuous instability, low conversion efficiency and regional restrictions, it will not be the most direct source of energy in our daily life for a period of time. It is crucial to develop new energy conversion and storage systems in which the energy delivery can be adapted in a controlled manner to the market demand.

Fortunately, the battery is an ideal energy storage device due to its safety of use, reliable performance, convenient carrying and reasonable price; it directly converts the chemical energy reversibly into electrical energy through an electrochemical oxidation-reduction reaction. Alessandro Volta in 1800 created the first electrochemical cell by connecting copper (positive electrode) and zinc plates (negative electrode) separated by cloth (separator) impregnated with sulphuric acid (electrolyte). This type of cell is called a primary battery, which cannot be recharged. With the continuous development of the battery technology, rechargeable batteries as nickel-cadmium and nickel-metal hydride ones were created and widely used in various fields of human life. Nonetheless, the problems of these devices are their low specific energy and power, and shorter cycle life, which makes them insufficient to fulfill the current requirements of portable devices (laptops, cell phones, etc.) and electric vehicles. Besides, some of the components from nickel-cadmium batteries are environmentally unfriendly. Therefore, during the last decades, the development of electrochemical energy storage components with higher specific energy and power has become the most critical problem for researchers and engineers.

Among the various energy storage technologies, a metal-ion battery is a promising solution for large-scale storage of electricity, due to its high energy conversion efficiency, and simple maintenance. Li-ion batteries (LIBs), which have become familiar power sources in the portable electronic market since their first commercialization by Sony in the early 1990s, are the primary candidates for energy storage systems. The Nobel Prize in Chemistry 2019 was awarded jointly to John B. Goodenough, M. Stanley Whittingham and Akira Yoshino, who were pioneers in the development of LIBs, confirming the strong impact of this

technology, which was a revolution in our way of life. The introduction of LIBs into the automotive market as the battery of choice for powering hybrid electric vehicles (HEVs), plug-in hybrid electric vehicles (PHEVs) and electric vehicles (EVs) could reduce the dependence on fossil fuels. As lithium, the primary ingredient in LIBs, is in particular located in countries posing political issues, the increasing demand for this metal associated with these new and large-scale applications is expected to skyrocket its price, affecting the reserves as it is not a naturally abundant element. Based on the calculations, the global Li consumption in 2019 was nearly 93800 tons [1]; hence, the present mineable resources could be sustained for approximately 65 years at most at an average growth rate of 5% per year, making the implementation of the above-mentioned applications very costly.

As an alternative to lithium is needed to realize large-scale applications, Na-ion batteries (NIBs) have attracted a considerable research attention in recent years. Sodium, the fourth most abundant element on Earth, has a seemingly unlimited distribution with vast supplies of its precursors. The cost of sodium carbonate (about \$250 per ton) [2] compared to lithium carbonate (about \$12700 per ton in 2021) [3] provides a compelling rationale for developing NIBs as an alternative to LIBs. In addition, contrary to lithium, sodium does not alloy with aluminum, enabling the use of light and low-cost aluminum current collectors instead of copper, allowing the mass and production cost of the batteries to be reduced. The specific energy of NIBs is as high as ca. 130 Wh kg⁻¹, however, their short cycle life and low power (less than 350 W kg⁻¹) remain the limiting factors for a number of applications [4, 5].

At the same time, capacitors, another traditional energy storage device, are widely used in electronic devices, communication equipment, household appliances and other fields. Among them, the electrochemical capacitors, and particularly electrical double-layer capacitors (EDLCs), have attracted the attention of scientific researchers and manufacturers, owing to their relatively high specific energy (in comparison with traditional capacitors), while keeping superior characteristics such as fast charge and discharge capabilities, long cycle life, super high instantaneous specific power. With the development and rise of electric vehicles, this type of capacitors gradually occupies an increasingly important position. As the charge is stored electrostatically on the active surface of the electrodes, EDLCs operating in organic electrolytes display a specific power as high as 10 kW kg⁻¹, yet the specific energy is lower than 10 Wh kg⁻¹ [6].

Strategies for designing high performance sodium-ion capacitors

From the foreword, it appears clearly that, for applications, the weak point of metal-ion batteries is their relatively low specific power, whereas for EDLCs, it is the low specific energy (Fig. 1). Therefore, hybrid metal-ion capacitors (*e.g.*, Li-ion capacitors - LICs), which implement a battery-like negative electrode (that gives a plateau in its charge-discharge profile) and porous carbons as positive EDL one (characterized by the triangular shape of the charge-discharge profile), have appeared at the beginning of the 2000s to be an excellent alternative to combine in a single device the high voltage of metal-ion batteries and higher power capability of EDLCs. As shown in Fig. 1, the specific energy of LIC can be as high as ca. 80 Wh kg⁻¹, and the specific power as high as ca. 5 kW kg⁻¹ [7-9].

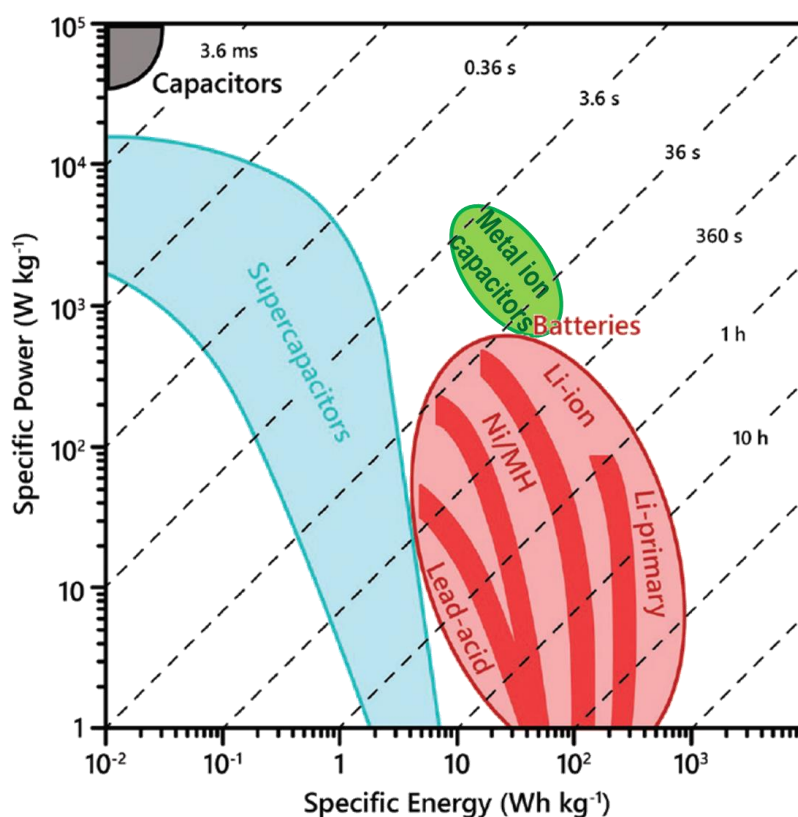


Fig. 1. Comparison of the specific energy and power for various electrochemical energy storage devices. Adapted from [6-9].

Due to the aforementioned massive consumption of lithium resources and its rising price, for the same reasons as NIBs, the Na-ion capacitors (NICs) with electrochemical similarities to the LICs have been proposed as an alternative. Nonetheless, the operation of NICs requires to presodiate the negative electrode, in order to form the solid electrolyte interphase (S.E.I.)

and insert sodium into the anodic material structure; this operation requires an additional step which increases the cost of the devices. Besides, although alloys as potential anodic host have a higher sodium insertion/deinsertion potential than hard carbons, enabling to avoid sodium plating during the operation of the cells, their major flaw during cycling is a high volumetric variation leading to the pulverization of the active material followed by a loss of the electrical contact with the current collector; in other words, the depth of sodium insertion in these hosts should be carefully controlled to enhance their stability during cycling. More importantly, the sodiation potential of the negative electrode and the mass of AC in the positive electrode must be optimized to get the best compromise between the longest life span and specific energy of the hybrid device at a given power.

In order to address these issues, the dissertation is divided into five chapters:

The first chapter introduces the literature background on the electrochemical energy storage systems, including EDLCs, NIBs and NICs. The charging/discharging mechanisms, the performance of these systems, the organic electrolytes, together with the main types of electrode materials are presented. The last part of the chapter details the two premetallation technologies, based either on including a metallic auxiliary electrode in the MICs or adding a sacrificial metallic salt in the positive EDL electrode. In the last case, the metallic salt is irreversibly oxidized, and the metal ions are transferred to the negative electrode, what dramatically simplifies the cell construction.

As graphite cannot be used as a host for sodium due to its low intercalation capability, hard carbons (HCs) are quite often applied as anodic hosts in NIBs and NICs. However, the low potential of sodium insertion in HCs precludes their application at high currents, due to the risk of sodium plating, which may lead to thermal runaway and explosion of the devices. Among the alternative anodes explored for NIBs, Sn_4P_3 with a theoretical specific capacity of 1132 mAh g^{-1} and suitable insertion potential (ca. $0.3 \text{ V vs. Na/Na}^+$) is one of the essential Na^+ storage hosts, which consequently looks very attractive for NICs. Therefore, the second chapter summarizes the publication entitled “*High performance hybrid sodium-ion capacitor with tin phosphide used as battery-type negative electrode*” and presents the publication as an attachment. In this chapter, Sn_4P_3 is synthesized by high-energy milling of red phosphorus and tin powders. After the physico-chemical characterization of the obtained material by X-ray diffraction (XRD) and scanning electron microscopy (SEM), Sn_4P_3 -based electrodes are

prepared and tested electrochemically by galvanostatic charge/discharge down to different vertex potentials. After the identification of an optimized sodium insertion potential limit, the Sn_4P_3 negative electrode is presodiated in a separate cell and then combined with an activated carbon (AC) positive EDL electrode to assemble an $\text{AC}/\text{Na}_x\text{Sn}_4\text{P}_3$ NIC. The NIC performance (capacitance, life span and specific energy vs. power) is finally determined, showing an advantage of the realized NICs over other systems reported in the literature.

Related to the above-mentioned statement that the anodic host must be premetallated in a separated cell before realizing a MIC, it has been previously proposed in the literature on LICs to incorporate a sacrificial lithium source together with AC in the positive electrode, and to electrochemically transfer it to the anodic host, thus realizing the LIC is a single cell. This strategy offers the advantage of simplifying the cell construction and reducing its cost. Therefore, it has been applied in the third chapter, which includes a summary of the publication entitled “*Na₂S sacrificial cathodic material for high performance sodium-ion capacitors*” and presents the publication itself as an attachment. For this purpose, two ACs of different microporous texture were selected, and then the stability limits of electrodes made from these carbons are established by the S-method to determine the potential of electrolyte oxidation. Thereafter, the irreversibility of sodium extraction from an AC- Na_2S electrode is tested by cyclic voltammetry and galvanostatic charge/discharge at potentials lower than the afore established oxidation limit of the electrolyte. Nitrogen adsorption/desorption at 77K is used to compare the cumulative DFT surface area and pore volume of the oxidized electrodes as well as pristine AC- Na_2S and AC electrodes. Then, $\text{AC}-\text{Na}_2\text{S}/\text{Sn}_4\text{P}_3$ cells are constructed in the same electrolyte, and Na_2S is oxidized to irreversibly extract the sodium ions, which are then transferred to the Sn_4P_3 host, allowing the $\text{AC}/\text{Na}_x\text{Sn}_4\text{P}_3$ NIC to be realized and cycled to determine its performance. Even though this strategy is attractive, it is worth noting that Na_2S is sensitive to moisture, and imposes preparing the electrodes under the controlled atmosphere of a glove-box; therefore, it seems preferable to implement an air-stable sacrificial material, what is described in the next chapter.

The fourth chapter deals with the implementation of $\text{Na}_2\text{C}_4\text{O}_4$ as the sacrificial material, which turned out to solve the main disadvantages encountered with Na_2S , *i.e.*, it can be manipulated in the presence of moisture. The chapter contains a summary of the publication entitled “*Advantageous carbon black deposition during the irreversible electrochemical oxidation of $\text{Na}_2\text{C}_4\text{O}_4$ used as a presodiation source for the anode of sodium-ion systems*” and

the publication itself. The electrochemical oxidation of the AC- $\text{Na}_2\text{C}_4\text{O}_4$ electrodes is studied in the same conditions as in chapter III, and in addition, *operando* electrochemical mass spectrometry is implemented to identify the gas produced during the oxidation of the $\text{C}_4\text{O}_4^{2-}$ anion. Nitrogen adsorption/desorption at 77 K is used to determine the changes of porosity between the pristine and the oxidized electrodes, whereas Raman spectroscopy is implemented to identify the eventual solid deposits remaining after the electrochemical oxidation of the AC- $\text{Na}_2\text{C}_4\text{O}_4$ electrodes. The impact of the deposited solids is also investigated by measuring the electrical conductivity of the oxidized electrodes. AC- $\text{Na}_2\text{C}_4\text{O}_4//\text{Sn}_4\text{P}_3$ cells are constructed in the same electrolyte, and sodium is inserted in Sn_4P_3 by oxidative transfer from $\text{Na}_2\text{C}_4\text{O}_4$; once the AC// $\text{Na}_x\text{Sn}_4\text{P}_3$ NICs are realized, they are cycled to determine their performance. After cycling, the S.E.I. formed on the anodic material is analysed by infrared spectroscopy to interpret its effect on optimizing the life span of the devices. Finally, the improved performance of the NICs prepared with help of $\text{Na}_2\text{C}_4\text{O}_4$ is discussed in the light of the various analyses which were realized.

Although we successfully realized AC// $\text{Na}_x\text{Sn}_4\text{P}_3$ NICs in the previous chapters, the major problem during the sodiation of the Sn_4P_3 alloy is its volumetric expansion, which depends on the presodiation potential. The significant change in electrode volume leads to the pulverization of the active material followed by a loss of electrical contact with the current collector, which is directly reflected by the failing of the NICs. Hence, one of the objectives of the fifth chapter was to determine a strategy to circumvent these problems. The chapter summarizes the manuscript entitled “A strategy for designing more durable sodium-ion capacitors with optimized output energy” and includes the manuscript itself as attachment. To optimize the performance of the anodes based on Sn_4P_3 , a hydrothermal hard carbon (HCG) with spherical particles is synthesized and mixed with the Sn_4P_3 alloy to partly absorb its volumetric variations during cycling. The buffer effect of HCG in the HCG/ Sn_4P_3 electrodes during sodium insertion is demonstrated by *operando* electrochemical dilatometry. To simultaneously increase the specific energy and life span of the NICs, the capacity ratio between the anode and the positive electrode is matched by varying the low presodiation potential of Sn_4P_3 and/or the mass of AC. Finally, on the basis of the various results obtained during this systematic study, recommendations to design optimized NICs based on the Sn_4P_3 anodic materials are presented.

Strategies for designing high performance sodium-ion capacitors

The manuscript ends with a general conclusion highlighting and discussing the essential results. Finally, perspectives for further research work in hybrid metal-ion capacitors based on organic electrolytes are suggested.

Chapter I

Literature review

This bibliography part aims at introducing electrochemical energy storage systems, such as electrical double-layer capacitors (EDLCs), Na-ion batteries (NIBs) and Na-ion capacitors (NICs), as well as their storage mechanisms, together with the organic electrolytes and the main types of electrode materials which they implement. Based on a battery-type anode and an EDL-type positive electrode, NICs have attracted much attention because of their comparable performance to Li-ion capacitors (LICs), alongside abundant sodium resources, which allow reducing their cost. Generally, the positive electrode of NICs is the same as in EDLCs, whereas the negative electrode and electrolyte are the same as those in NIBs. Due to the need for the necessary presodiation of the negative electrode, the implementation of an adapted sacrificial material in the composition of the positive electrode is the more reasonable solution for the realization of NICs, which will be detailed in the last part of this chapter.

1. Electrical double-layer capacitors (EDLCs)

1.1 Principle and properties of EDLCs

The electrical double-layer (EDL) model, first proposed by Helmholtz, describes the charge separation at the electrode/electrolyte interface on the surface of a planar and conductive electrode immersed in an electrolyte [10]. In this model, the accumulated charges on the surface of the electrode are balanced by the electrostatic adsorption of a counterion monolayer from the electrolyte, resulting in two layers of opposite charges at the interface, *i.e.*, electrons on the surface of the electrical conductor and the monolayer of ions accumulated close to the surface of the electrode in the electrolytic solution [10].

Electrical double-layer capacitors (EDLCs), also known as supercapacitors, are capacitive energy storage devices, that can store energy through a physical ion adsorption/desorption process at the electrode-electrolyte interface when there is a potential difference between the two electrodes (as shown in Fig. 2) and separated by a porous membrane to avoid electrical short circuits [11]. Basically, the accumulated charge on the surface of each electrode is balanced by adsorbing the opposite ionic charge from the electrolyte. Owing to the electrostatic charge separation, the capacitance C (often known as the electrochemical double-layer capacitance) of EDLC can be expressed by the formula (1):

$$C = A \frac{\epsilon_r \epsilon_0}{d} \quad (1)$$

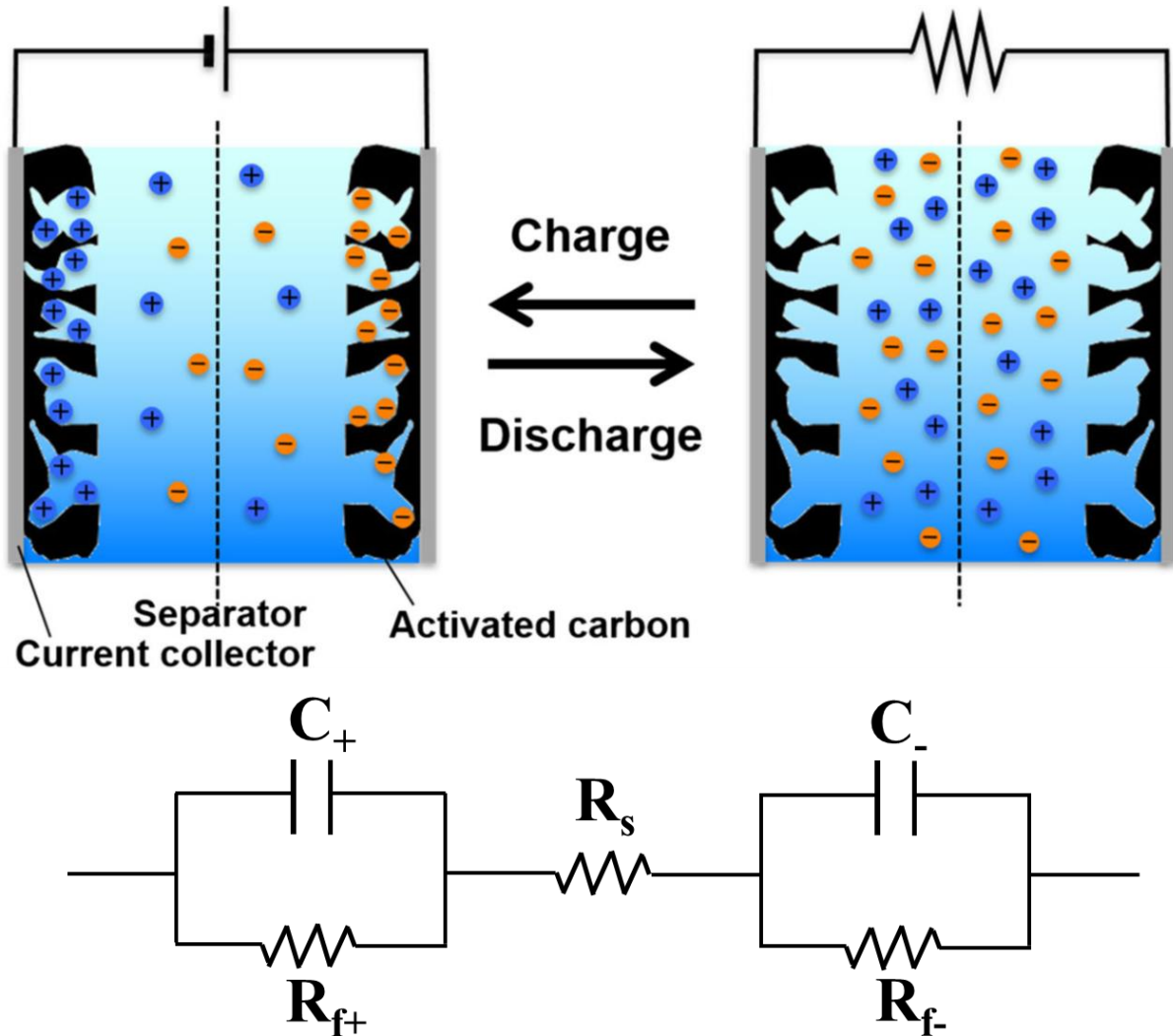


Fig. 2. Schematic representation of an EDLC using porous carbon electrodes during charge and discharge. (grey: current collectors, black: activated carbon, orange: cations, and blue: anions) [11]. In the corresponding equivalent circuit, R_{f+} , R_{f-} , R_s stand for the charge transfer resistance of the positive and negative electrodes, and the equivalent series resistance of the EDLC; and C_+ , C_- for the capacitance of the positive and negative electrodes, respectively [12].

Where ϵ_0 ($8.85 \times 10^{-12} \text{ F m}^{-1}$) is the permittivity of vacuum, ϵ_r is the relative dielectric constant of the electrolyte, d (m) is the average approaching distance of ions on the surface of the electrode, and A (m^2) as the accessible surface area of the electrode. Considering the relative

dielectric constant of the electrolyte ($\epsilon_r < 100$) and the approaching distance d (a few 10^{-10} m), the double-layer capacitance values are in the range of tens of mF cm^{-2} . Materials with high specific surface area (SSA) have been used to increase the total electrode capacitance, among which, porous carbon can meet all the requirements owing to its large SSA ($>1500 \text{ m}^2 \text{ g}^{-1}$), electrical conductivity, electrochemical stability and low cost [13, 14]. According to these principles, Becker proposed the first patent of the EDLC with porous carbon electrodes and sulfuric acid as its electrolyte in 1957 [15]. Later, Standard Oil of Ohio Corporation started designing another EDLC device with carbon materials alongside an organic electrolyte in 1970 [16]. Subsequently, Nippon Electric Company sold EDLCs based on an aqueous electrolyte in 2001 [16]. Since then, EDLCs have been used for a wide range of applications, such as consumer electronics, memory backup systems and industrial power and energy management [17, 18].

Many works have been focused initially on the fabrication of high SSA carbons (*e.g.*, activated carbons). Researchers observed that ions are easily stored in subnanometric pores, and consequently they may be desolvated [19, 20], revealing the significance of both SSA and pore size distribution on carbon electrode properties [21, 22]. Since then, alternative EDL theories and models have been proposed and developed to understand the charge storage mechanisms in nanoporous carbons, which has been made possible to understand better the ion environment and ion fluxes in these confined pores by the vital development of theoretical studies, as well as analytical techniques [13].

As shown in Fig. 2, an EDLC can be regarded as two capacitors connected in series, and consequently its capacitance C_{EDLC} (F) is given by formula (2):

$$\frac{1}{C_{EDLC}} = \frac{1}{C_p} + \frac{1}{C_N} \quad (2)$$

where C_p and C_N (F) are the capacitance values of the positive and negative electrodes, respectively. Thus, due to the differences in the size and mobility of cations and anions, C_{EDLC} is primarily determined by the smallest of the two capacitance values, which are substantially unequal. Hence, the overall C_{EDLC} of any “symmetric” capacitor is only half that of the individual capacitance values which are approximately equal. Usually, the “specific capacitance” or “gravimetric capacitance” (F g^{-1}) of cells or electrodes is more prevalent in the scientific literature. Considering that the mass of an EDLC is twice that of one electrode, the specific capacitance of EDLC is one-fourth that of a single electrode. From the applied

point of view, the industry is more interested in the volumetric parameters. Therefore, carbons with subnanometric pores with higher density than mesoporous carbons are preferred and very effective for EDL storage [19, 20]. Electrodes for EDLCs must be clearly described, including the information on the respective mass ratios between the active material, conductive agent and binder used in their fabrication. Moreover, the material mass loading per electrode area in units of mg cm^{-2} is essential for other researchers to clearly evaluate the electrochemical properties of both the material and device as a whole, especially when comparing against results from different laboratories or commercial products. At the academic level, the calculated capacitance values of cells, either per one electrode or two electrodes, are considered as the coating mass of the electrode material without the current collector. For practical applications in the commercial market, all metrics are expressed per the overall mass (or volume) of EDLCs, which includes the package, electrodes (materials + current collector), electrolyte and separator [23].

The specific energy (E , Wh kg^{-1}) is the energy stored by a unit mass of a capacitor; it is given by the formula (3):

$$E = \frac{1}{2} CU^2 \quad (3)$$

where U is the maximum voltage of the device and C its capacitance. Burke *et al.* [24, 25] and also Conway *et al.* [26] emphasized a more practical point that the available specific energy is delivered from U to $0.5U$ and is consequently $3/8 CU^2$. Yet, the remaining specific energy from $0.5U$ to 0 is $1/8 CU^2$, which is 3 times smaller than the delivered one from U to $0.5U$.

The specific power output (P , W kg^{-1}) of a capacitor can be principally derived from dividing the specific energy (E , Wh kg^{-1}) by the discharge time (t , h) as in equation (4):

$$P = \frac{E}{t} \quad (4)$$

Obviously, the maximum specific power output is determined by the minimum discharge time.

The time constant τ is an indicator of the power capability, which is given by equation (5):

$$\tau = RC \quad (5)$$

where R stands for the resistance and C the capacitance of the EDLC [25]. Actually, E and P are linked in the Ragone plot (Fig. 1), where the diagonals represent the time constant [27].

1.2 Carbon materials for EDLCs

Carbon materials for EDLCs must have a high specific surface area, while having the highest density. Therefore, essentially microporous carbons (such as activated carbons and CDCs) are practically preferred in EDLCs. The properties of carbon materials for EDLCs are primarily determined by the accessibility of pores and the pore size distribution. According to the IUPAC, the pores can be classified into three domains, namely, micropores (up to 2 nm), mesopores (2-50 nm), and macropores (> 50 nm); the nanosized micropores can be subdivided into super- (>0.7 nm) and ultra-micropores (<0.7 nm) [28]; materials with pores exceeding hundreds of nanometers are most often classified as nonporous. The type of porosity in materials affects the SSA, ions transport, and charge storage [29, 30]. A bimodal porosity with interconnected micropores and mesopores (so-called hierarchical carbons) is currently considered ideal because the actual charge storage predominately occurs in the smaller micropores; the larger pores (preferably mesopores) provide a rapid mass transport of the electrolyte ions to the micropores [29-31]. Therefore, the porosity development needs to be controlled to some extent to overmaster the charge storage capacity of carbons.

Carbons for EDLCs can be prepared by cheap processes from low-cost and abundant bio-sourced precursors, with a high electrical conductivity allowing for a limited ohmic drop during an electrochemical polarization [17]. In the case of nanoporous carbons, which are widely used as EDLC electrode materials, an extremely high SSA (> 2000 m² g⁻¹), as well as an adjustable pore size distribution, can be achieved through various processes, including carbonization/activation, templating, *etc.* [12]. Also, the carbons should have the desirable properties to meet the requirements for practical applications, *e.g.*, low cost, well-balanced micro-mesoporosity, high density, reduced surface oxygenated functionality. As shown in Fig. 3, various carbon materials with several dimensionalities can be used for EDLC applications, including 0-dimensional (0D) onion-like carbons [32], 1D carbon nanotubes [33] and carbon fibers [34], 2D graphene [35], and 3D porous carbons (activated carbons (ACs) [36], carbide-derived carbons (CDCs) [37], template carbons [38]). As only ACs and CDCs meet the practical requirements for commercial EDLCs, other carbons are excluded from the detailed description given below.

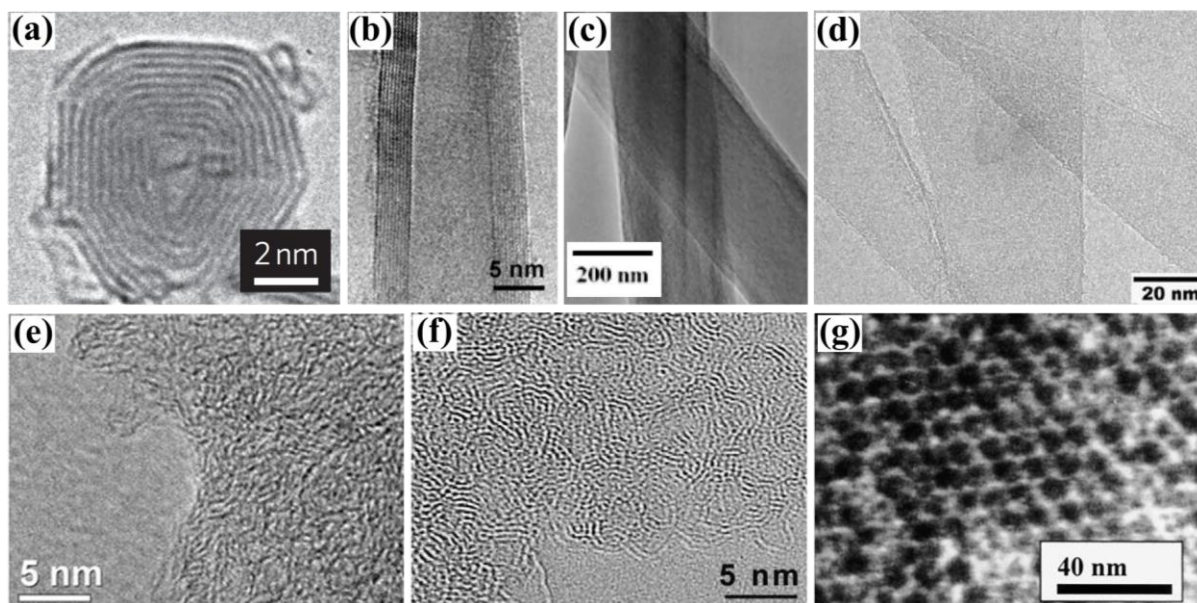


Fig. 3. Transmission electron microscopy (TEM) images of various carbons with several dimensionalities for EDLCs: (a) onion-like carbons [32], (b) carbon nanotubes [33], (c) carbon fibers [34], (d) graphene nanosheets [35], (e) activated carbons - ACs [36], (f) carbide derived carbons - CDCs [37], and (g) template carbons [38], respectively. For practical applications in EDLCs, dense materials with well-balanced micro-mesoporosity, *i.e.*, ACs [39] and CDCs [40, 41], are preferred.

1.2.1 Activated carbons (ACs)

Activated carbons (ACs) are amorphous porous materials containing mainly sp^2 carbon atoms. Generally, they are prepared from various natural or synthetic organic precursors, which are first pre-carbonized and then physically or chemically activated (to open the porosity and create new pores) [13, 14]. Physical activation usually occurs in a high-temperature range of 700 - 1000 °C under oxidizing atmospheres (*e.g.*, CO_2 or steam), whereas chemical activation requires a lower temperature range of 400 - 700 °C with chemical reagents (such as KOH, $ZnCl_2$, *etc.*) [30, 42, 43]. However, as these oxidizing atmospheres create surface functional groups, and it is known that the stability of organic electrolytes is strongly decreased by the presence of such functionalities, post-treatments (*e.g.*, heating under inert gas flow) are used to eliminate these surface functionalities [44]. ACs are highly porous, with a broad range of pore size, from tenths of nanometers to few nanometers, resulting in a high SSA, mainly ranging from 1000 to 2000 $m^2 g^{-1}$, which is predominantly determined by the carbon precursor and the activation conditions. ACs have been widely used

as EDLC electrode materials due to their relatively good electrical properties and high SSA, especially lower-cost, allowing commercial EDLCs with a long life span ($> 10^6$ cycles) to be produced [45]. During the past few years, the electrochemical performance of AC-based electrodes has been significantly improved to reach 100 F cm^{-3} or exceed 200 F g^{-1} in nonaqueous-based electrolytes [46, 47], which has been mainly achieved by tuning the pore size in the micropore range below 1.5 nm. In aqueous electrolytes, AC-based electrodes enable to deliver capacitance values ranging from 100 to 300 F g^{-1} , depending on the pore size distribution and surface functional groups, with the weakness of a low specific energy associated with the limited voltage window [48, 49].

1.2.2 Carbide-derived carbons (CDCs)

Carbide-derived carbons (CDCs) are generally produced by selective etching of metals from various metal carbides (*e.g.*, TiC) [50]. The carbon structure and particle size are controlled by the type of carbide precursor [51]. CDCs can offer the critical advantage of tuned pore size (below 2 nm) and pore size distribution according to the synthesis parameters such as temperature and time. Generally, CDCs can exhibit a high SSA ranging from 1000 to $2000 \text{ m}^2 \text{ g}^{-1}$, with a narrow pore size distribution in the nanometer and sub-nanometer range. Taking the TiC-CDCs as an example, the average pore size can be tuned with 0.05 nm accuracy from 0.68 to 1.1 nm by changing the chlorination temperature from 500 to $1000 \text{ }^\circ\text{C}$ [19]. Due to the controlled narrow pore size distribution in the micropore range, CDCs have been extensively utilized as model materials to understand the fundamental of EDL formation in porous materials [19, 52], which has helped in identifying the capacitance increase in nanopores. TiC-CDCs with a specific capacitance of 160 F g^{-1} were reported in an ionic liquid, leading to a high volumetric capacitance of 85 F cm^{-3} [52]. Subsequently, several approaches have been proposed to design CDCs with high EDL capacitance and high-rate performance, including reducing the CDC particle size and adding mesopores [53, 54]. Also, the ReaxFF reaction field and quench molecular dynamics (QMD) simulations were used to generate atomic, extensible models for CDCs (Fig. 4) [55]. According to such simulations, Palmer *et al.* found that the structural changes of CDCs were similar in the model and the experiment. These changes have significant effects on the pore size distribution, specific surface area, and adsorption isotherms [56]. However, the synthesis of the precursor carbides

is very complicated, and etching from carbide to CDC requires toxic Cl_2 . Collectively, these complex processes significantly increase the production cost of CDCs.

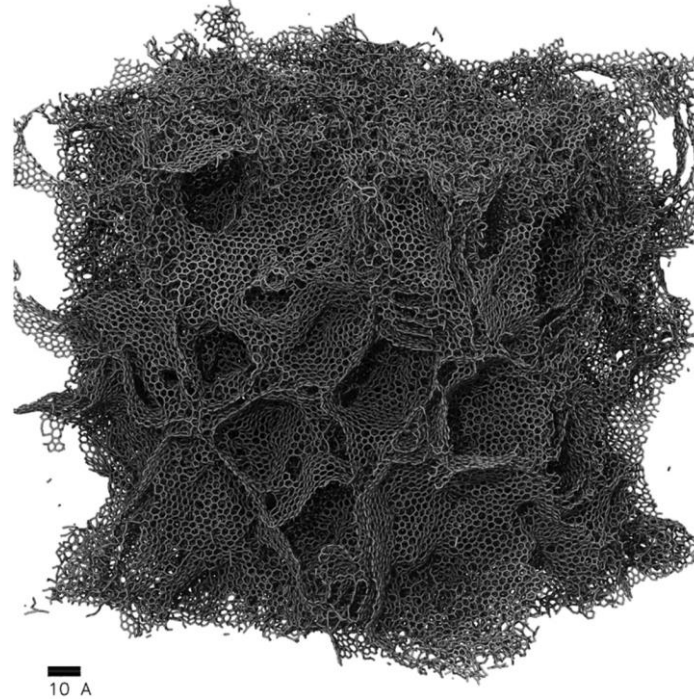


Fig. 4. Model of a CDC generated via QMD simulation with a ReaxFF force field [55]; the 200,000 carbon atoms build up a cubic box of length 25 nm with various sizes of nanopores. The nanoporous domains are constituted of stacking graphene-like sheets containing defects such as non-hexagonal rings creating a curvature.

1.3 Electrolytes for EDLCs

The main disadvantage of EDLCs is their lower specific energy than batteries (as shown in Fig. 1 of the General Introduction) [6]. According to formula (3), the specific energy of this type of capacitor is mainly increased by boosting the working voltage depending on the types of electrolytes [57]. An electrolyte for EDLCs should:

- ❖ be an excellent ion conductor to ensure a high specific power;
- ❖ be conducive to maintain a minimum self-discharge;
- ❖ have a wide electrochemical stability window (ESW) - suitable for the higher or lower potential of positive or negative electrode materials, so that EDLC can have a high working voltage;

- ❖ be adaptable to a wide temperature range, to ensure that EDLC can normally work under extreme temperature conditions;
- ❖ allow good safety, *i.e.*, low flammability, and not react with other EDLC components, such as electrodes, separator and assembly materials;
- ❖ be environmentally friendly, so that it can be promoted into practical applications.

Generally, electrolytes are divided into aqueous, organic and ionic liquids.

1.3.1 Aqueous electrolytes

An aqueous electrolyte is solution containing a suitable concentration of acids, bases or neutral salts in water. Its advantages include a high ionic conductivity (*e.g.*, 409 mS cm^{-1} for $1 \text{ mol L}^{-1} \text{ H}_2\text{SO}_4$ [58]), contributing to lower equivalent series resistance (ESR) values, and a very low cost induced by manufacturing conditions under air atmosphere. Compared with the other two types of electrolytes, aqueous electrolytes have additional advantages of smaller ions size and higher ionic conductivity, further providing ELDCs of larger capacitance and faster charge and discharge rate [59].

As we all know, the ESW of water is 1.23 V, which is the main reason to limit the working voltage of the aqueous EDLCs, with boundary potentials related to the hydrogen and oxygen evolution reactions of water. Therefore, the ESW is the most effectively enlarged through increasing the hydrogen evolution overpotential by introducing hydroxyl anions in the porosity of carbon, what locally increases the pH and triggers a shift in the Nernst potential [60]. There are three main ways reported today to increase the operating voltage of EDLCs with aqueous electrolytes: (i) by adjusting the pH of the electrolyte to reduce the activity of the water decomposition reaction [61, 62]; (ii) by adding active redox additives to inhibit the hydrogen and oxygen evolution reactions [63]; (iii) by reducing the amount of available water and consequently inhibiting its redox activity with water-in-salt electrolytes (*e.g.*, a voltage of 1.8 V can be reached with AC/AC capacitors in $20 \text{ mol kg}^{-1} \text{ LiTFSI}$ electrolyte) [64].

1.3.2 Organic electrolytes

An organic electrolyte is mainly composed of an organic solvent together with an organic or inorganic salt. As the carrier of ion transmission, the organic solvent should be able to dissolve a sufficient amount of salt, and display a low viscosity, a low melting point and a

high boiling point at the same time [65]. Because the salt needs to be dissolved at its optimal concentration, *i.e.*, the concentration ensuring the highest conductivity, the organic solvent should have polar groups such as sulfonyl (S=O), nitrile (C≡N) and carbonyl (C=O). The commonly used types of organic solvent, with a high dipole moment and a high dielectric constant, currently on the market, include acetonitrile (ACN) [66], ethylene carbonate (EC) [67], dimethyl carbonate (DMC) [68], N,N-dimethylformamide (DMF) [69] and propylene carbonate (PC) [70]. The salt in such electrolytes should have a weak anion-cation interaction to ensure a greater solubility in the organic solvent. The commonly used salts mainly include tetraethylammonium tetrafluoroborate (TEA-BF₄) [65], 1-ethyl-3-methylimidazolium tetrafluoroborate (EMIm-BF₄) [71], 1-ethyl-1-methylpyrrolidinium tetrafluoroborate (MEPY-BF₄) [72], etc. Since organic electrolytes meet the requirements for a wide ESW (*e.g.*, 0 - 3.5 V for 1.5 mol L⁻¹ TEABF₄ in ACN) [73], they are generally used in commercial EDLCs. Besides, EDLCs based on TEABF₄ in ACN can be used down to -40°C, what is an advantage compared to most aqueous media and ILs. However, the conductivity of 0.65 mol L⁻¹ TEABF₄ in PC or ACN is 10.6 mS cm⁻¹ or 49.6 mS cm⁻¹ [74], lower than that of aqueous electrolytes. In addition, the flammability, toxicity and volatility of organic electrolytes have brought certain safety issues, imposing further optimizations and improvements. Moisture in the electrolytes and/or porous carbon is also a significant issue, as few ppm of water may strongly reduce the ESW. Therefore, it has a dramatic consequence on the production costs of EDLCs, since the electrolyte and all the other components must be dramatically dried.

1.3.3 Ionic liquid electrolytes

An ionic liquid, also known as low-temperature molten salt, is a new type of electrolyte material, which received a widespread attention recently [75]. The ionic fluidity of ionic liquids allows them to be used directly as electrolytes in EDLCs [76]; they also display the advantages of low vapor pressure, low volatility, good wettability, non-flammability, and high thermal stability, with a wide ESW up to 4.5 V [77].

Although such electrolytes have many advantages, they still have a series of defects limiting their practical applications. Firstly, due their low ionic conductivity (less than 20 mS cm⁻¹) [78] and high viscosity restricting the movements of ions, the EDLCs made with such electrolytes have a worse rate performance than those with organic electrolytes, and they generally do not operate at low temperature [79]. Secondly, they are environmentally

sensitive, so that they need to be manipulated in an absolutely water-free environment during their preparation, storage and use, resulting in complex manufacturing processes with high costs [80]. Therefore, there will be a long way before ionic liquids will be widely used as high-performance electrolytes.

2. Na-ion batteries (NIBs)

Na-ion batteries (NIBs) started to be developed in parallel to Li-ion batteries (LIBs) in the 1980s [81, 82]. However, the lithium equivalents exhibit a higher specific energy owing to their lower mass, resulting in their domination of both research and commercial fields, as well as the exponential growth of the portable electronics market in the 1990s. Though recent reports have indicated that NIBs could compete with LIBs in terms of specific energy [83, 84], there are several obstacles to overcome, including insufficient cycle life and the need to discover new materials to enhance the properties of positive and negative electrodes, before they become a commercial reality [85]. In the last few years, the research on NIBs has significantly increased to address these obstacles so that this emerging energy storage technology will soon become available.

2.1 Principles of NIB operation

Fig. 5 shows a schematic representation of a NIB where Na^+ ions shuttle between the cathode (*e.g.*, NaMnO_2 or NaFeO_2 layered metal oxides) and anode (*e.g.*, hard carbon) through a sodiated organic electrolyte [86, 87]. During the charge, the sodium ions are extracted from the positive electrode at a high potential (*e.g.*, $> 3.0 \text{ V}$ vs. Na/Na^+), and are then inserted in the negative electrode at a low potential (*e.g.*, $< 1.0 \text{ V}$ vs. Na/Na^+). From the thermodynamic perspective, the electrons are pumped ‘uphill’ from the positive to the negative electrodes through the external circuit during charging. On the contrary, during the discharge, the reverse process occurs, where the Na^+ ions are extracted from the anode and re-inserted into the cathode, while the electrons pass through the external circuit.

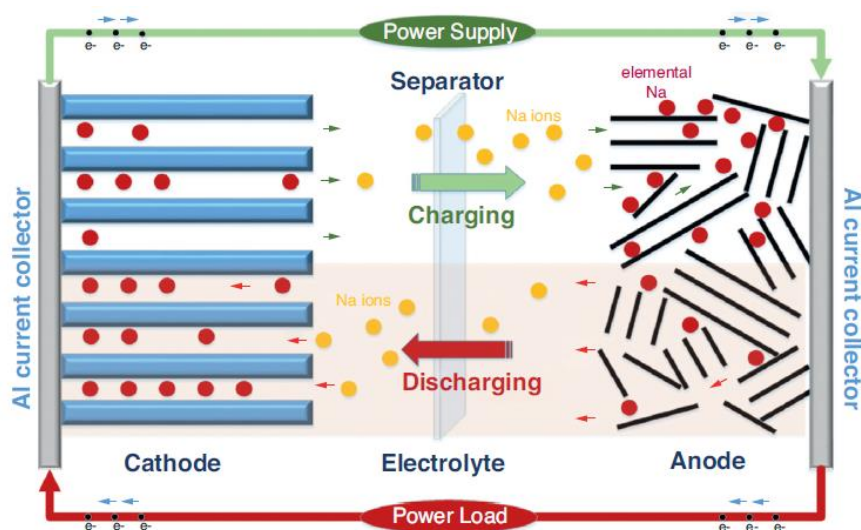


Fig. 5. Scheme of a typical NIB composed of a layered metal oxide cathode and a hard carbon (HC) anode. During the charge, Na^+ are inserted in the anode, as illustrated in the top portion of the scheme; during the discharge, they migrate in the opposite direction, as illustrated in the lower part [87].

2.2 Organic electrolytes for NIBs

Generally, electrolytes applied in NIBs comprise a sodium salt, a solvent, and an additive is sometimes included to form a stable S.E.I. [88]. The optimization of electrolytes can be achieved by carefully selecting and reasonably matching these components for desirable electrochemical properties.

A generic list of properties required for an electrolyte of a NIB is as follows [89]:

- chemically stable – during cell operation, no chemical reactions of the electrolyte with the separator, the electrodes, the current collectors and the packaging materials;
- electrochemically stable – large ESW;
- thermally stable – both the melting and boiling points should be well outside the operating temperature range;
- ionically conductive and electronically insulating – to sustain the cell operation by facile Na^+ transport and minimize the self-discharge, respectively;
- low toxicity, limited environmental hazards;
- prepared based on sustainable chemistries – abundant elements and the lowest possible impact on the synthesis process (energy, pollution, *etc.*);

- minimize total cost, including materials and production.

2.2.1 Sodium salt

The salt is one of the significant components of the electrolyte, with profound effects on the final performance. Among the properties directly affecting the choice of the salt, the most important ones are: (i) its solubility in the solvent, allowing sufficient carriers to exist, (ii) its stability for the widest ESW, *i.e.*, no chemical reactions with the solvent, electrodes, and current collectors, and (iii) the absence of toxicity.

The most used types of sodium salt in NIBs are listed in Fig. 6. The mainly applied anions are ClO_4^- , BF_4^- , PF_6^- , CF_3SO_3^- (Tf), $[\text{N}(\text{CF}_3\text{SO}_2)_2]^-$ (TFSI) and $[\text{N}(\text{SO}_2\text{F})_2]^-$ (FSI) [90-93]. During charging, the anion is usually the part of electrolytes oxidized at first, and consequently determines the upper limit of ESW.

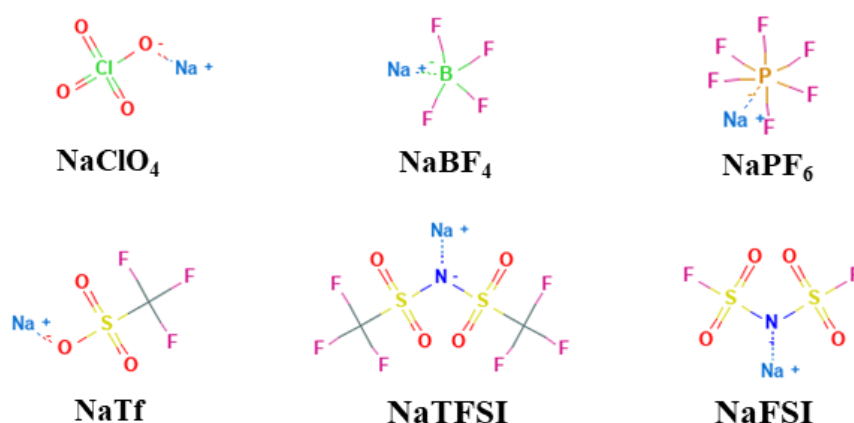


Fig. 6. The most common salts used for NIBs with liquid electrolytes. Sodium perchlorate (NaClO_4), sodium tetrafluoroborate (NaBF_4), sodium hexafluorophosphate (NaPF_6), sodium trifluoromethanesulfonate (NaTf), Sodium trifluoromethanesulfonimide (NaTFSI), sodium bis(fluorosulfonyl)imide (NaFSI).

The most commonly used salt in NIBs is NaClO_4 , likely which may be due to a combination of historical and cost reasons. In addition to safety, a particularly problematic issue is that NaClO_4 is notoriously difficult to dry [94]. Though the water content of electrolytes is seldom reported in the literature, NaClO_4 -based electrolytes do usually exhibit higher water content (> 40 ppm) as compared to NaPF_6 -based ones (< 10 ppm), even after drying the powder at 80°C under vacuum overnight. The second most popular type of salt is

indeed NaPF₆, which enables comparisons with many studies on LIBs. Despite the issues related to Al corrosion, NaTFSI and NaFSI have become strong candidates for sodium salt of choice; NIB electrolytes based on these two salts display a higher thermal stability than with both NaPF₆ and NaBF₄, and a higher conductivity than with NaTf. It is worth pointing out that FSI has an unclear status yet when considering corrosion issues; the early reports on aluminum by FSI were later attributed to Cl impurities left over from the salt synthesis process; still, a recent paper reports on the corrosion of stainless steel [95].

2.2.2 Solvent

The selected solvent should meet the following criteria: (i) display a relatively high dielectric constant to facilitate the salt dissociation and limit ion pairing; (ii) have a low viscosity to improve the mobility of ions; (iii) be electrochemically stable vs. reduction and oxidation during cell operation; (iv) have a wide liquid range (*i.e.*, low melting point and high boiling point) and (v) be nontoxic and economical [96].

The main types of solvents used for electrolytes of NIBs are shown in Fig. 7. So far, the carbonate esters are either of cyclic type (*e.g.*, propylene carbonate (PC) and ethylene carbonate (EC)) or linear type (*e.g.*, ethylmethyl carbonate (EMC), dimethyl carbonate (DMC) and diethyl carbonate (DEC)). PC and EC are the most attractive solvents for NIBs owing to their high dielectric constant, stable chemical and electrochemical properties, though no single solvent can meet all the requirements of batteries. For example, a NIB with PC-based electrolytes suffers from significant capacity decay over time, which is attributed to the continuous decomposition of PC and growth of a solid electrolyte interphase (S.E.I.) film [97, 98]. Pure EC is unsuitable for being a solvent at ambient temperature because of its high melting point (36.4 °C). Nevertheless, EC is a favorable co-solvent, especially of PC, in an optimized electrolyte system, because it is an effective ingredient to form a protective S.E.I. layer [98, 99]. Linear carbonate esters (*e.g.*, EMC, DMC, and DEC) have a lower viscosity and melting point than cyclic carbonate esters, which are often used as the co-solvent with cyclic carbonate (EC or PC), to obtain an electrolyte with better performance. For example, graphite has long been considered unsuitable as an anode for NIBs because suitable binary intercalation compounds cannot be formed with sodium [100, 101]. Recently, Jache *et al.* reported the successful application of graphite as a NIB anode in a diglyme-based electrolyte, where diglyme is co-intercalated with sodium to form a ternary intercalation compound [101].

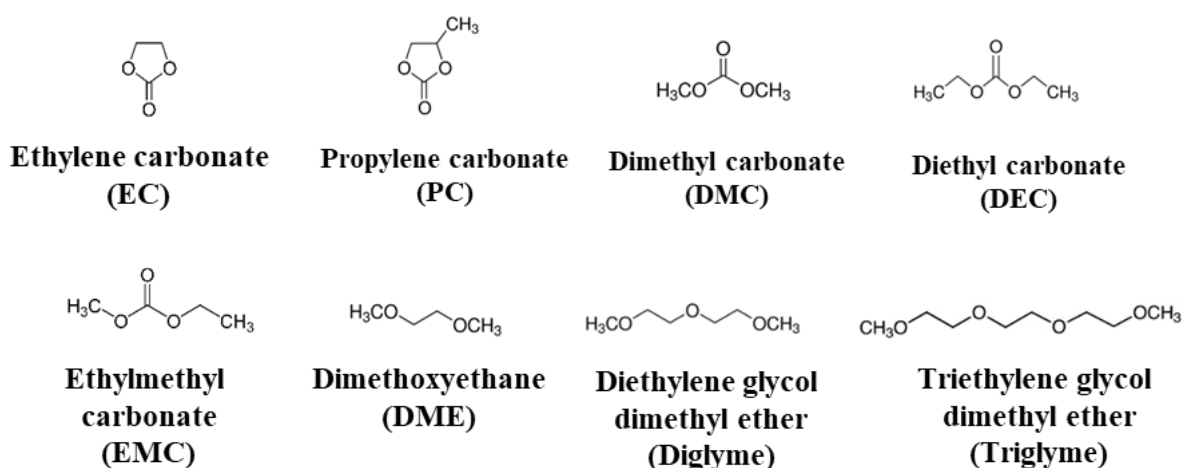


Fig. 7. The most common solvents used for NIBs with liquid electrolytes.

2.2.3 Additive

Another significant component, which is often needed to create a functional electrolyte is the additive with less than 5 wt%. Generally, the additive is used to form a stable solid electrolyte interphase (S.E.I.) [102], which is also required for battery safety issues such as reducing flammability and preventing overcharging [103, 104]. Several kinds of additive have been screened for electrolytes of NIBs, including fluoroethylene carbonate (FEC), vinylene carbonate (VC), ethylene sulphite (ES), and the doubly fluorinated EC (DFEC); a clear advantage of FEC compared to others has been shown [105]. Interestingly, VC, very popular in LIBs, was not found to act for NIBs in the same way. The benefits of FEC are clearly proven for electrode materials displaying a significant volumetric expansion, such as SnO_2 , Sb, red phosphorus and Sn_4P_3 [106-109].

2.3 Anodic materials for NIBs

As illustrated in Fig. 8, there are mainly three types of anodic materials for NIBs: carbon-based, conversion and alloying [102]; organic compounds have so far received less attention as potential anode materials for NIBs due to the successful development of the other materials. Carbon-based materials exhibit a relatively low sodium storage capability ($\sim 300 \text{ mAh g}^{-1}$), which may be insufficient to meet the requirements of high-energy NIBs. The conversion and alloying materials, with 2-3 times that of carbon-based anodes, have broad application prospects in high-energy NIBs. Unfortunately, a major challenge is the large

volume change occurring during the sodium insertion/deinsertion processes, which may easily cause the material to crumble, thus inducing the exfoliation of electrodes from the current collectors.

Anode materials are one of the most crucial components, which directly affect the cycle life, output voltage and whole specific energy of NIBs. In general, a promising anode candidate for NIBs should meet the following requirements: high specific capacity, good cycling stability, superior rate performance, and appropriate reaction potential to avoid sodium plating.

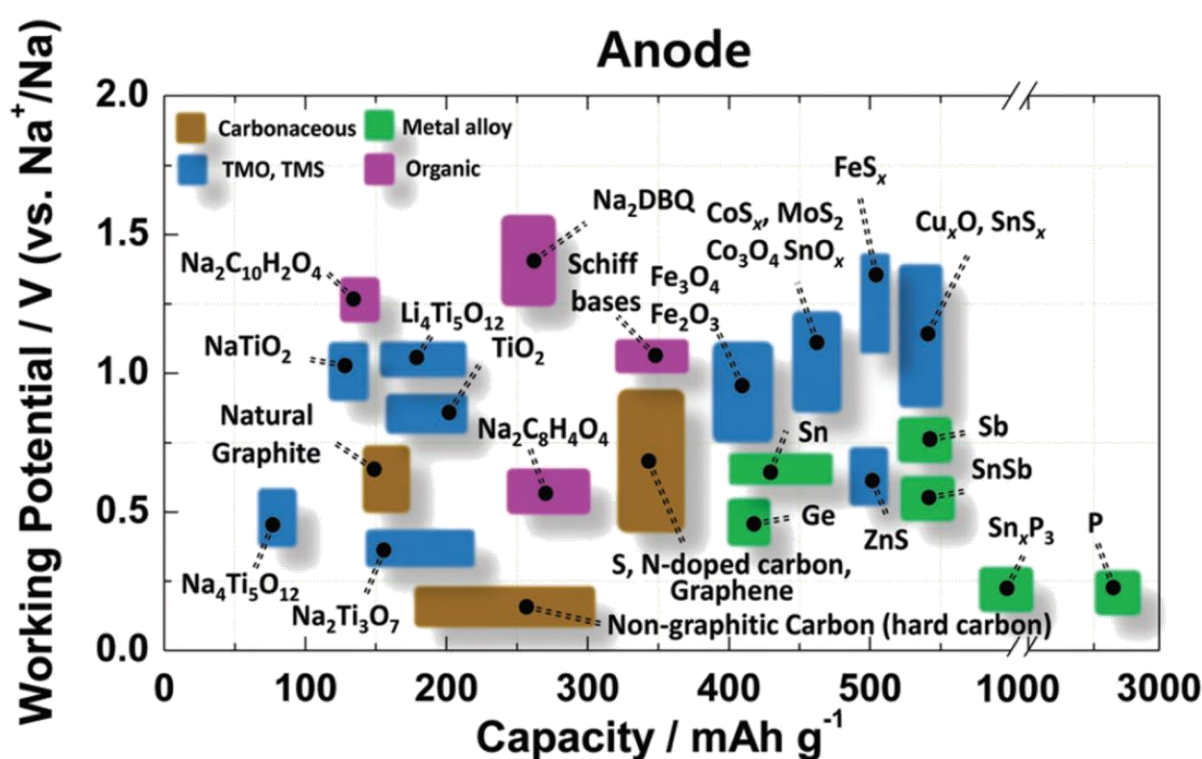


Fig. 8. Plot of average working potential vs. practical capacity of promising anodic materials for NIBs [102].

2.3.1 Carbon-based materials

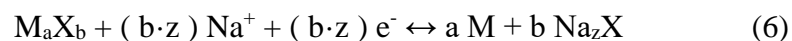
Many carbon materials have been used to explore the mechanism of sodium storage, such as graphitized and non-graphitized carbon [110, 111], which are widely recognized because their structure has an interesting ability to store alkali metals. Similar to lithium, which is easily intercalated into graphite to form Li-graphite intercalation compounds [112], the electrochemical reaction between Na^+ and graphite has also been studied since the 1980s. As

this reaction is significantly hindered, the first principle was used to calculate the formation energy of Na-graphite intercalation compounds. The results showed that, because the graphite structure did not match the radius of Na^+ , these compounds are thermodynamically unstable, so that only a very small amount of sodium can be intercalated [113]. However, a recent study by Jache *et al.* showed that solvated Na^+ could be intercalated into graphite to form a ternary graphite intercalation compound [101].

Hard carbons (HCs), with a suitable reversible capacity (about 300 mA h g^{-1}), are a popular anodic material which has been largely investigated for NIBs, though its low operating potential (close to 0 V vs. Na/Na^+) might be the cause of sodium plating [111, 114-116]. HCs can be obtained by carbonization of environmentally friendly, cheap, and renewable bio-sources, representing a great advantage in terms of cost, as well as large-scale production and commercialization [111]. Despite several promising HCs being proposed and tested, the basic understanding of the sodium storage mechanisms is still lacking [117]. Early works on the mechanism by Stevens and Dahn stated that Na^+ could be first inserted into regions of parallel graphene layers at a higher potential, resulting in a sloping potential curve, and then could fill the nanoporosity between randomly stacked layers by an adsorption-like process [116, 118, 119]. Recent works by Grey *et al.* using *operando* ^{23}Na solid-state nuclear magnetic resonance (ssNMR) in an in-house designed electrochemical cell confirmed such a mechanism [120]. The first stage, in the sloping region from open circuit potential to $180 \text{ mV vs. Na/Na}^+$, shows a signal close to 0 ppm , revealing the presence of ionic sodium. In the second stage, below $180 \text{ mV vs. Na/Na}^+$, the signal shifts progressively up to 760 ppm , characterizing metallic sodium clusters (Fig. 9). From *ab initio* calculations, it was concluded that the larger interlayer spacing is not the only factor promoting Na embedding; vacancy defects in HCs can also greatly facilitate the insertion of Na^+ because of the strong ionic bond between defects and Na^+ ions [121].

2.3.2 Conversion materials

Conversion materials (*e.g.*, transition-metal oxides, transition-metal sulfides) undergo phase transitions during the absorption and release of sodium, according to the reversible reaction schematized by equation (6):



where M is a metal and X is a non-metal. For a typical conversion reaction, M is a transition metal such as Fe, Co, Ni, Cu and Mn, and X includes O, N, F, S, Se and P. The metal M may form amorphous or crystalline nanoparticles, while nucleated Na_zX tends to be distributed around the metal M nanoparticles. The ideal state is that a bi-continuous conductive network is created by both of them, which is beneficial for the conduction of electrons/sodium ions and the reversibility of the conversion reaction. The interface between the electronically conductive M phase and the ionic conductive Na_zX phase can further store sodium ions, generating an additional capacity [122].

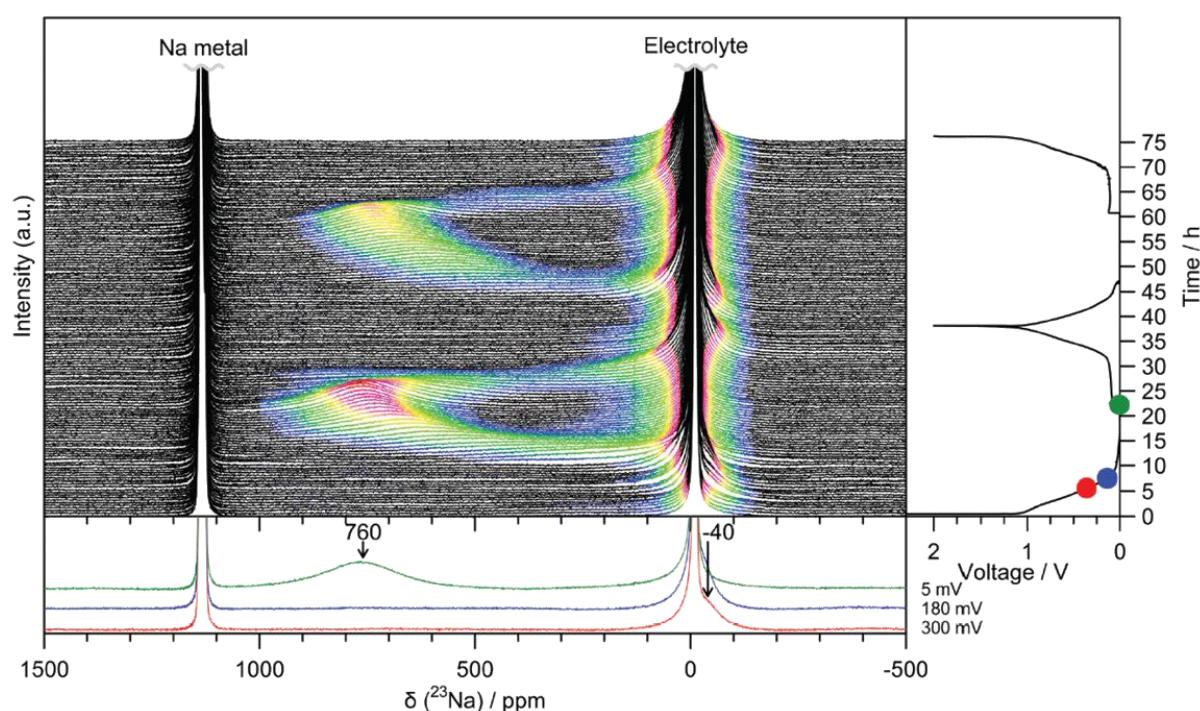


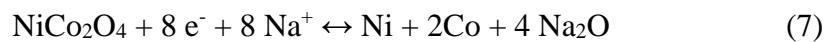
Fig. 9. *Operando* ^{23}Na NMR spectra for an electrochemical cell with a hard carbon working electrode and a sodium disc counter/reference electrode in NaPF_6 electrolyte [120]. The cell was cycled at a current of $C/20$ ($C = 300 \text{ mAh g}^{-1}$) between 2 V and 5 mV vs. Na/Na^+ and held at 5 mV vs. Na/Na^+ until the applied current dropped to $C/100$. The result of two galvanostatic cycles is shown on the right side.

A conversion reaction is a multi-electron transfer process with a high theoretical capacity. In addition, since the working potential of the conversion reaction depends on the ionicity of the M-X bond, the electrochemical potential can be adjusted as needed [123]. Conversion reaction electrode materials have been extensively studied in LIBs and NIBs because of their

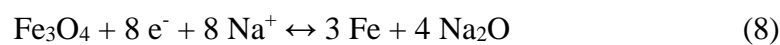
higher capacity than intercalation reaction materials. In addition, nanomaterials can provide more electrode-electrolyte contacts and shorten the diffusion distance of Na^+ in the material, thereby bringing higher rate performance. However, their application is restricted by problems, *e.g.*, low first coulombic efficiency, cycle stability and energy efficiency caused by the potential hysteresis between insertion and deinsertion during cycling. As each conversion cycle exposes a new electrode surface, the latter accelerates the electrolyte decomposition. A potential hysteresis is an inherent characteristic of conversion reactions, mainly due to the ohmic voltage drop, the reaction over-potential (related to the ionicity of the M-X bond), and the uneven spatial distribution of the electrochemically active phase [124]. Meanwhile, as the volume of the electrode changes significantly during the transformation reaction, it leads the electrode to powdering, with a resulting decrease of electrical conductivity and finally capacity. The stress caused by volumetric changes can effectively be released by employing nanostructured materials [125]. By optimizing the material microstructure and electrode structure, the energy efficiency of NIBs based on a conversion reaction can be improved, and the potential lag when reversing the reaction can also be reduced [126].

(1) Transition-metal oxides

Alcantara *et al.* were the first to report the concept of conversion reaction material for NIBs, showing that spinel NiCo_2O_4 had the potential to be used for the negative electrode [127]. The conversion reaction of NiCo_2O_4 can be expressed by equation (7):



To understand whether the conversion reaction is feasible in NIBs, Klein *et al.* systematically studied the fundamental thermodynamic properties of the conversion reaction materials [128], and calculated that the potential for this reaction with oxides in NIBs is usually around 0.96 V vs. Na/Na^+ , lower than the reaction potential in LIBs, which can ensure the high specific energy of NIBs based on transition metal oxide anodes compared with LIBs. Fe-based oxides, which are abundant and environmentally friendly, have been extensively studied as potential anode materials for NIBs, and it has been proposed that the conversion reaction mechanism of Fe_3O_4 with Na^+ follows the equation (8):



The formation of Fe metal and Na_2O was confirmed by *ex-situ* selected area electron diffraction (SAED) (Fig. 10a) [129]. It was observed that Fe_3O_4 has a reversible capacity of

366 mAh g⁻¹, with an initial coulombic efficiency of 57% (as shown in Fig. 10b). This capacity is much lower than both the theoretical value of 926 mAh g⁻¹ for the entire conversion reaction and the reversible capacity of 932 mAh g⁻¹ observed in lithium-ion cells; such a low value could be primarily due to the slow sodium insertion/extraction kinetics because of the too high ionic radius of the Na⁺ ions. Similar observations were made with other conversion reaction compounds [102, 128, 130, 131], what may originate from (i) the sluggish kinetics of Na⁺ transfer due to its relatively large ion size and (ii) a different nature of the S.E.I. layer formed in Na cells [132-135].

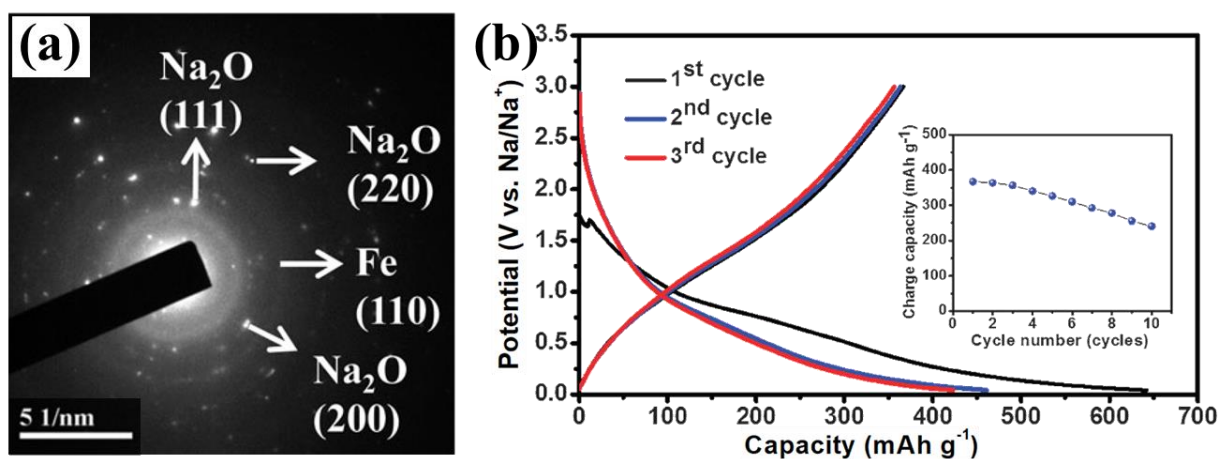
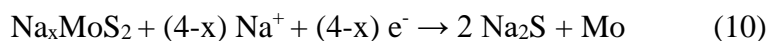


Fig. 10. (a) Selected area electron diffraction patterns of the Fe₃O₄ electrode after the first discharge to 0.04 V vs. Na/Na⁺ [129]; (b) Galvanostatic discharge/charge of Fe₃O₄ at 0.06 C in the potential window of 0.04-3.0 V vs. Na/Na⁺; the inset shows the variation of the charge capacity vs. the cycle number [129].

(2) Transition-metal sulfides

Similar to oxides, transition metal sulfides store sodium ions through conversion reactions with a high theoretical capacity; compared with the corresponding oxides, sulfides display more obvious advantages. The bond between the sulfur and metal atoms in sulfides is weaker than that between oxygen and metal in oxides, what will cause sodium to be inserted in metal sulfides, whereas metal oxides are more prone to sodium deinsertion [136]. Also, the mechanical stability of sulfides is higher because of their smaller volume changes [137]. Therefore, many transition metal sulfides have been studied as anode materials for high-capacity NIBs. For example, MoS₂ is a layered material in which Na⁺ can be intercalated

between the layers as shown in equation (9) [138], and when the potential is lower than 0.4 V vs. Na/Na⁺, the conversion reaction occurs as in equation (10):



The capacity provided by the insertion reaction (equation (9)) is relatively low, while the theoretical capacity provided by the transformation reaction is 668 mAh g⁻¹. To solve the volume expansion caused by the conversion reaction, the researchers designed various nanostructures and fabricated composites with conductive carbon materials. In this context, Chen *et al.* reported a facile one-step spraying pyrolysis method to form MoS₂/C microspheres (Fig. 11a) [139], in which the interlayer distance between the MoS₂ nanosheets is 0.64 nm (as shown in Fig. 11b). This material demonstrated a stable cycling performance at 1 A g⁻¹, with a capacity of 390 mAh g⁻¹ after 2500 cycles (as shown in Fig. 11c), mainly attributed to the uniform distribution and reduced aggregation of the MoS₂ nanosheets in carbon backbones.

2.3.3 Alloying materials

Alloying reaction materials originating mainly from groups IVA and VA, especially Si, Ge, Sn, P and Sb are desirable negative electrode materials because of their high capacity during the alloying-dealloying reaction with Na⁺ below 1.0 V vs. Na/Na⁺ [140]. The alloying mechanism is represented by equation (11):



(X: Sn, P, Sb, Bi, Ge, etc.)

This reaction occurs with significant volume changes during alloying-dealloying, causing complex mechanical stresses on the active particles, eventually leading the electrodes to powdering [141]. So far, researchers have carried out many designs of electrode structure to tentatively solve these volumetric variations.

(1) Sn-based materials

Sn is considered to be one of the most promising anodic hosts, which forms a Na₁₅Sn₄ phase at full alloying, with a high theoretical capacity of 847 mAh g⁻¹ [142], and an enormous volume expansion of about 420%. Such a high volume change causes continuous pulverization of the electrodes, with a loss of conductive contact and an accelerated capacity

degradation. Coating carbon on Sn powder or constructing a composite with a carbon matrix can effectively buffer the volume expansion and provide excellent conductive paths [142]. A self-supporting electrode was prepared with a 3D core-shell structure Sn@CNT nanocolumn array grown on carbon paper [143], with a high reversible capacity of 519 mAh g^{-1} after 100 cycles at 0.5C. Two-dimensional graphene can also act as a physical barrier to buffer the volume change of Sn and prevent the agglomeration of nanoparticles [144], with a reversible capacity of 413 mAh g^{-1} with ca. 2 % fading after 100 cycles at 100 mA g^{-1} .

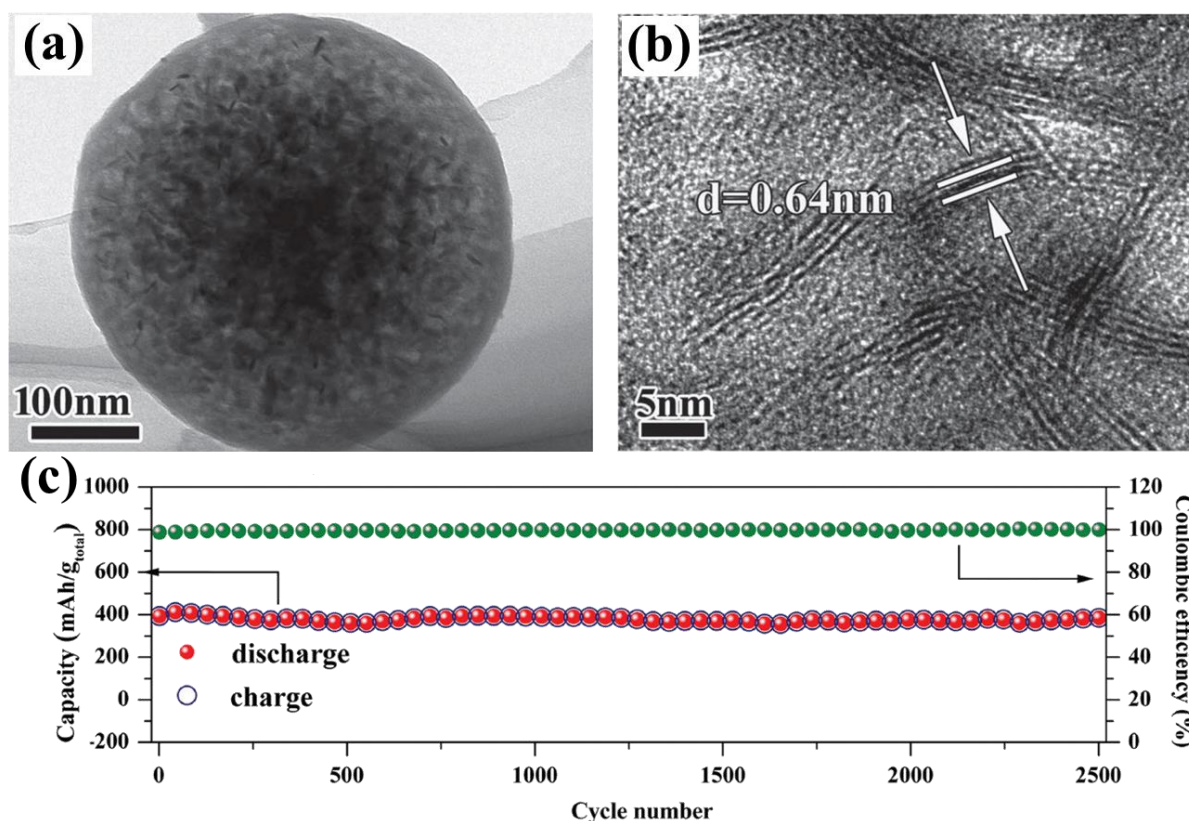


Fig. 11. (a) TEM and (b) HRTEM images of a MoS₂/C microsphere [139]; (c) Charge/discharge capacity and coulombic efficiency of a MoS₂/C electrode during galvanostatic cycling at 1.0 A g^{-1} [139].

(2) P-based materials

Owing to its low molecular mass and high number of electrons transferred ($3e^-$), phosphorous has a theoretical capacity of 2596 mAh g^{-1} [145-147]. Among the allotropes of phosphorus [148], amorphous red phosphorus and orthorhombic black phosphorus have great potential as anodic materials for sodium ion storage. The actual application of these two

materials is restricted by the huge volume change (ca. 490%) during the alloying reactions. Recently, researchers have designed various amorphous phosphorus-based materials by adding a carbon matrix in the attempt to achieve a high capacity and a stable cycle life. The red-phosphorus-impregnated carbon nanofiber composite prepared by a vaporization–condensation method [148], displayed a reversible capacity of 1522 mAh g⁻¹ and a reversible capacity of 1020 mAh g⁻¹ after 5000 cycles at 1 A g⁻¹. Black phosphorus is thought to consist of 2D phosphorene single-layers with a spacing up to 3.2 Å, meaning that Na⁺ (with a radius of 1.02 Å) can be stored between the phosphorene layers [149]. Sun *et al.* prepared nanostructured black phosphorene-graphene composites, in which black phosphorene is between graphene sheets forming a sandwich structure [150]; this material displayed a high reversible capacity of 2440 mAh g⁻¹ at a current density of 0.05 A g⁻¹ and a capacity retention of 85% after 100 cycles. *In-situ* TEM and *ex-situ* XRD investigations demonstrated that the large capacity of a black phosphorene-graphene anode is achieved owing to a dual mechanism of sodium ions intercalation between the phosphorene layers, followed by the formation of a Na₃P alloy.

(3) Sb-based materials

At full alloying of antimony with sodium, the Na₃Sb phase with a theoretical specific capacity of 660 mAh g⁻¹ was formed and its volume expansion reached 390% [151]. To reduce the volume changes and accelerate the kinetics of the alloying reaction, many researches are devoted to the design of nanostructures and composites with conductive carbon materials. A composite with antimony uniformly fixed on multilayer graphene has been prepared through chemical bonding [152]; it demonstrated an initial reversible capacity of 452 and 210 mAh g⁻¹ at 5 and 0.1 A g⁻¹, respectively, and a reversible capacity retention of 90% after 200 cycles at 0.1 A g⁻¹. Compared with micron-sized antimony particles, monodisperse antimony nanocrystals with an average particle size of 10-20 nanometers [153] demonstrated a significantly improved rate performance and cycle stability.

(4) SnSb-based materials

Mixed alloys such as SnSb and Sn₄P₃ can also be used as anode materials for NIBs; among them, SnSb displays a high theoretical capacity of 752 mAh g⁻¹ [154]. *In-situ* TEM [155] proved that the Na₃Sb and Na_{3.75}Sn phases are formed successively during the sodium

insertion in a β -SnSb anode, and that the Na_3Sb phase is desodiated before the $\text{Na}_{3.75}\text{Sn}$ phase during sodium deinsertion; finally, Sb is alloyed with the desodiated Sn, allowing nanocrystalline β -SnSb to be restored (see Fig. 12a). The variation of the β -SnSb volume with time shows a final expansion by 210%, which is much smaller than that of either pure Sn or Sb. Therefore, a β -SnSb alloy anode shows a better cycling stability than the pure Sn or Sb phases (Fig. 12b). However, during cycling, the segregation of a crystalline Sn phase results in a capacity decay. Hence, the sodium insertion/deinsertion in SnSb follows the reversible sequential electrochemical reactions as shown in equations (12) and (13) [151]:

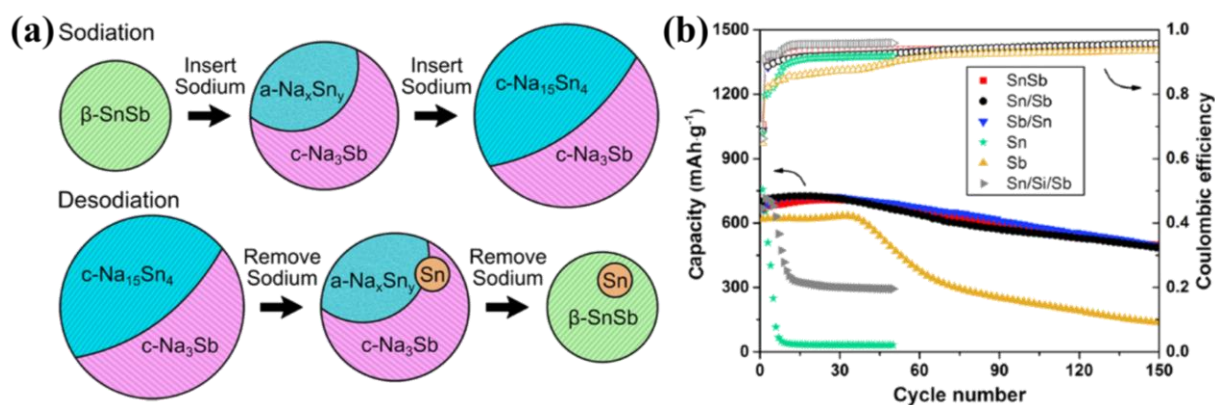
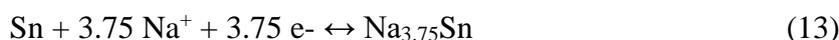


Fig. 12. (a) Schematic illustration of the identified phase transitions during a sodium insertion/deinsertion cycle in β -SnSb [155]; (b) Cycling performance and coulombic efficiency of Sn, Sb, SnSb, bilayer Sn(top, 50nm)/Sb(bottom, 50nm) or Sb(top, 50nm)/Sn(bottom, 50nm) and trilayer Sn(top, 49nm)/Si(middle, 2nm)/Sb(bottom, 49nm) films at 200 mA g^{-1} [155].

To improve the stability and rate performances of SnSb electrodes, hybrid composites made of SnSb nano-particles uniformly dispersed on RGO have been prepared with a hydrothermal method and subsequent thermal reduction [156]; the formation of the RGO-SnSb nanocomposites effectively suppresses the volumetric changes and prevents from the agglomeration of the SnSb particles. When applied as an anode in NIBs, RGO-SnSb showed an excellent rate performance (80 mAh g^{-1} at 15 A g^{-1}) and cycling stability (reversible capacity from 407 mAh g^{-1} to 361 mAh g^{-1} after 80 cycles at 0.1 A g^{-1}). Moreover, a SnSb-in-

plane nano-confined 3D N-doped porous graphene network (3D SnSb@N-PG), fabricated by a NaCl-template method combined with spray drying, was applied as anode for NIBs and gave a capacity retention of nearly 100% after 4000 cycles at a high current density at 10 A g^{-1} , without any morphological and structural changes [157]. The N-doped porous graphene network buffers the huge volumetric changes of the SnSb nanocrystals during the sodium insertion/deinsertion, and also enhances the electrode conductivity, whereas the SnSb nanocrystals (10-15 nm) provide short Na^+ diffusion paths.

(5) Sn_4P_3 -based materials

Among the alloys, Sn_4P_3 has attracted a considerable attention because of its high theoretical gravimetric and volumetric capacity of 1132 mAh g^{-1} and 6650 mAh cm^{-3} , respectively (Fig. 13) and high electronic conductivity of 30.7 S cm^{-1} [109]. In the first investigation of the electrochemical performance of ball-milled Sn_4P_3 as a NIB anode [109], a reversible capacity of 718 mAh g^{-1} at a low redox potential of ca. $0.3 \text{ V vs. Na/Na}^+$ has been claimed.

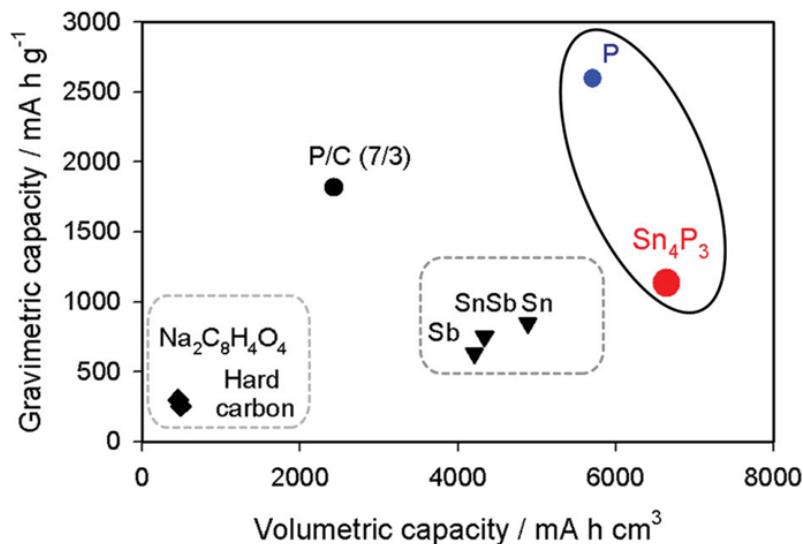


Fig. 13. The theoretical volumetric and gravimetric capacity of various anode materials for NIBs [109].

According to first-principle molecular dynamics simulations [158], the sodium insertion process of Sn_4P_3 can be depicted as follows: in the initial stage of the reduction reaction, the Sn-P bonds of Sn_4P_3 are broken and Na^+ reacts with P to form Na_xP due to the strong

preference of Na for P over Sn; meanwhile, Sn nano particles are formed. As the reduction continues, the Na_xP phase is transformed into Na_3P , and the Sn particles react with Na^+ to give Na_ySn , and eventually at the end of reduction $\text{Na}_{15}\text{Sn}_4$ particles confined in a Na_3P matrix. Therefore, the first Na^+ insertion process can be expressed as:



The sodium insertion/extraction mechanism in Sn_4P_3 was verified by *ex-situ* XRD (Fig. 14) [159]: in the initial stage of sodium insertion down to 0.25 V vs. Na/Na^+ , the Sn_4P_3 lattice is transformed into Na_3P and metallic Sn; after a complete discharge to 0.01 V vs. Na/Na^+ , the Na_3P signal is enhanced and the $\text{Na}_{15}\text{Sn}_4$ alloy is formed. During the charge up to 0.5 V vs. Na/Na^+ , the signal of the $\text{Na}_{15}\text{Sn}_4$ phase disappears and the Sn signals becomes stronger, manifesting the Na^+ extraction reaction. However, when the electrode is charged back to 2 V vs. Na/Na^+ , the absence of any XRD reveals a low crystallinity of the final reaction products.

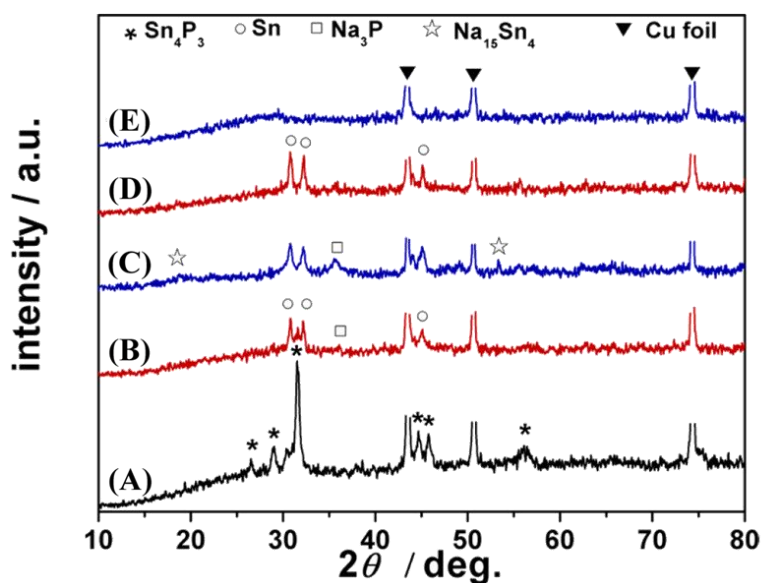


Fig. 14. *Ex-situ* XRD patterns of a Sn_4P_3 /carbon electrode at different discharge and charge states: (A) fresh electrode; (B) after the 1st discharge to 0.25 V vs. Na/Na^+ ; (C) after completion of the 1st discharge to 0.01 V vs. Na/Na^+ ; (D) after the 1st charge to 0.5 V vs. Na/Na^+ ; and (E) full charge to 2.0 V vs. Na/Na^+ . Here, the discharging process represents the sodium insertion [159].

The size of Sn_4P_3 nanostructures is a crucial factor for anode performance. Size-adjustable core-shell Sn_4P_3 -C nanospheres were fabricated with a carbonization/reduction and

phosphorization process [160]. Among the various sizes which were prepared (see Fig. 15a and 15b), the electrodes made of 140 nm $\text{Sn}_4\text{P}_3\text{-C}$ nanospheres have been reported to demonstrate a reversible capacity of ca. 500 mAh g^{-1} after 100 cycles at 1 A g^{-1} (see Fig. 15c) and 420 mAh g^{-1} after 2000 cycles at 2 A g^{-1} .

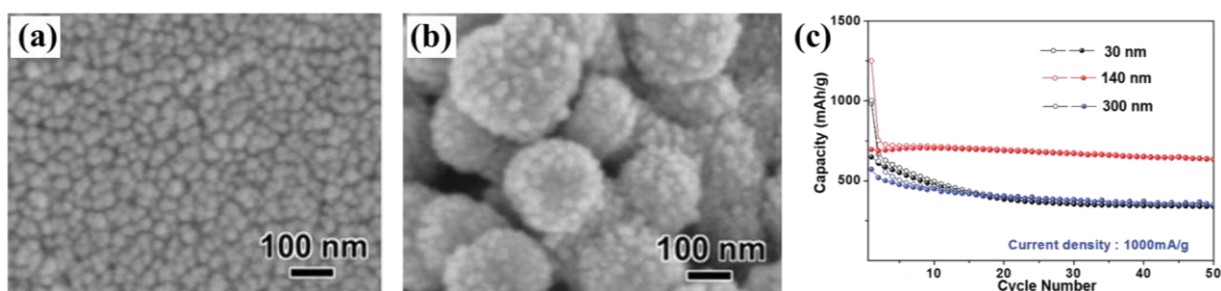


Fig. 15. SEM images of (a) 30 nm and (b) 300 nm-sized $\text{Sn}_4\text{P}_3\text{-C}$ nanospheres and (c) cyclability of 30, 140, and 300 nm-sized $\text{Sn}_4\text{P}_3\text{-C}$ nanosphere electrodes at 1000 mA g^{-1} [160].

2.4 Solid electrolyte interphase formation on negative electrodes

It is common for negative electrodes of sodium-based energy storage cells to experience an irreversible capacity loss during the first operating cycle. To provide an important example, Fig. 16 shows the constant current first insertion and deinsertion profile of an HC electrode [161], where it is seen that the capacity of the electrode at the end of the first reduction is higher than after its oxidation back to the starting potential; in other words, a "missing" capacity is not recovered during the subsequent cycles [162, 163].

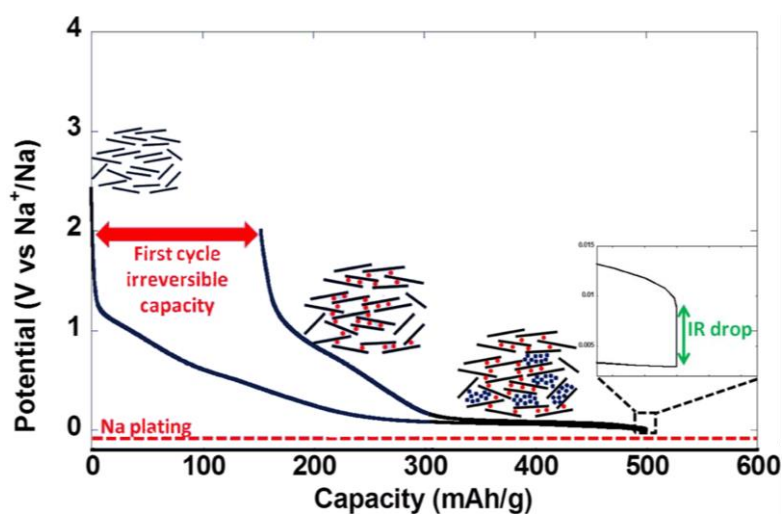


Fig. 16. Typical potential vs. capacity profile for a hard carbon electrode tested against a sodium counter electrode [161].

During the first reduction, as the electrode potential decreases, an electrochemical reaction occurs at the electrode/electrolyte interface, resulting in the irreversible formation of a solid electrolyte interphase (S.E.I.) [164], with a mosaic form consisting of different inorganic and organic reaction products of Na^+ with the electrolyte (as shown in Fig. 17a and 17b) [165, 166]; the loss of sodium in the S.E.I. formation is the primary reason for low initial coulombic efficiency (CE). However, this passivation layer plays a pivotal role in providing highly reversible cycling properties of anode materials. Electrolyte formulations have been adjusted to ensure that the S.E.I. has a good ionic conductivity and is a good electronic insulator to prevent the electrolyte decomposition after the deposition of a certain thickness [165, 167-169]. A good S.E.I. should meet the following criteria: (i) protect the electrode surface from a direct contact with the electrolyte, and (ii) allow the diffusion of desolvated ions and prevent the transport of electrons (the S.E.I. is a pure cationic conductor).

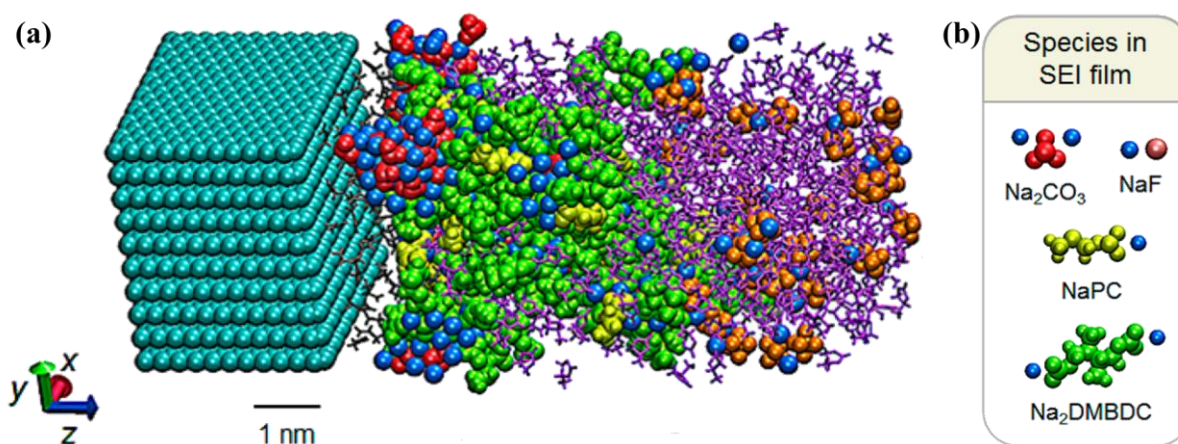


Fig. 17. (a) A computer model of a negative electrode with a deposited S.E.I. (the electrolyte is $1.1 \text{ mol L}^{-1} \text{ NaPF}_6$ in propylene carbonate); (b) Sodium is irreversibly lost in the formation of the S.E.I. species (*e.g.*, red: sodium carbonate (Na_2CO_3), orange: sodium fluoride (NaF), yellow: sodium propyl carbonate (NaPC), green: 3-dimethylsodium butylene dicarbonate (Na_2DMBDC)) [165].

For a long time, the S.E.I. research for LIBs has taken an absolute precedence over that for NIBs [170]. One of the first examples of S.E.I. research in NIBs was conducted by Komaba *et al.* in 2011 [167], who investigated the compounds formed on the surface of the hard carbon electrode after the first cycle in coin-type cells. *Ex-situ* XPS revealed the

presence of carbonate, Na_2CO_3 , and alkyl carbonate, ROCO_2Na (as shown in Fig. 18a), similarly to the case of a LIB surface. However, one critical difference between the S.E.I. of NIBs and LIBs was revealed by XPS after etching the surface of hard carbon electrodes with Ar^+ in the same conditions: the intensity of the oxygen signal from the S.E.I. disappeared more rapidly in NIBs than in LIBs. Further differences were found in the *ex-situ* TOF-SIMS analysis, as the S.E.I. fingerprint in NIBs was skewed more toward inorganic compounds, while in LIBs it was mainly composed of organic compounds (as shown in Fig. 18b and 18c), indicating that these differences of S.E.I. composition on HC anodes are the most likely due to different reactivities of sodium and lithium.

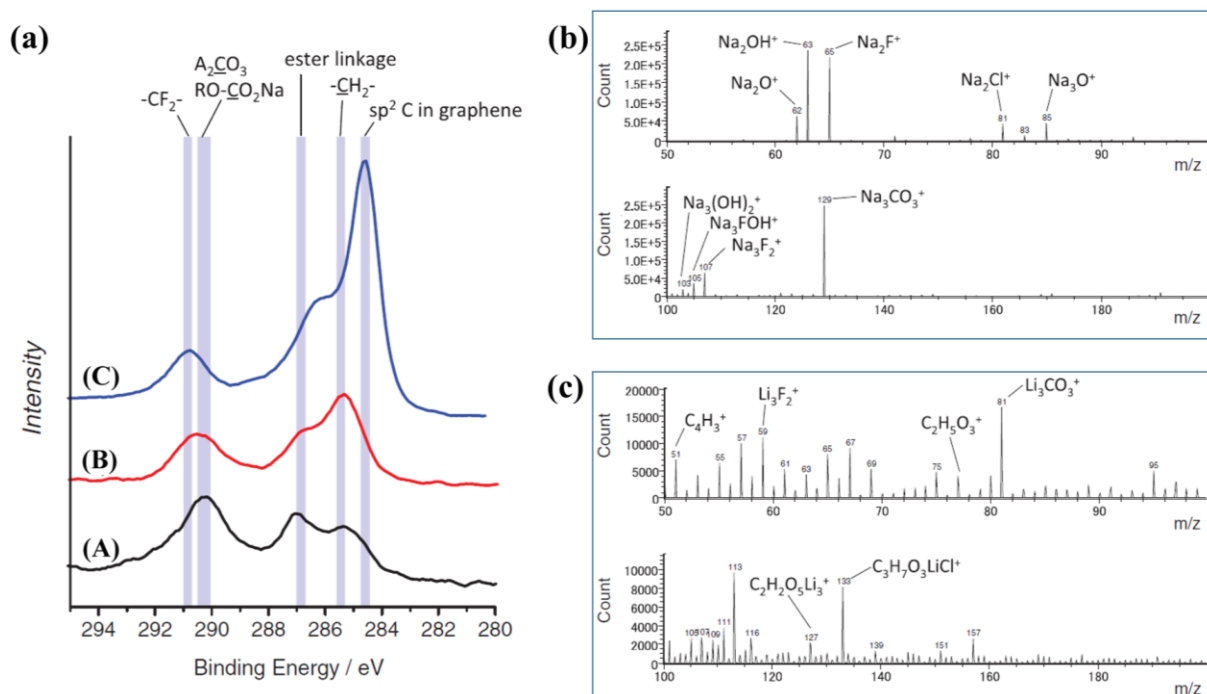


Fig. 18. (a) C1s XPS spectra of hard carbon (A) after sodium insertion/deinsertion (black curve), (B) after lithium insertion/deinsertion (red curve), and (C) in the pristine electrode (blue curve). TOF-SIMS positive ion spectra for the HC electrodes at the end of the first galvanostatic discharge/charge cycle in coin-type cells Li with (b) sodium or (c) lithium counter/reference electrodes [167].

Such differences in the S.E.I. layer formation were verified with a Fe_2O_3 electrode, where the Na-based S.E.I. layer is more homogenous than a Li-based S.E.I. [171]. In addition, the Na-based S.E.I. contains more carbonates and other $-\text{C}=\text{O}$ rich species and less long $-(\text{CH}_2)_x-$

hydrocarbon chains than those in Li-based S.E.I. [171]. To understand the disparity of Na-based S.E.I. layers, a fresh HC electrode was cycled in a series of Li/Na/Li environments, *i.e.*, with a Li counter electrode and a Li-based electrolyte, then with Na components, and finally it was cycled again with Li components (see Fig. 19a); the converse was done by cycling the HC electrode in successive Na/Li/Na environments (as shown in Fig. 19b) [172]. It was found that the S.E.I. formed in Na environments is inconsequential for cycling of a HC electrode with Li. However, the Li-based SEI layer is effective in controlling the Na-ions intercalation. According to these findings, it can be concluded that i) the capacity of a HC electrode for NIBs can effectively be tuned through the interplay of a Na/Li S.E.I. formation; ii) Na-based S.E.I.s are relatively porous, or more porous than Li-based ones at the very least, leading to a better capacity retention of Na-based S.E.I.s during long-term cycling.

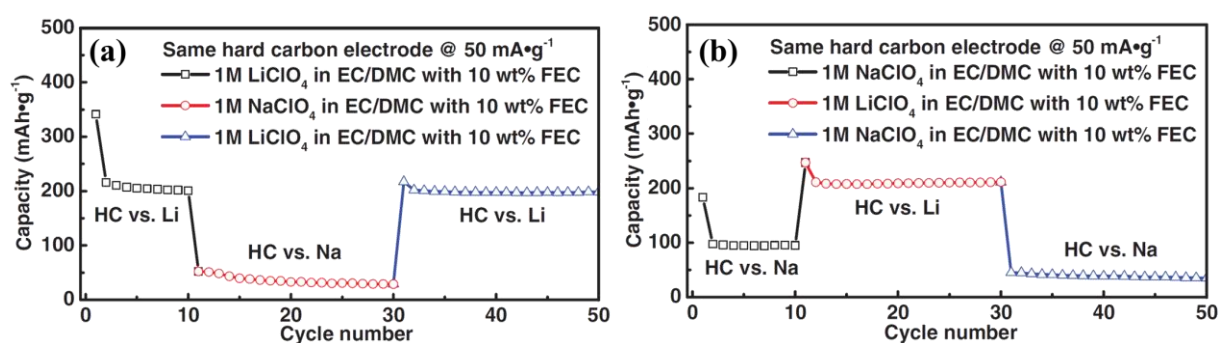


Fig. 19. Li/Na-ion insertion in hard carbon with a preformed SEI layer. (a) Electrochemical performance of the same hard-carbon electrode cycled subsequently in 1 mol L⁻¹ LiClO₄;EC/DMC with 10 wt% of FEC, 1 mol L⁻¹ NaClO₄;EC/DMC with 10 wt% of FEC and 1 mol L⁻¹ LiClO₄;EC/DMC with 10 wt% of FEC; (b) Electrochemical performance of the same hard-carbon electrode cycled subsequently in 1 mol L⁻¹ NaClO₄;EC/DMC with 10 wt% of FEC, in 1 mol L⁻¹ LiClO₄;EC/DMC with 10 wt% of FEC, and in 1 mol L⁻¹ NaClO₄;EC/DMC with 10 wt% of FEC [172].

In another study, colloidal probe microscopy revealed that the composition of the S.E.I. formed on the surface of a hard carbon electrode in a NIB is inhomogeneous, leading to heterogeneous physical and mechanical properties [173]; it demonstrates the need to devise a method leading to homogeneous S.E.I. formation, which can potentially lead to a more stable cycling. It was also shown that the S.E.I. layer on a Sn anode stemming from an electrolyte

solution in EC:DEC is primarily composed of Na₂O and Na₂CO₃, among which Na₂O has a much better ionic conductivity [174].

3. Na-ion capacitors (NICs)

The hybrid metal-ion capacitor was first proposed in 2001 by Amatucci [175], and subsequently, commercial hybrid LICs have been realized and mass-produced by JM Energy [176]. Since then, although many devices were successfully assembled, researchers are very concerned about the cost and future reserves of lithium, especially in large-scale energy devices and smart grid applications. Owing to the much wider distribution of sodium in the Earth crust (23,000 ppm) and its lower cost (ca. 3 \$ kg⁻¹ in 2021) in comparison to lithium (20 ppm, ca. 86 \$ kg⁻¹ in 2021) [177], Na-ion capacitors (NICs) would be an exciting alternative to LICs. Additionally, as aluminum does not form alloys with sodium at low potential, it is possible to replace copper current collectors with cheap and light aluminum current collectors, reducing the total mass and cost of the cells.

The advantages of a NIC vs. an EDLC can be easily understood by comparing the principles and galvanostatic charge/discharge profiles of EDLC and NIC cells. An EDLC consists of two porous carbon electrodes (generally made of activated carbon), which stores the energy owing to the reversible electrosorption of electrolyte ions at the electrode-electrolyte interface (see Fig. 20a). Hence, as it is an electrostatic surface storage, the amount of energy stored is relatively low, yet the power is very high. During the galvanostatic charge/discharge of an EDLC, the potential variations of the positive and negative electrodes demonstrate a triangular shape (Fig. 20b). NICs are composed of a sodium insertion negative electrode and an EDL-type positive electrode (Fig. 20c). During the galvanostatic charge/discharge of a NIC, the potential of the positive electrode varies linearly, while the low potential of the negative electrode is almost constant (Fig. 20d), what enhances the specific energy according to the classical formula (15) for capacitors.

$$E = \frac{1}{2} C (U_{\max}^2 - U_{\min}^2) \quad (15)$$

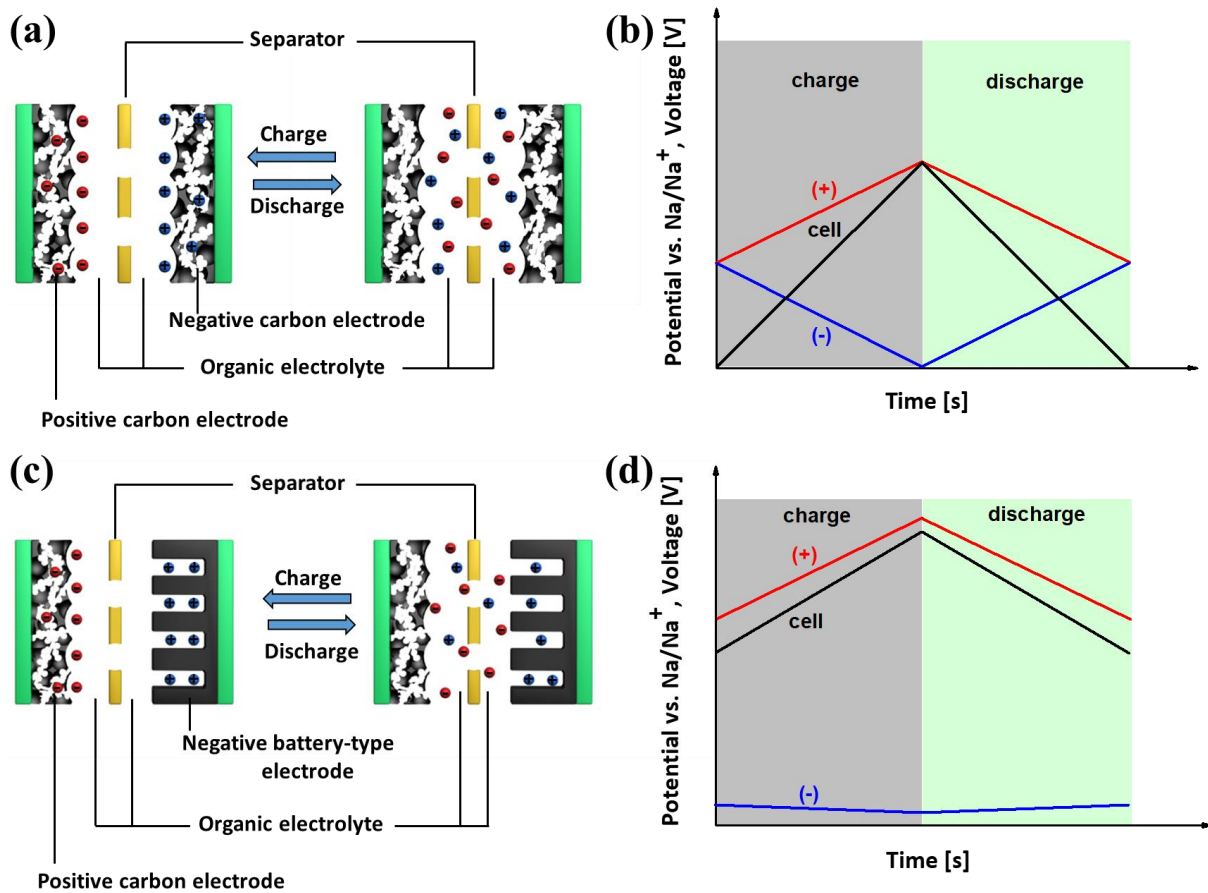


Fig. 20. Schematic representation of (a) an EDLC with activated carbon electrodes and (c) a NIC with a battery-type negative electrode and an activated carbon positive electrode. Charge/discharge profiles of (b) an EDLC and (d) a NIC where: red-potential of the positive electrode, blue-potential of the negative electrode and black-voltage of the cell.

To obtain the theoretical relation of capacitance and/or specific energy between a NIC and an EDLC (with the same electrolyte and same porous carbon for the positive electrode of the NIC and the two electrodes of the EDLC), it is assumed that the slope of the positive electrode potential is the same during the discharge of the two systems (Fig. 21). On the example of the data published in ref. [178], the voltage range (ΔU) during the discharge of the NIC and EDLC is from 3.8 V to 2.2 V and from 2.6 to 1.3 V, respectively. On these bases, and assuming that the potential of the negative electrode in the NIC is constant at 0.1 V vs. Na/Na⁺, the calculated ratio of the discharge capacity values, Q_{NIC} and Q_{EDLC} in Fig. 21, is expressed by the formula (16):

$$\frac{Q_{NIC}}{Q_{EDLC}} \approx 1.231 \quad (16)$$

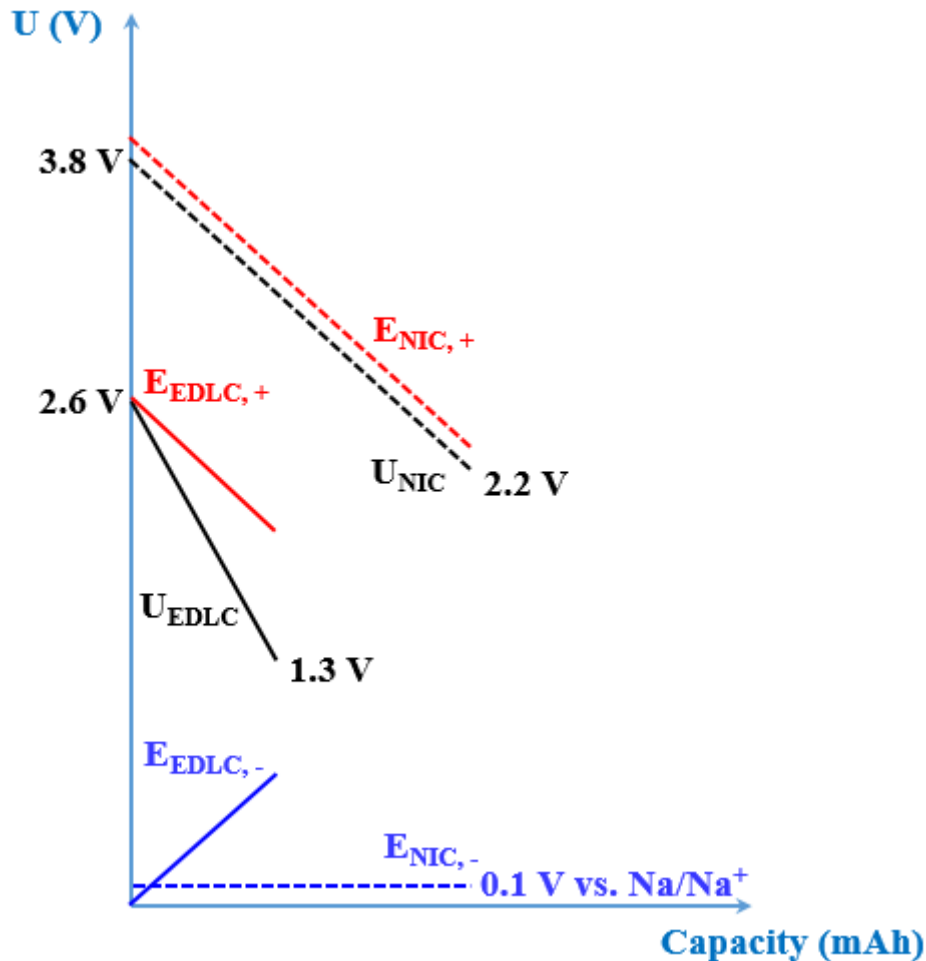


Fig. 21. Discharge profiles of an EDLC and a NIC. For the EDLC, the black, red and blue continuous lines represent the variations of the cell voltage, and potential of the positive and negative electrodes, respectively. For the NIC, the black, red and blue dashed lines represent the variations of the cell voltage, and potential of the positive and negative electrodes, respectively. The slope of the positive EDL electrode characteristics is the same for the NIC and the EDLC. In the chosen example, the potential of the negative electrode in the NIC is assumed to be constant at 0.1 V vs. Na/Na⁺; the NIC is discharged from 3.8 to 2.2 V and the EDLC from 2.6 to 1.3 V.

The expressions of the discharge capacity values, Q_{NIC} and Q_{EDLC} , are given by the equations (17) and (18), respectively:

$$Q_{NIC} = C_{NIC} \cdot \Delta U_{NIC} \quad (17)$$

$$Q_{EDLC} = C_{EDLC} \cdot \Delta U_{EDLC} \quad (18)$$

Then, by replacing Q_{NIC} and Q_{EDLC} by their expression in the formula (16), it comes:

$$\frac{Q_{NIC}}{Q_{EDLC}} \approx 1.231 = \frac{C_{NIC} \cdot \Delta U_{NIC}}{C_{EDLC} \cdot \Delta U_{EDLC}} \quad (19)$$

and by introducing the variation of the voltage values, ΔU_{NIC} and ΔU_{EDLC} , it gives:

$$\frac{C_{NIC}}{C_{EDLC}} \approx 2.0 \quad (20)$$

In this case, the output energy of the EDLC, E_{EDLC} , is given by application of the formula (15) where $U_{max} = 2.6$ V and $U_{min} = 1.3$ V = $U_{max}/2$:

$$E_{EDLC} = \frac{1}{2} C_{EDLC} (U_{max}^2 - U_{max}^2/4) = \frac{3}{8} C_{EDLC} \cdot U_{max}^2 = \frac{3}{8} C_{EDLC} \cdot 2.6^2 = 2.535 C_{EDLC}$$

In the case of the NIC, the output energy is:

$$E_{NIC} = \frac{1}{2} C_{NIC} (U_{max}^2 - U_{min}^2) = \frac{1}{2} C_{NIC} (3.8^2 - 2.2^2) = 4.8 C_{NIC}$$

Then, after taking into account the formula (20), it gives:

$$E_{NIC}/E_{EDLC} = 4.8/2.535 \cdot C_{NIC}/C_{EDLC} = 4.8/2.535 \cdot 2 = 3.8$$

Hence, from this calculation, it can be concluded that the output specific energy is about 4 times higher for a NIC than an EDLC, confirming the advantages of hybridization. To the best of our knowledge, in general, the positive electrode of NICs is made of active materials used in EDLCs, and the negative electrode is made of anodic materials used in NIBs, while the electrolyte is also the same as in a NIB. Though providing moderate advantages, some other components have also been specifically proposed for their application in NICs; information can be found in a number of review papers as refs. [179, 180-183]. However, in a NIB, the S.E.I. can be formed during the first charge using a part of sodium contained in the positive electrode; at the same time, another part of sodium is inserted in the anodic material. In the case of NICs, where the positive electrode is made of *e.g.*, activated carbon, there is no sodium source for the anodic materials as HC, alloys and conversion materials. Therefore, presodiation strategies of NICs must be developed.

4. Presodiation of anodic materials

The previous section explained that most of the anodic hosts which could be implemented in NICs do not contain inserted sodium. Therefore, these materials must be presodiated either by using a metallic sodium auxiliary electrode or by adding sacrificial sodiated materials in the positive EDL electrode.

4.1 Presodiation from a metallic sodium auxiliary electrode

In most of the published research papers concerning NICs, the presodiation is realized in a separate cell where the host material is used as a working electrode vs. a sodium counter/reference electrode; to perform the sodiation, the working electrode is discharged with a low current [178]. Then, the presodiated material must be extracted from the cell under a moisture- and oxygen-free atmosphere and mounted as the anode in another cell with a positive EDL electrode; this reassembling step increases the expenditure and reduces the possibility to use this strategy in a commercial way. To circumvent this cell reassembly, one option is to use a single cell constituted of three electrodes (positive, negative and sodium auxiliary electrode) (see Fig. 22) [184]. A dedicated discharging step between the host material and the auxiliary electrode forms the S.E.I. and sodiates the host material to the desired level without the need for cell reconstruction.

Nonetheless, this presodiation method enabled by an auxiliary electrode requires additional cell components, *e.g.*, one additional separator and one additional current collector for the auxiliary electrode, which lead to reducing the specific energy of such constructed NICs. Besides, compared with lithium, the higher reactivity of sodium may reduce the safety of NICs. Therefore, it is desirable to develop an alternative presodiation route that may be less costly and dangerous, without reducing the specific energy of cells. Such an approach would also bring an opportunity for a faster commercialization for presodiation of NICs.

4.2 Sacrificial materials in positive electrodes

Most recently, sacrificial materials (also called metal-containing additives) have gathered great attention because of their relatively simple implementation into state-of-the-art industrial cell manufacturing procedures. Sacrificial materials have already been implemented in NIBs and NICs [185, 186], and also in LICs [187, 188]. In general, the

Strategies for designing high performance sodium-ion capacitors

sacrificial materials for NICs should possess four different vital features to be regarded as a beneficial presodiation agent:

- they should exhibit a high irreversible capacity to reduce their amount, and consequently fingerprint in the positive EDL electrode, after their electrochemical oxidation;
- their oxidation, *i.e.*, the sodium extraction, should occur at a sufficiently low potential to avoid the electrolyte oxidation;
- they should be compatible with standard industrial processing, which includes compatibility with current positive electrode active materials, solvents, binders, conductive agents, electrolytes and also handling in the ambient atmosphere;
- their oxidation products after sodium extraction should be electrochemically stable, and should also be thermally, chemically and mechanically stable, and should not be harmful to the device.

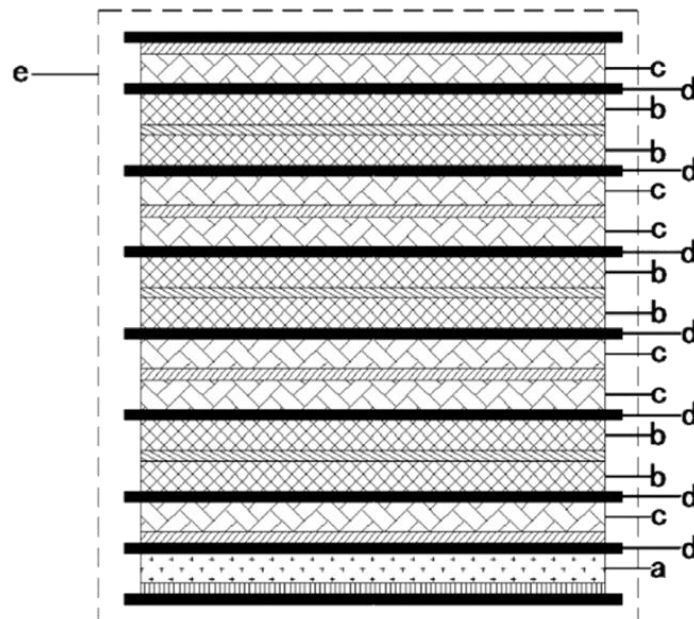


Fig. 22. A schematic diagram of the laminated-type NIC configuration: a, b, c, d and e are the sodium metal for presodiation, positive electrode, anode, separator and outer package, respectively [184].

Generally, the sacrificial material is incorporated into the positive electrode and irreversibly oxidized during charging by applying a high potential to the positive electrode;

simultaneous to this oxidation reaction, the Na^+ ions released from the additive are transferred for presodiating the negative electrode to a particular chemical state [187, 188]. The process is schematically depicted in Fig. 23 for the particular case of a positive electrode of a NIC [188].

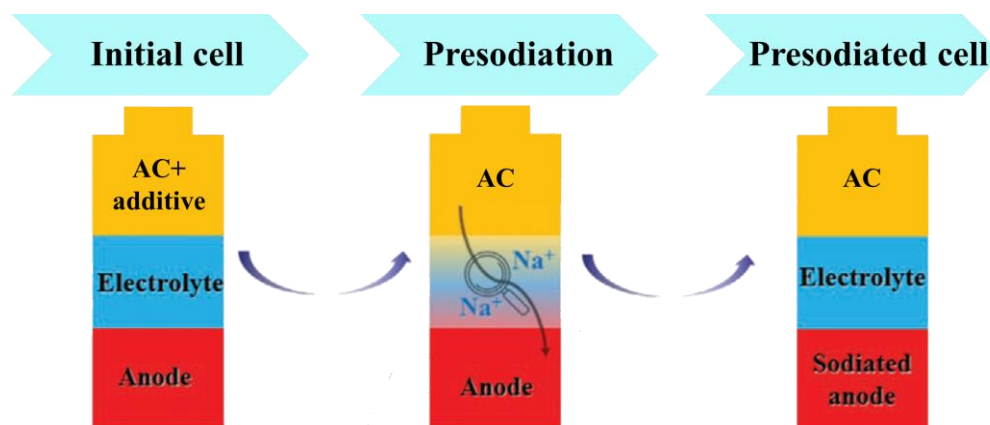


Fig. 23. Illustration of the use of a sacrificial presodiation material added in the positive AC electrode of a NIC. The extra sodiated material introduced in the positive electrode is irreversibly oxidized to release Na^+ during the first sodium extraction [188].

Various sacrificial materials have been suggested for this purpose (Table 1). For example, NaN_3 is stable in air and displays a low oxidation potential of 3.5 V vs. Na/Na^+ [189, 190], with a theoretical capacity of 412 mAh g^{-1} , giving only N_2 as an oxidation product. Although these properties might indicate it as a desirable sacrificial compound, the literature mentions the toxicity and explosiveness of NaN_3 [191]. Na_2S with a high theoretical capacity of 687 mAh g^{-1} has been successfully applied in Na-S batteries [192-194]. NaNH_2 and NaBH_2 were applied as sacrificial materials in NICs [195, 196], though their sensitivity to moisture is a serious disadvantage; indeed, all steps of manufacturing, including even the preparation of electrodes, require the controlled atmosphere of a glove-box. The oxidation of Na_2CO_3 [197] releases dioxygen as one of the decomposition products which parasitically may react with a sodiated negative electrode; in the case of both EDTA-4Na [198] and DTPA-5Na [199], the decomposition products are dioxygen and dihydrogen, and also H_2O is an intermediate product which may reduce the ESW of the electrolyte [199]. Hence, all these sacrificial materials have some disadvantages, which preclude their use for practical applications.

Strategies for designing high performance sodium-ion capacitors

Table 1. Characteristics of sacrificial materials satisfying most of the required criteria for their application in sodium-ion systems.

Sacrificial material	Targeted application	Oxidation potential (V vs. Na/Na ⁺)	Theoretical capacity (mAh g ⁻¹)	Measured irreversible capacity (mAh g ⁻¹)	Oxidation products	Ref.
NaN ₃	NIB	ca. 3.5	412	ca. 280	N ₂	189
Na ₂ C ₄ O ₄	NIB	ca. 3.6	339	ca. 186	C, CO ₂	191
NaNH ₂	NIC	ca. 3.8	687	ca. 680	N ₂ , H ₂ , N ₂ H ₄	195
NaBH ₄	NIC	ca. 2.4	708	ca. 700	B, H ₂	196
Na ₂ CO ₃	NIB	ca. 4.0	506	ca. 253	CO ₂ , O ₂	197
EDTA-4Na	NIB	ca. 3.7	237	ca. 300	C ₃ N, CO, H ₂ O, H ₂ , O ₂	198
DTPA-5Na	NIB	ca. 3.9	266	ca. 300	C ₃ N, CO, H ₂ O, H ₂ , O ₂	199
Na ₂ NiO ₂	NIB	from 2.0 to 3.6	236	ca. 189	NaNiO ₂	200
NaCrO ₂	NIB	from 3.0 to 4.2	251	ca. 229	Na _{0.06} CrO ₂	201
Na ₂ C ₂ O ₄	NIB	ca. 4.3	400	ca. 389	CO ₂	206
Na ₂ C ₆ O ₆	NIC	ca. 4.5	250	ca. 150	C ₆ O ₆	207

Na₂NiO₂ can be irreversibly oxidized into NaNiO₂ [200], which remains as a dead mass in the positive electrolyte; however, Na₂NiO₂ is not decomposed in a dry air environment, what is an advantage for the manufacturing and manipulation of electrodes. NaCrO₂ is irreversibly oxidized from 3.0 V to 4.2 V vs. Na/Na⁺ [201] and has been used as a sacrificial material to compensate the S.E.I. formation in the Na₃(VO)₂(PO₄)₂F//HC NIB. The capacity retention after 50 cycles was increased from 21.4% Na₃(VO)₂(PO₄)₂F//HC NIB to 80% after incorporating NaCrO₂ in the cathode. However, the remaining Na_{0.06}CrO₂ after decomposition reaction contributes to a dead mass in the cell.

Recently, organic sacrificial materials started to attract scientific attention, because they are stable in the air [202], and their oxidation products are CO and CO₂ [198, 199]. CO is not stable at room temperature, and according to the exothermic Boudouard reaction, it can be disproportionated into carbon and CO₂ [202]. More importantly, CO₂ might form an efficient Na₂CO₃ passivation film on the surface of the negative electrode and chemically stabilizes the S.E.I. formation [203-205]. In addition, organic sacrificial materials are made from abundant and environmentally friendly precursors.

For example, $\text{Na}_2\text{C}_2\text{O}_4$ displays a relatively high theoretical capacity (ca. 400 mAh g^{-1}), yet its high oxidation potential of ca. $4.3 \text{ V vs. Na/Na}^+$ precludes its use in electrochemical energy storage systems [206], as the sodium extraction may be accompanied by a possible oxidation of the electrolyte. $\text{Na}_2\text{C}_6\text{O}_6$ as a sodium source also exhibits a very high extraction potential of ca. $4.5 \text{ V vs. Na/Na}^+$ [207]. However, $\text{Na}_2\text{C}_4\text{O}_4$ with a theoretical capacity of 339 mAh g^{-1} , and an oxidation potential ca. $3.6 \text{ V vs. Na/Na}^+$ (below the oxidation potential of the electrolyte), appears very promising [185, 191, 208]. However, the reported irreversible oxidation capacity values of 186 mAh g^{-1} , 256 mAh g^{-1} , and 275 mAh g^{-1} [185, 191, 208] are much lower than the theoretical value of 339 mAh g^{-1} , suggesting that the performance of this material could be optimized by an appropriate design of electrodes.

Overall, sacrificial materials are able to compensate for the active sodium loss of negative electrode materials and are an excellent alternative for their presodiation. Nevertheless, more research has to focus on the effects of residues in the positive EDL electrode of NICs and gas production during the decomposition of the presodiation agent. A significant disadvantage of most sacrificial materials is the additional mass remaining in the positive electrode if they do not fully decompose upon their oxidation.

5. Conclusion

In the last few years, NICs have emerged as new energy storage cells utilizing the combination of battery-type and capacitive electrodes. As it was shown in this bibliography review, well-performing activated carbons (ACs) were developed for EDLCs and are commercially available at a reasonable price; they can also be implemented in NICs. Hence, as far as electrode materials are concerned, one of the main problems for designing high performance NICs is the selection of an appropriate anodic material. Herein, we have shown that HCs, with their low sodium insertion/deinsertion potential, allow the voltage range of NICs to be extended, certainly providing a dramatic improvement in specific energy, yet at the expense of sodium plating during cycling and possible thermal runaway. The conversion and alloying materials represent a better alternative to avoid any possible Na-metal plating/stripping reaction under high current rates. However, the slightly elevated potential and limited reversibility of the conversion materials certainly preclude the realization of high specific energy sodium-ion systems. Sn_4P_3 is one of the essential Na^+ storage hosts from the NIB point of view, owing to its relatively lower working potential (ca. $0.3 \text{ V vs. Na/Na}^+$),

though being sufficiently high to avoid sodium plating. Unfortunately, Sn_4P_3 has the same issues (large volume expansion and pulverization of the electrode material particles during sodium insertion) as other alloys. The combination of Sn_4P_3 with carbon materials has been shown an effective strategy to improve the reversible Na^+ storage performance. For these reasons, we have selected Sn_4P_3 as our anodic host to realize NICs, and a part of our work has also been dedicated to realizing $\text{Sn}_4\text{P}_3/\text{HC}$ electrodes (with spherical HC particles) to buffer the volumetric variations of Sn_4P_3 .

The realization of NICs requires first to presodiate the host anodic material. The concept of NIC with sacrificial sodium source incorporated together with AC in the positive EDL electrode seems the most interesting to simplify the cell construction and thereof reduce the cost of the device. In this literature review, we have shown that none of the to-date investigated sacrificial materials satisfies the four required criteria. Therefore, in this dissertation, we have selected to investigate the oxidation properties (and also properties of the resulting NICs) of two sacrificial materials presenting a good compromise: i) Na_2S , though being sensitive to moisture, displays a high irreversible capacity which allows its content in the positive electrode to be reduced; ii) $\text{Na}_2\text{C}_4\text{O}_4$, though having a moderate irreversible capacity, is stable in air and can be oxidized at a relatively low potential. In the case of the latter, it will be even demonstrated that the decomposition products profitably enhance the NIC performance.

Finally, to the best of our knowledge, the balancing of electrodes (mass and/or capacity) is almost totally ignored in the literature on NICs and very seldom considered in the case of LICs. The last part of the manuscript will be dedicated to addressing this issue.

Chapter II

High performance hybrid sodium-ion capacitor with tin phosphide used as battery-type negative electrode

1. Summary of the publication

As explained in the bibliography review of this dissertation (chapter I), the specific energy of hybrid sodium-ion capacitors (NICs) is largely dependent of the maximum voltage reached by the cells. Therefore, it is necessary to implement anodic materials with the lowest redox potential, while avoiding sodium plating during cycling at high current, what excludes any hard carbon. Therefore, the objective of the study described in the publication “High performance hybrid sodium-ion capacitor with tin phosphide used as battery-type negative electrode” was to develop a cost-affordable anode material displaying a low irreversible capacity and a relatively high reversible capacity, as well as the lowest sodium insertion potential, to allow sodium plating at high current density to be avoided.

Among the materials which can be implemented as anodic hosts in Na-ion systems, it has been shown that sodium forms rich alloys with tin-based compounds, yielding a high theoretical capacity from ca. 850 mAh g⁻¹ for Sn to 1130 mAh g⁻¹ for Sn₄P₃ [109, 159]. Hence, a low mass content of Sn-based materials can be utilized in the construction of NICs, what is beneficial for the specific capacitance and energy outputs of the system. Consequently, in the attached publication, the anodic material of choice was Sn₄P₃, and optimal conditions were defined to obtain it by high-energy mechanical milling of red phosphorus with micrometric tin (Fig. 24a). The diffractogram of the as-synthesized alloy is in line with the literature data and corresponds to the rhombohedral phase belonging to the *R3m* space group (ICDD card No. 73–1820). The thereof obtained Sn₄P₃ electrode displays the lowest irreversible capacity (83 mAh g⁻¹ at a low limit potential of 0.1 V vs. Na/Na⁺) today reported in the Na-ion literature [109, 159, 209-212]. Such favourable performance was achieved owing to the optimization of the active material synthesis parameters, *e.g.*, by reducing the mixing time to 4 h instead of 6 h in ref. [159] or 30 h in ref. [209] and by adjusting the balls to powder mass ratio to 24. Considering the evolution of reversible and irreversible capacity of Sn₄P₃ electrodes during galvanostatic cycling at 0.025 A g⁻¹ down to selected low insertion potentials, a stable life span with constant irreversible capacity was observed only if the low limit potential is equal or higher than 0.1 V vs. Na/Na⁺. The further sodiation of Sn₄P₃ electrodes down to 0.01 V vs. Na/Na⁺ causes a large volumetric expansion and the pulverization of the active material, leading to the electrical disconnection of the particles and deterioration of the reversible capacity. Since the irreversible capacity values after the first sodium insertion were similar for cut-off potentials from 0.1 to 0.2 V vs. Na/Na⁺, the optimal

Strategies for designing high performance sodium-ion capacitors

low limit potential of 0.1 vs. Na/Na^+ was selected, as it gave the lowest irreversible to reversible capacity ratio.

Based on the above-mentioned findings, Sn_4P_3 was presodiated down to 0.1 V vs. Na/Na^+ in a separate cell (Fig. 24b) to give $\text{Na}_x\text{Sn}_4\text{P}_3$, with $x = 9$. Then AC// $\text{Na}_9\text{Sn}_4\text{P}_3$ NICs were assembled with an EDL positive electrode made of activated carbon (AC) and the previously prepared $\text{Na}_9\text{Sn}_4\text{P}_3$ anode, using a separator soaked in NaClO_4 (EC:PC, vol. ratio = 1:1) electrolyte and a sodium pin as reference (Fig. 24c); according to literature data [213, 214], we selected equal masses of AC and Sn_4P_3 .

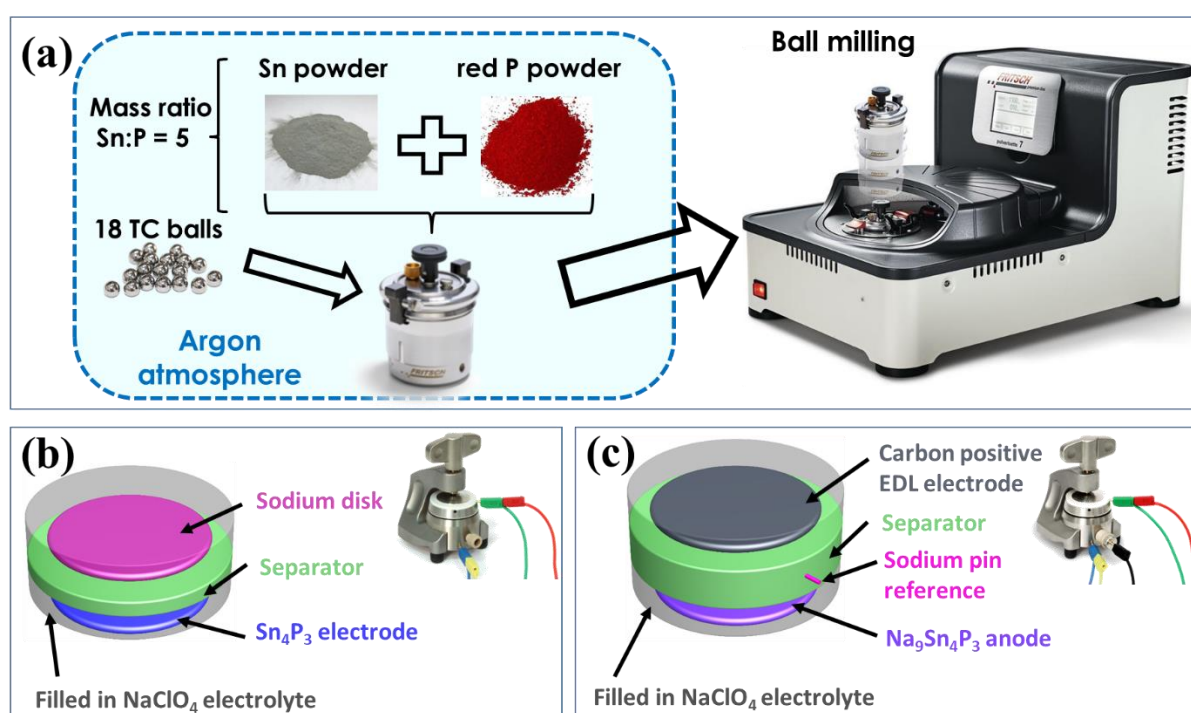


Fig. 24. (a) Synthesis of Sn_4P_3 powder using a planetary ball mill (Pulverisette 7 premium line, Fritsch [215]); (b) Scheme of the cell used for the presodiation of Sn_4P_3 as working electrode, while using a sodium disk as counter/reference electrode; (c) Scheme of a NIC with a $\text{Na}_9\text{Sn}_4\text{P}_3$ anode, a carbon positive EDL electrode and a sodium pin as the reference electrode to monitor the potential of the individual electrodes during cycling of the NICs. The electrochemical cells were based on using ECC-REF (EI-cell) assemblies.

The life span and specific energy of the cells was determined by cycling at 0.2 A g^{-1} (per total mass of the electrodes) in the voltage range from 2.2 V to 3.8 V, and the Ragone plots were obtained by discharging the NICs from 3.8 V to 2.2 V at a constant power. The

Strategies for designing high performance sodium-ion capacitors

AC//Na₉Sn₄P₃ NIC displayed a high specific energy of 39 Wh kg⁻¹ (calculated per total mass of electrodes), as well as an excellent life span, with a capacitance retention of 94% after 6,500 cycles, showing a remarkable advantage over other NICs reported in the literature. Since the presented NIC is realized in two separate steps, the next chapters of the dissertation are dedicated to improving its realization and performance by implementing sacrificial materials used as a potential source of sodium; a special attention will also be paid to the balancing of electrodes.

Chapter III

Na₂S sacrificial cathodic material for high performance sodium-ion capacitors

1. Summary of the publication

The concept of the attached publication entitled “*Na₂S sacrificial cathodic material for high performance sodium-ion capacitors*”, is to simplify the construction of NICs by applying a composite positive electrode containing a sacrificial sodium source in addition to the activated carbon (AC) EDL material. Sodium sulphide, Na₂S, owing to its high theoretical capacity of 687 mAh g⁻¹ and low irreversible sodium extraction potential ca. 2.2 V vs. Na/Na⁺ in electrolytes such as 1.5 mol L⁻¹ NaClO₄ and 0.3 mol L⁻¹ NaNO₃ in tetraethylene glycol dimethyl ether (TEGDME) [192] or 1.5 mol L⁻¹ NaClO₄ and 0.2 mol L⁻¹ NaNO₃ in TEGDME [193], appears as a sacrificial material of choice. For the preparation of the positive electrode, two industrial activated carbons differing in their porous texture were selected – the microporous Maxsorb (Kansai Coke and Chemicals), and the micro/mesoporous BP2000 (Cabot). Potential window opening measurements by cyclic voltammetry, while applying the stability limit criterion proposed by Kötzt *et al.* [216], allowed maximum safe potential values of 4.1 V and 4.2 V vs. Na/Na⁺ to be established for the Maxsorb and BP2000 electrodes, respectively, when using 1 mol L⁻¹ NaClO₄ in EC:PC (vol. ratio 1:1) as an electrolyte. Taking into consideration these determined potential limits, the irreversibility of sodium extraction from Na₂S (*i.e.*, irreversibility of Na₂S oxidation) from Na₂S-Maxsorb and Na₂S-BP2000 composite electrodes was confirmed by cyclic voltammetry (CV) and galvanostatic charge/discharge vs. a sodium counter/reference electrode. The full extraction of sodium was confirmed by the energy dispersive spectroscopy (EDS) analysis of the polarized electrodes, which did not detect any trace of sodium. However, some traces of sulphur ca. 3.4 wt% were revealed, suggesting that residues, probably in the form of polysulfides, are still present in the oxidized electrodes. Nonetheless, the nitrogen adsorption/desorption analyses of the AC-Na₂S composite electrodes show that the initially partly blocked porosity of the ACs (by the presence of Na₂S) is almost totally restored after the electrochemical oxidation.

Thereafter, AC-Na₂S//Sn₄P₃ cells were constructed in 1 mol L⁻¹ NaClO₄ in EC:PC (1:1 vol. ratio) electrolyte, incorporating Sn₄P₃ as a negative electrode (prepared according to the description included in the previous chapter) and Na₂S as a sacrificial material in the EDL positive AC electrodes. During the presodiation step (Fig. 25a), Na₂S was oxidized to irreversibly extract the sodium ions, which were then transferred to the Sn₄P₃ host. It is worth noting that, as the Na₂S amount in the positive composite electrodes can be reduced owing to its high irreversible capacity, the risks of mechanical degradation of these electrodes during

the presodiation step are also significantly reduced. Subsequently, the resulting AC//Na_xSn₄P₃ NICs constituted of an EDL positive electrode and sodiated Sn₄P₃ anode (Fig. 25b) were cycled at 0.18 A g⁻¹ (per total mass of the electrodes) in the voltage range from 2.0 V to 3.8 V, and demonstrated the triangular characteristics of a capacitor (black continuous line in Fig. 25b).

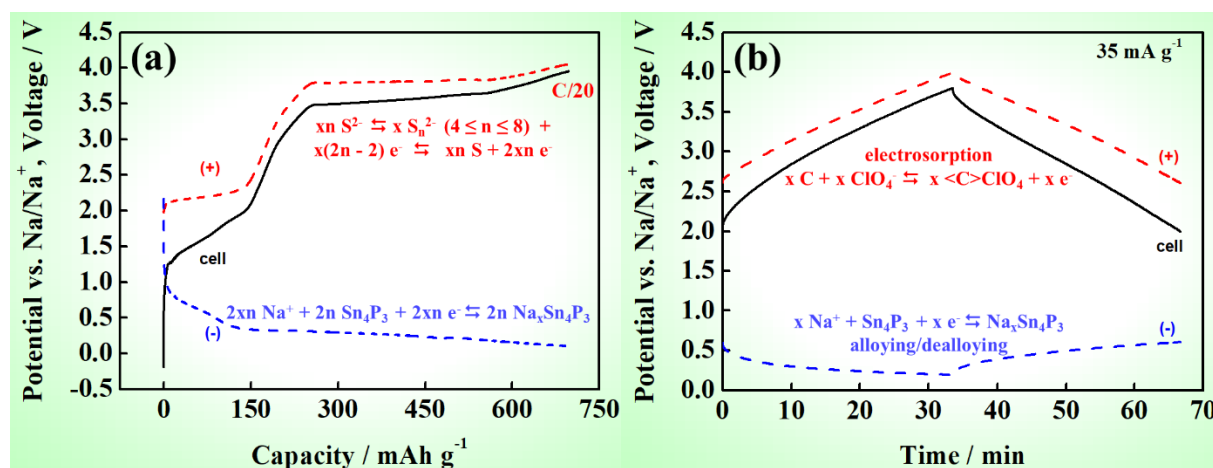


Fig. 25. (a) Galvanostatic sodium transfer from a Maxsorb-Na₂S electrode to Sn₄P₃ at C/20 (where C corresponds to the theoretical capacity of Na₂S, *i.e.*, 687 mAh g⁻¹), using a Maxsorb-Na₂S//Sn₄P₃ cell. The potential was limited to 4.1 V vs. Na/Na⁺ or 0.1 V vs. Na/Na⁺ for the positive or negative electrodes, respectively. (b) GCPL characteristics of the Maxsorb//Na_xSn₄P₃ NIC at a current density of 35 mA g⁻¹ (per total mass of electrodes) in the voltage range from 2.0 V to 3.8 V. The black continuous, red dashed and blue dotted lines represent the cell voltage, and the potential of the positive and negative electrodes, respectively. The electrolyte was 1 mol L⁻¹ NaClO₄ in EC/PC (vol ratio 1:1) and a sodium pin was used as the reference electrode. All the electrochemical tests were done in ECC-REF (E1-cell).

All the NICs exhibited a stable life span with a discharge capacitance retention of 97% and 93% after 3,500 cycles for Maxsorb//Na₁₅Sn₄P₃ and BP2000//Na₁₅Sn₄P₃, respectively, proving that Na₂S can be successfully used as a sacrificial material. Nonetheless, the system implementing Maxsorb displayed a higher capacitance and specific energy (C=33 F g⁻¹ and E=48 Wh kg⁻¹ at 1 kW kg⁻¹) than the NIC with BP2000 (C=25 F g⁻¹ and E=35 Wh kg⁻¹ at 1

kW kg⁻¹), confirming that the capacitance of hybrid cells depends strongly on the type of porous carbon electrode.

Certainly, the presented solution is a competitive technology to hybrid capacitors realized in two steps in terms of technical performance and cost. However, due to the residues which remain in the EDL electrode after the oxidation of Na₂S, as well as the sensitivity of the latter to moisture imposing the preparation of electrodes in a controlled inert atmosphere, further attempts to identify a more adapted sacrificial material for NICs are presented in the next chapter.

Chapter IV

Advantageous carbon deposition during the irreversible electrochemical oxidation of $\text{Na}_2\text{C}_4\text{O}_4$ used as a presodiation source for the anode of sodium-ion systems

1. Summary of the publication

According to the previous chapter, Na_2S can be successfully used as a sacrificial material for the presodiation of Sn_4P_3 . However, its sensitivity to moisture complicates the preparation of electrodes, which must be realized in the air and moisture-free atmosphere of a glove box. In addition, the residual sulfur remaining after the oxidation of AC- Na_2S electrodes might partly block their porosity and be also the cause of detrimental side effects as self-discharge. Hence, it is essential to find new possibilities fulfilling the criteria of an ideal sacrificial material. Therefore, the aim of chapter IV with the attached publication entitled “*Advantageous carbon deposition during the irreversible electrochemical oxidation of $\text{Na}_2\text{C}_4\text{O}_4$ used as a presodiation source for the anode of sodium-ion systems*” is to better identify the oxidation products of $\text{Na}_2\text{C}_4\text{O}_4$ and to incorporate it in NICs for the presodiation of the Sn_4P_3 anodic material; it is noteworthy that, according to the literature [185, 191, 208], the oxidation products of $\text{C}_4\text{O}_4^{2-}$, *i.e.*, carbon (supposed to be produced, yet not experimentally characterized in ref. [185, 191, 208]) and CO_2 should not perturb the performance of the obtained NICs.

To get rid of any undesirable phenomenon related to the oxidation of the carbon surface, the maximum safe potential of the electrolyte is first determined by the S-method on electrodes made of the YP80F carbon; in other words, all the further investigations involving this carbon will be realized at potentials lower than the determined value of 4.1 V vs. Na/Na^+ . The irreversibility of sodium extraction from C65- $\text{Na}_2\text{C}_4\text{O}_4$ electrodes is confirmed by CV and galvanostatic charge from OCP to 4.1 V vs. Na/Na^+ , revealing an irreversible capacity of 342 mAh g^{-1} , which is in line with the theoretical value of 339 mAh g^{-1} . The gases detected by using *operando* electrochemical mass spectrometry during the galvanostatic oxidation of the C65- $\text{Na}_2\text{C}_4\text{O}_4$ electrode are CO and CO_2 . As the measured mass of the oxidized electrode is higher than the calculated one in the hypothesis of a complete elimination of $\text{Na}_2\text{C}_4\text{O}_4$ from the electrode, it suggests that the $\text{C}_4\text{O}_4^{2-}$ anion is oxidized to give CO, which is further disproportionated to give CO_2 together with a carbon deposit.

To verify this assumption about carbon, pristine YP80F, fresh YP80F- $\text{Na}_2\text{C}_4\text{O}_4$ and oxidized YP80F- $\text{Na}_2\text{C}_4\text{O}_4$ electrodes are analysed by nitrogen adsorption/desorption at 77 K, confirming that the porosity of YP80F is partly blocked after the oxidation of $\text{Na}_2\text{C}_4\text{O}_4$. Interestingly, the mesopore volume of the oxidized YP80F- $\text{Na}_2\text{C}_4\text{O}_4$ electrode is higher than for YP80F, and a new peak with its maximum ca. 13 nm appears in the pore size distribution,

revealing the presence of interparticle mesopores as *e.g.*, found in carbon blacks. To characterize the fingerprint of deposited carbon, the Raman spectra of the pristine YP80F and oxidized YP80F- $\text{Na}_2\text{C}_4\text{O}_4$ electrodes are recorded and compared to the SC2A carbon black as well as an oxidized YP80F- NaN_3 electrode, which should liberate only N_2 during the oxidation process. The position of the G1 and G2 peaks remains unchanged for the YP80F and oxidized YP80F- $\text{Na}_2\text{C}_4\text{O}_4$ electrode, whereas the D1 peak is upshifted from 1330 to 1345 cm^{-1} and the D2 one from 1224 to 1245 cm^{-1} , what can be connected to the suggested carbon deposition [217]. Remarkably, the G1, G2, D1, D2 peaks of the SC2A carbon black and oxidized YP80F- $\text{Na}_2\text{C}_4\text{O}_4$ electrode are located at the same positions. Additionally, the seven-fold increase of the electrical conductivity of the oxidized YP80F- $\text{Na}_2\text{C}_4\text{O}_4$, in comparison to the pristine YP80F electrode, is an additional evidence confirming the carbon deposition. From the above, it can be concluded that the electrochemical oxidation of a YP80F- $\text{Na}_2\text{C}_4\text{O}_4$ electrode leads to the formation of CO, which is further partly disproportionated into CO_2 and carbon [202]; the YP80F electrode is blended by carbon which enhances its conductivity, what is extremely profitable on the point of view of a capacitor application.

Subsequently, a cell is built with a YP80F- $\text{Na}_2\text{C}_4\text{O}_4$ positive electrode together with a Sn_4P_3 anodic host, using the 1 mol L^{-1} NaClO_4 in EC:PC electrolyte and a metallic sodium pin as a reference electrode. As in the previous chapter, the first step is the NIC's realization by the electrochemical oxidation of $\text{Na}_2\text{C}_4\text{O}_4$ with simultaneous sodium transfer to the Sn_4P_3 anodic host (as shown in Fig. 26). The obtained YP80F// $\text{Na}_{15}\text{Sn}_4\text{P}_3$ NIC is cycled at 0.18 A g^{-1} (per total mass of the electrodes) in the voltage range from 2.0 V to 3.8 V, demonstrating an excellent life span with a capacitance retention of 94 % after 11,000 cycles, much better than for the NIC presented in chapter II, where Sn_4P_3 was sodiated in a separate cell (the capacitance retention of 94% was obtained after 6,500 cycles). Such a remarkable life span of the YP80F// $\text{Na}_x\text{Sn}_4\text{P}_3$ NIC is attributed to the CO_2 oxidation product of the $\text{C}_4\text{O}_4^{2-}$ anion, which enables to form a Na_2CO_3 film passivating very efficiently the surface of the $\text{Na}_{15}\text{Sn}_4\text{P}_3$ anode. The relevant evidence for the presence of Na_2CO_3 is found by a characteristic peak at 1514 cm^{-1} [203, 204] in the infrared spectrum of the Sn_4P_3 electrode obtained after the oxidative sodium transfer from $\text{Na}_2\text{C}_4\text{O}_4$. Hence, it can be concluded that $\text{Na}_2\text{C}_4\text{O}_4$ is an easy to handle sacrificial material, which facilitates the production of electrodes and enables to realize sodium-ion systems of significantly enhanced performance in one step.

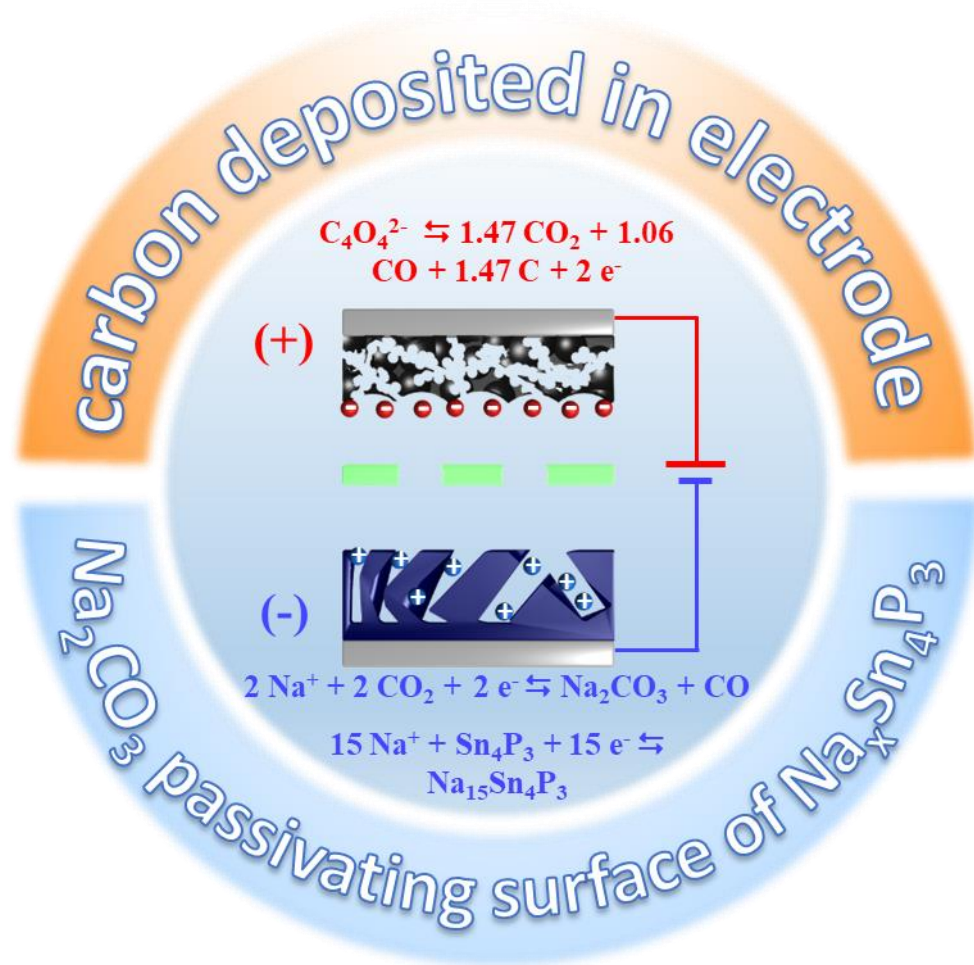


Fig. 26. Scheme representing the presodiation of the Sn_4P_3 electrode (represented in dark blue) by oxidation of the AC- $\text{Na}_2\text{C}_4\text{O}_4$ electrode (represented in black); Na^+ and ClO_4^- are shown as blue and red balls, respectively.

Chapter V

A strategy for designing more durable sodium-ion capacitors with optimized output energy

1. Summary of the publication

As it was mentioned in the bibliography part of the thesis (chapter I), to maximize the life span of NICs, it is crucial to develop anodic materials able to work under high current loads. Hence, the aim of the last chapter (together with the attached publication submitted to Energy Environmental Science) entitled “*A strategy for designing more durable sodium-ion capacitors with optimized output energy*” was to optimize both the Sn₄P₃-based anodic material and the capacity ratio, Q₋/Q₊, between the negative and positive electrodes of the NIC.

To absorb the volumetric variations of the negative electrode, HCG/Sn₄P₃ composites were prepared by ball-milling mixing of Sn₄P₃ with spherical hydrothermal hard carbon (HCG) particles specially prepared by hydrothermal carbonization followed by annealing at 1000°C. As the low presodiation potential (E_{p-}) of the Sn₄P₃-based electrodes dramatically influences their stability during cycling, we measured the height changes of HCG/Sn₄P₃ and Sn₄P₃-based electrodes by *operando* electrochemical dilatometry down to selected potentials E_{p-} of 0.28, 0.22 and 0.10 V vs. Na/Na⁺, using a cell where metallic sodium was the reference/counter electrode. As it is known from the literature [218] that the height change of a HCG electrode is negligible during sodium insertion [218], a theoretical value of relative height change was calculated for HCG/Sn₄P₃ at each E_{p-}, by taking into account the values of height change measured on the Sn₄P₃ electrode and applying the rule of mixtures. We found that the calculated values of height change for the HCG/Sn₄P₃ electrode are noticeably higher than the measured ones for any E_{p-}, what proves unambiguously that HCG effectively buffers the volumetric variations of Sn₄P₃.

Then, Na_x(HCG/Sn₄P₃) anodes were prepared by sodium insertion down to low insertion potentials E_{p-} of 0.28, 0.22 and 0.10 V vs. Na/Na⁺, and they were used to assemble NICs with adjusted capacity ratios, Q₋/Q₊, between the negative and positive electrodes. According to the literature on LICs [219], the capacity ratio between the graphite-based anode and the EDL electrode should be ca. 6 to maximize the specific energy and power metrics of a LIC. Therefore, we adjusted the Q₋/Q₊ of the NICs around this value, *i.e.*, to 5, 7.5, 10; these various Q₋/Q₊ were obtained by adjusting E_{p-} at the above-mentioned values and/or the mass of the positive AC electrode. Hence, three series of NICs with these capacity ratios were assembled where: (i) the Na_x(HCG/Sn₄P₃) anodes were prepared by setting E_{p-} of the HCG/Sn₄P₃ electrode to the limits of 0.10 V, 0.22 V and 0.28 V vs. Na/Na⁺, while imposing

the mass of the anodic host and adjusting accordingly the mass of the YP80F positive electrode to a constant value; (ii) the low insertion potential found in the previous step as advantageous (0.22 V vs. Na/Na⁺) was kept constant, while the targeted Q-/Q₊ of 10, 7.5, 5 were obtained by imposing a constant mass of the anodic host and varying the mass of the positive YP80 electrode; (iii) the Q-/Q₊ identified in the two previous steps as favorable (7.5) was kept constant by imposing a constant mass of HCG/Sn₄P₃ anodic material with setting its E_{p-} to the values of 0.10, 0.22, 0.28 V vs. Na/Na⁺, while varying the mass of the positive YP80F electrode.

In the voltage range from 2.0 to 3.8 V, the longest life span of the YP80F//Na_x(HCG/Sn₄P₃) NICs (10,200 cycles), was found for the cell with Q-/Q₊ = 7.5, where the negative electrode was sodiated down to a potential of 0.22 V vs. Na/Na⁺. Based on this information, we can expect that this E_{p-} provides a good compromise between a sufficient capacity and a moderate expansion of the anode. Considering the energy metrics of the NICs, it is worth noting that, when the mass of the positive electrode was changed, the specific energy of the NICs varied in the same proportions as their specific capacitance. The highest specific energy (63 Wh kg⁻¹ at 1 kW kg⁻¹) was obtained for the NIC with Q-/Q₊ = 5, where the negative electrode was sodiated down to a potential of 0.22 V vs. Na/Na⁺; however, the life span of this cell was very poor (the end-of-life criterion was reached only after 2,700 cycles).

The comparison of the results from the three series of experiments revealed the complexity of the realized research, since the life span and the energy output of the YP80F//Na_x(HCG/Sn₄P₃) NICs are connected in an antagonistic manner with the mass of the positive electrode. Despite the benefits resulting from an increased mass of this electrode, as higher discharge capacitance and thus specific energy output of the NIC, the application of a positive electrode with a higher mass entails an issue of faster negative electrode degradation, due to the higher current circulating in the system. Therefore, the best compromise between the life span (end-of-life criterion reached after 10,200 cycles) and specific energy output (55 Wh kg⁻¹ at 1 kW kg⁻¹) was found for the NIC with Q-/Q₊ of 7.5 obtained by limiting the presodiation potential of the HCG/Sn₄P₃ electrode to 0.22 V vs. Na/Na⁺.

General conclusion

So far, three main issues exist in the development of well-performing NICs, *i.e.*, finding a suitable i) anode including an appropriate active material, eventually together with an additive to improve the mechanical properties; ii) method for presodiating this host; and iii) capacity ratio, Q_-/Q_+ , between the negative and positive electrodes for optimizing the performance.

In this context, Sn_4P_3 was found to be an interesting anodic material for NICs owing to its a high theoretical capacity of 1132 mAh g^{-1} (allowing to adjust the sodium insertion depth appropriately) and relatively low insertion potential (ca. $0.3 \text{ V vs. Na/Na}^+$), profitably higher than for hard carbons subject to sodium plating at high currents. However, it was revealed by *operando* dilatometry that Sn_4P_3 -based electrodes undergo considerable changes of their height during sodium insertion/deinsertion, what ultimately provokes their pulverization and at least partial detachment from the current collectors. This issue was partly solved by adding a hydrothermal hard carbon (HCG) with spherical particles in the preparation to form HCG/ Sn_4P_3 electrodes. The second part of the solution was also given by the *operando* dilatometry investigations revealing that a limit insertion potential of $0.22 \text{ V vs. Na/Na}^+$ allows a sufficiently high capacity to be reached, with a moderate volumetric expansion.

Two presodiation methods were tested in this manuscript by use of i) a separate cell, where the Sn_4P_3 -based working electrode was sodiated vs. a sodium counter/reference electrode; the obtained $\text{Na}_x\text{Sn}_4\text{P}_3$ was transferred to another cell with a positive EDL electrode to realize the NIC; ii) a unique cell where the EDL electrode incorporates a sacrificial sodiated material, from which sodium is transferred to the Sn_4P_3 host by electrochemical oxidation, leading to the realization of the NIC. Clearly, the data presented in chapters III and IV show the great advantages of the second method, owing to its simplicity and even the improved properties of the NIC when $\text{Na}_2\text{C}_4\text{O}_4$ is used as a sacrificial material. These were i) a seven-fold increase of the positive EDL electrode conductivity and ii) the formation of Na_2CO_3 in the S.E.I. passivating layer coating the $\text{Na}_x(\text{HCG}/\text{Sn}_4\text{P}_3)$ anode; both are owing to the disproportionation reaction of carbon monoxide, CO, formed during the electrochemical oxidation of the $\text{C}_4\text{O}_4^{2-}$ anion.

The capacity ratio, Q_-/Q_+ , between the $\text{Na}_x(\text{HCG}/\text{Sn}_4\text{P}_3)$ anode and the activated carbon electrode was adjusted either by controlling the low sodium insertion potential, E_{p-} , and/or the mass of the positive electrode; the selected values of Q_-/Q_+ were 5, 7.5, 10 to fit with the value of 6 already adopted in the case of LICs implementing a graphite negative host. The

conducted systematic study confirmed 0.22 V vs. Na/Na⁺ as an optimal presodiation potential limit and enabled to demonstrate that the life span of the NICs and their specific energy are oppositely influenced by the mass of the positive EDL electrode. The best compromise was obtained for $Q_-/Q_+ = 7.5$, with a capacitance retention higher than 80% for more than 10,000 cycles and a specific energy of 55 Wh kg⁻¹ at 1 kW kg⁻¹.

Although we realized a noticeable progress in the complicated understanding of the NICs properties, and we obtained promising results after this work, the road is still paved by several scientific problems that have not been totally solved. For example, the capacity ratio study should be now conducted, while applying a sacrificial material in the positive electrode. The products resulting from the sacrificial material oxidation may cause changes in the two electrodes and consequently affect the optimized parameters. Besides, related to the volumetric variations of the anodes, information on the sodium diffusion rate could help in determining a maximum current. Finally, as all the experiments were realized in conventional laboratory cells, it would be of prime importance to transfer them to pouch-type cells, which would allow to simulate more closely the behavior of an industrial-type NIC based on the knowledge gathered during the realization of this work.

References

- [1] http://www.yole.fr/Li-ionBatteryRecycling_MarketUpdate.aspx
- [2] <https://www.alibaba.com/showroom/sodium-carbonate-price-per-ton.html>
- [3] <https://www.metal.com/search?keyword=lithium%20carbonate&type=price>
- [4] W. Zhang, Y. Liu, Z. Guo, *Sci. Adv.*, 5 (2019) eaav7412.
- [5] E. Kharbachi, O. Zavorotynska, M. Latroche, F. Cuevas, V. Yartys, M. Fichtner, *J. Alloys Compd.*, 817 (2020) 153261.
- [6] T. S. Mathis, N. Kurra, X. Wang, D. Pinto, P. Simon, Y. Gogotsi, *Adv. Energy Mater.*, 9 (2019) 1902007.
- [7] D. P. Dubal, O. Ayyad, V. Ruiz, P. Gómez-Romero, *Chem. Soc. Rev.*, 44 (2015) 1777-1790.
- [8] L. M. D. Silva, R. Cesar, C. M. R. Moreira, J. H. M. Santos, L. G. D. Souza, B. M. Pires, R. Vicentini, W. Nunes, H. Zanin, *Energy Storage Mater.*, 27 (2020) 555-590.
- [9] B. Babu, P. Simon, A. Balducci, *Adv. Energy Mater.*, 10 (2020) 2001128.
- [10] H. Helmholtz, *Ann. Phys.*, 165 (1853) 353-377.
- [11] Y. Kado, Y. Soneda, H. Hatori, M. Kodama, *J. Solid State Electrochem.*, 23 (2019) 1061-1081.
- [12] F. Béguin, V. Presser, A. Balducci, E. Frackowiak, *Adv. Mater.*, 26 (2014) 2219-2251.
- [13] P. Ratajczak, M. E. Suss, F. Kaasik, F. Béguin, *Energy Storage Mater.*, 16 (2019) 126-145.
- [14] G. Wang, L. Zhang, J. Zhang, *Chem. Soc. Rev.*, 41 (2012) 797-828.
- [15] B. E. Conway, *Electrochemical supercapacitors: scientific fundamentals and technological applications*, Kluwer Academic/Plenum, New York, 1999.
- [16] B. K. Kim, S. Sy, A. Yu, J. Zhang, *Handbook of Clean Energy Systems*, (2015) 1-25.
- [17] L. L. Zhang, X. S. Zhao, *Chem. Soc. Rev.*, 38 (2009) 2520-2531.
- [18] W. Raza, F. Ali, N. Raza, Y. Luo, K. H. Kim, J. Yang, S. Kumar, A. Mehmood, E. E. Kwon, *Nano Energy*, 52 (2018) 441-473.
- [19] J. Chmiola, G. Yushin, Y. Gogotsi, C. Portet, P. Simon, P. L. Taberna, *Science*, 313 (2006) 1760-1763.
- [20] E. Raymundo-Piñero, K. Kierzek, J. Machnikowski, F. Béguin, *Carbon*, 44 (2006) 2498-2507.
- [21] H. Shi, *Electrochim. Acta*, 41 (1996) 1633-1639.
- [22] G. Salitra, A. Soffer, L. Eliad, Y. Cohen, D. Aurbach, *J. Electrochem. Soc.*, 147 (2000) 2486.

- [23] M. D. Stoller, R. S. Ruoff, *Energy Environ. Sci.*, 3 (2010) 1294-1301.
- [24] J. Zhao, Y. Gao, A. F. Burke, *J. Power Sources*, 363 (2017) 327-340.
- [25] J. Zhao, A. F. Burke, *Adv. Energy Mater.*, 11 (2021) 2002192.
- [26] W. G. Pell, B. E. Conway, *J. Power Sources*, 136 (2004) 334-345.
- [27] E. Catenaro, D. M. Rizzo, S. Onori, *Appl. Energy*, 291 (2021) 116473.
- [28] K. S. W. Sing, D. H. Everett, R. A. W. Haul, L. Moscou, R. A. Pierotti, J. Rouquérol, T. Siemieniowska, *Pure Appl. Chem.*, 57 (1985) 603-619.
- [29] E. Frackowiak, F. Béguin, *Carbon*, 39 (2001) 937-950.
- [30] A. G. Pandolfo, A. F. Hollenkamp, *J. Power Sources*, 157 (2006) 11-27.
- [31] M. E. Suss, T. F. Baumann, M. A. Worsley, K. A. Rose, T. F. Jaramillo, M. Stadermann, J. G. Santiago, *J. Power Sources*, 241 (2013) 266-273.
- [32] D. Pech, M. Brunet, H. Durou, P. Huang, V. Mochalin, Y. Gogotsi, P. L. Taberna, P. Simon, *Nat. Nanotechnol.*, 5 (2010) 651-654.
- [33] J. H. Lehman, M. Terrones, E. Mansfield, K. E. Hurst, V. Meunier, *Carbon*, 49 (2011) 2581-2602.
- [34] Z. Zhou, C. Lai, L. Zhang, Y. Qian, H. Hou, D. H. Reneker, H. Fong, *Polymer*, 50 (2009) 2999-3006.
- [35] G. Wang, X. Shen, J. Yao, Ji. Park, *Carbon*, 47 (2009) 2049-2053.
- [36] J. Xu, N. Yuan, J. M. Razal, Y. Zheng, X. Zhou, J. Ding, K. Cho, S. Ge, R. Zhang, Y. Gogotsi, R. H. Baughman, *Energy Storage Mater.*, 22 (2019) 323-329.
- [37] J. Chmiola, G. Yushin, R. Dash, Y. Gogotsi, *J. Power Sources*, 158 (2006) 765-772.
- [38] A. B. Fuertes, S. Alvarez, *Carbon*, 42 (2004) 3049-3055.
- [39] I. Yang, D. Kwon, M. S. Kim, J. C. Jung, *Carbon*, 132 (2018) 503-511.
- [40] V. Presser, M. Heon, Y. Gogotsi, *Adv. Funct. Mater.*, 21 (2011) 810-833.
- [41] S. Ratso, N. R. Sahraie, M. T. Sougrati, M. Käärik, M. Kook, R. Saar, P. Paiste, Q. Jia, J. Leis, S. Mukerjee, F. Jaouen, K. Tammeveski, *J. Mater. Chem. A*, 6 (2018) 14663-14674.
- [42] D. Lozano-Castelló, M. A. Lillo-Ródenas, D. Cazorla-Amorós, A. Linares-Solano, *Carbon*, 39 (2001) 741-749.
- [43] F. Caturla, M. Molina-Sabio, F. Rodríguez-Reinoso, *Carbon*, 29 (1991) 999-1007.
- [44] S. Tazibet, P. Lodewyckx, Y. Boucheffa, *Adsorption*, 20 (2014) 545-553.
- [45] S. Patrice, Y. Gogotsi, *Nat. Mater.*, 19 (2020) 1151-1163.

- [46] L. Wei, M. Sevilla, A. B. Fuertes, R. Mokaya, G. Yushin, *Adv. Energy Mater.*, 1 (2011) 356-361.
- [47] L. Wei, M. Sevilla, A. B. Fuertes, R. Mokaya, G. Yushin, *Adv. Funct. Mater.*, 22 (2012) 827-834.
- [48] J. Yan, Q. Wang, T. Wei, Z. Fan, *Adv. Energy Mater.*, 4 (2014) 1300816.
- [49] C. Peng, X. Yan, R. Wang, J. Lang, Y. Ou, Q. Xue, *Electrochim. Acta*, 87 (2013) 401-408.
- [50] Y. Gogotsi, A. Nikitin, H. Ye, W. Zhou, J. E. Fischer, B. Yi, H. C. Foley, M. W. Barsoum, *Nat. Mater.*, 2 (2003) 591-594.
- [51] P. Simon, Y. Gogotsi, *Acc. Chem. Res.*, 46 (2013) 1094-1103.
- [52] C. Largeot, C. Portet, J. Chmiola, P. L. Taberna, Y. Gogotsi, P. Simon, *J. Am. Chem. Soc.*, 130 (2008) 2730-2731.
- [53] H. J. Liu, J. Wang, C. X. Wang, Y. Y. Xia, *Adv. Energy Mater.*, 1 (2011) 1101-1108.
- [54] M. Rose, Y. Korenblit, E. Kockrick, L. Borchardt, M. Oschatz, S. Kaskel, G. Yushin, *Small*, 7 (2011) 1108-1117.
- [55] C. Zhan, C. Lian, Y. Zhang, M. W. Thompson, Y. Xie, J. Wu, P. R. C. Kent, P. T. Cummings, D. Jiang, D. J. Wesolowski, *Adv. Sci.*, 4 (2017) 1700059.
- [56] J. C. Palmer, A. Llobet, S. H. Yeon, J. E. Fischer, Y. Shi, Y. Gogotsi, K. E. Gubbins, *Carbon*, 48 (2010) 1116-1123.
- [57] Y. Wang, W. H. Zhong, *ChemElectroChem*, 2 (2015) 22-36.
- [58] K. Lota, A. Sierczynska, I. Acznik, *Chemik*, 67 (2013) 1138-1145.
- [59] M. P. Bichat, E. Raymundo-Piñero, F. Béguin, *Carbon*, 48 (2010) 4351-4361.
- [60] M. Yu, Y. Lu, H. Zheng, X. Lu, *Chem. Eur. J.*, 24 (2018) 3639-3649.
- [61] F. Wan, J. Zhu, S. Huang, Z. Niu, *Batter. Supercaps*, 3 (2020) 323-330.
- [62] P. Ratajczak, F. Béguin, *ChemElectroChem*, 5 (2018) 2518-2521.
- [63] S. E. Chun, B. Evanko, X. Wang, D. Vonlanthen, X. Ji, G. D. Stucky, S. W. Boettcher, *Nat. Commun.*, 6 (2015) 7818.
- [64] E. P. Yambou, F. Beguin, *Electrochim. Acta*, (2021) 138687.
- [65] D. Jiang, Z. Jin, D. Henderson, J. Wu, *J. Phys. Chem. Lett.*, 3 (2012) 1727-1731.
- [66] Q. Dou, S. Lei, D. W. Wang, Q. Zhang, D. Xiao, H. Guo, A. Wang, H. Yang, Y. Li, S. Shi, X. Yan, *Energy Environ. Sci.*, 11 (2018) 3212-3219.
- [67] N. S. Nadiah, F. S. Omar, A. Numan, Y. K. Mahipal, S. Ramesh, K. Ramesh, *Int. J. Hydrog. Energy*, 42 (2017) 30683-30690.

- [68] C. R. Yang, Y. Y. Wang, C. C. Wan, *J. Power Sources*, 72 (1998) 66-70.
- [69] P. Han, G. Xu, X. Han, J. Zhao, X. Zhou, G. Cui, *Adv. Energy Mater.*, 8 (2018) 1801243.
- [70] P. Liu, M. Verbrugge, S. Soukiazian, *J. Power Sources*, 156 (2006) 712-718.
- [71] L. Hamenu, A. Madzvamuse, M. Hu, L. Mohammed, C. Y. Bon, S. J. Kim, W. I. Cho, J. Park, J. M. Ko, *Curr. Appl. Phys.*, 17 (2017) 1639-1645.
- [72] H. V. T. Nguyen, K. Kwak, K. K. Lee, *Electrochim. Acta*, 299 (2019) 98-106.
- [73] H. W. Jung, L. Hamenu, H. S. Lee, M. Latifatu, K. M. Kim, J. M. Ko, *Curr. Appl. Phys.*, 15 (2015) 567-570.
- [74] C. Zhong, Y. Deng, W. Hu, J. Qiao, L. Zhang, J. Zhang, *Chem. Soc. Rev.*, 44 (2015) 7484-7539.
- [75] A. Lewandowski, A. Świdzka-Mocek, *J. Power Sources*, 194 (2009) 601-609.
- [76] Z. Lei, Z. Liu, H. Wang, X. Sun, L. Lu, X. S. Zhao, *J. Mater. Chem. A*, 1 (2013) 2313-2321.
- [77] A. Balducci, R. Dugas, P. L. Taberna, P. Simon, D. Plée, M. Mastragostino, S. Passerini, *J. Power Sources*, 165 (2007) 922-927.
- [78] A. Likitchatchawankun, G. Whang, J. Lau, O. Munteshari, B. Dunn, L. Pilon, *Electrochim. Acta*, 338 (2020) 135802.
- [79] A. Brandt, S. Pohlmann, A. Varzi, A. Balducci, S. Passerini, *MRS Bull.*, 38 (2013) 554-559.
- [80] C. Fu, Y. Kuang, Z. Huang, X. Wang, Y. Yin, J. Chen, H. Zhou, *J. Solid State Electrochem.*, 15 (2011) 2581-2585.
- [81] M. S. Whittingham, *Prog. Solid. State Ch.*, 12 (1978) 41-99.
- [82] A. S. Nagelberg, W. L. Worrell, *J. Solid State Chem.*, 29 (1979) 345-354.
- [83] S. W. Kim, D. H. Seo, X. Ma, G. Ceder, K. Kang, *Adv. Energy Mater.*, 2 (2012) 710-721.
- [84] K. Chayambuka, G. Mulder, D. L. Danilov, P. H. L. Notten, *Adv. Energy Mater.*, 10 (2020) 2001310.
- [85] J. Deng, W. B. Luo, S. L. Chou, H. K. Liu, S. X. Dou, *Adv. Energy Mater.*, 8 (2018) 1701428.
- [86] H. Pan, Y. S. Hu, L. Chen, *Energy Environ. Sci.*, 6 (2013) 2338-2360.
- [87] J. Tang, A. D. Dysart, V. G. Pol, *Curr. Opin. Chem. Eng.*, 9 (2015) 34-41.
- [88] J. Song, B. Xiao, Y. Lin, K. Xu, X. Li, *Adv. Energy Mater.*, 8 (2018) 1703082.

- [89] G. G. Eshetu, G. A. Elia, M. Armand, M. Forsyth, S. Komaba, T. Rojo, S. Passerini, *Adv. Energy Mater.*, 10 (2020) 2000093.
- [90] K. L. Browning, R. L. Sacci, G. M. Veith, *J. Electrochem. Soc.*, 164 (2017) A580-A586.
- [91] A. Bhide, J. Hofmann, A. K. Dürr, J. Janek, P. Adelhelm, *Phys. Chem. Chem. Phys.*, 16 (2014) 1987-1998.
- [92] J. Lee, Y. Lee, J. Lee, S. M. Lee, J. H. Choi, H. Kim, M. S. Kwon, K. Kang, K. T. Lee, N. S. Choi, *ACS Appl. Mater. Interfaces*, 9 (2017) 3723-3732.
- [93] R. Väli, A. Laheäär, A. Jänes, E. Lust, *Electrochim. Acta*, 121 (2014) 294-300.
- [94] D. J. Devlin, P. J. Herley, *React. Solids*, 3 (1987) 75-84.
- [95] T. Evans, J. Olson, V. Bhat, S. H. Lee, *J. Power Sources*, 269 (2014) 616-620.
- [96] H. Che, S. Chen, Y. Xie, H. Wang, K. Amine, X. Z. Liao, Z. F. Ma, *Energy Environ. Sci.*, 10 (2017) 1075-1101.
- [97] A. Ponrouch, E. Marchante, M. Courty, J. M. Tarascon, M. R. Palacín, *Energy Environ. Sci.*, 5 (2012) 8572-8583.
- [98] M. Dubois, J. Ghanbaja, D. Billaud, *Synth. Met.*, 90 (1997) 127-134.
- [99] P. Thomas, J. Ghanbaja, D. Billaud, *Electrochim. Acta*, 45 (1999) 423-430.
- [100] K. Nobuhara, H. Nakayama, M. Nose, S. Nakanishi, H. Iba, *J. Power Sources*, 243 (2013) 585-587.
- [101] B. Jache, P. Adelhelm, *Angew. Chem. Int. Ed.*, 53 (2014) 10169-10173.
- [102] J. Y. Hwang, S. T. Myung, Y. K. Sun, *Chem. Soc. Rev.*, 46 (2017) 3529-3614.
- [103] H. Kim, J. Hong, K. Y. Park, H. Kim, S. W. Kim, K. Kang, *Chem. Rev.*, 114 (2014) 11788-11827.
- [104] N. Yabuuchi, K. Kubota, M. Dahbi, S. Komaba, *Chem. Rev.*, 114 (2014) 11636-11682.
- [105] S. Komaba, T. Ishikawa, N. Yabuuchi, W. Murata, A. Ito, Y. Ohsawa, *ACS Appl. Mater. Interfaces*, 3 (2011) 4165-4168.
- [106] Y. X. Wang, Y. G. Lim, M. S. Park, S. L. Chou, J. H. Kim, H. K. Liu, S. X. Dou, Y. J. Kim, *J. Mater. Chem. A*, 2 (2014) 529-534.
- [107] A. Darwiche, C. Marino, M. T. Sougrati, B. Frayssie, L. Stievano, L. Monconduit, *J. Am. Chem. Soc.*, 134 (2012) 20805-20811.
- [108] J. Qian, X. Wu, Y. Cao, X. Ai, H. Yang, *Angew. Chem.*, 125 (2013) 4731-4734.
- [109] Y. Kim, Y. Kim, A. Choi, S. Woo, D. Mok, N. S. Choi, Y. S. Jung, J. H. Ryu, S. M. Oh, K. T. Lee, *Adv. Mater.*, 26 (2014) 4139-4144.

- [110] M. S. Balogun, Y. Luo, W. Qiu, P. Liu, Y. Tong, *Carbon*, 98 (2016) 162-178.
- [111] X. Dou, I. Hasa, D. Saurel, C. Vaalma, L. Wu, D. Buchholz, D. Bresser, S. Komaba, S. Passerini, *Mater. Today*, 23 (2019) 87-104.
- [112] Y. F. Reynier, R. Yazami, B. Fultz, *J. Electrochem. Soc.*, 151 (2004) A422.
- [113] Z. Wang, S. M. Selbach, T. Grande, *RSC Adv.*, 4 (2014) 4069-4079.
- [114] F. Xie, Z. Xu, Z. Guo, M. M. Titirici, *Prog. Energy*, 2 (2020) 042002.
- [115] P. Yu, W. Tang, F. F. Wu, C. Zhang, H. Y. Luo, H. Liu, Z. G. Wang, *Rare Met.*, 39 (2020) 1019-1033.
- [116] D. A. Stevens, J. R. Dahn, *J. Electrochem. Soc.*, 147 (2000) 1271-1273.
- [117] M. Dahbi, N. Yabuuchi, K. Kubota, K. Tokiwa, S. Komaba, *Phys. Chem. Chem. Phys.*, 16 (2014) 15007-15028.
- [118] D. A. Stevens, J. R. Dahn, *J. Electrochem. Soc.*, 148 (2001) A803.
- [119] D. A. Stevens, J. R. Dahn, *J. Electrochem. Soc.*, 147 (2000) 4428.
- [120] J. M. Stratford, P. K. Allan, O. Pecher, P. A. Chater, C. P. Grey, *Chem. Commun.*, 52 (2016) 12430-12433.
- [121] P. C. Tsai, S. C. Chung, S. K. Lin, A. Yamada, *J. Mater. Chem. A*, 3 (2015) 9763-9768.
- [122] C. C. Chen, J. Maier, *Phys. Chem. Chem. Phys.*, 19 (2017) 6379-6396.
- [123] M. Jiang, X. Wang, Y. Shen, H. Hu, Y. Fu, X. Yang, *Electrochim. Acta*, 186 (2015) 7-15.
- [124] L. Li, R. Jacobs, P. Gao, L. Gan, F. Wang, D. Morgan, S. Jin, *J. Am. Chem. Soc.*, 138 (2016) 2838-2848.
- [125] Y. G. Guo, J. S. Hu, L. J. Wan, *Adv. Mater.*, 20 (2008) 2878-2887.
- [126] H. Zhang, I. Hasa, S. Passerini, *Adv. Energy Mater.*, 8 (2018) 1702582.
- [127] R. Alcántara, M. Jaraba, P. Lavela, J. L. Tirado, *Chem. Mater.*, 14 (2002) 2847-2848.
- [128] F. Klein, B. Jache, A. Bhide, P. Adelhelm, *Phys. Chem. Chem. Phys.*, 15 (2013) 15876-15887.
- [129] S. Hariharan, K. Saravanan, V. Ramar, P. Balaya, *Phys. Chem. Chem. Phys.*, 15 (2013) 2945-2953.
- [130] P. K. Nayak, L. Yang, W. Brehm, P. Adelhelm, *Angew. Chem. Int. Ed.*, 57 (2018) 102-120.
- [131] L. P. Wang, L. Yu, X. Wang, M. Srinivasan, Z. J. Xu, *J. Mater. Chem. A*, 3 (2015) 9353-9378.

- [132] J. L. Xu, X. Zhang, Y. X. Miao, M. X. Wen, W. J. Yan, P. Lu, Z. R. Wang, Q. Sun, *Appl. Surf. Sci.*, 546 (2021) 149163.
- [133] X. Tao, Y. Li, H. Wang, X. Lv, Y. Li, D. Xu, Y. Jiang, Y. Meng, *J. Colloid Interface Sci.*, 565 (2020) 494-502.
- [134] D. Y. Park, S. T. Myung, *ACS Appl. Mater. Interfaces*, 6 (2014) 11749-11757.
- [135] B. Huang, K. Tai, M. Zhang, Y. Xiao, S. J. Dillon, *Electrochim. Acta*, 118 (2014) 143-149.
- [136] X. Yang, F. Xiao, S. Wang, J. Liu, M. K. H. Leung, D. Y. W. Yu, A. L. Rogach, *J. Mater. Chem. A*, 7 (2019) 11877-11885.
- [137] W. H. Ryu, J. W. Jung, K. Park, S. J. Kim, I. D. Kim, *Nanoscale*, 6 (2014) 10975-10981.
- [138] Z. Hu, L. Wang, K. Zhang, J. Wang, F. Cheng, Z. Tao, J. Chen, *Angew. Chem. Int. Ed.*, 53 (2014) 12794-12798.
- [139] Y. Lu, Q. Zhao, N. Zhang, K. Lei, F. Li, J. Chen, *Adv. Funct. Mater.*, 26 (2016) 911-918.
- [140] M. Lao, Y. Zhang, W. Luo, Q. Yan, W. Sun, S. X. Dou, *Adv. Mater.*, 29 (2017) 1700622.
- [141] Y. Kim, K. H. Ha, S. M. Oh, K. T. Lee, *Chem. Eur. J.*, 20 (2014) 11980-11992.
- [142] C. Kim, K. Y. Lee, I. Kim, J. Park, G. Cho, K. W. Kim, J. H. Ahn, H. J. Ahn, *J. Power Sources*, 317 (2016) 153-158.
- [143] X. Xie, K. Kretschmer, J. Zhang, B. Sun, D. Su, G. Wang, *Nano Energy*, 13 (2015) 208-217.
- [144] B. Luo, T. Qiu, D. Ye, L. Wang, L. Zhi, *Nano Energy*, 22 (2016) 232-240.
- [145] J. Ni, L. Li, J. Lu, *ACS Energy Lett.*, 3 (2018) 1137-1144.
- [146] F. Yang, H. Gao, J. Chen, Z. Guo, *Small Methods*, 1 (2017) 1700216.
- [147] P. Santhoshkumar, N. Shaji, M. Nanthagopal, J. W. Park, C. Senthil, C. W. Lee, *J. Power Sources*, 470 (2020) 228459.
- [148] Y. Liu, Q. Liu, C. Jian, D. Cui, M. Chen, Z. Li, T. Li, T. Nilges, K. He, Z. Jia, C. Zhou, *Nat. Commun.*, 11 (2020) 1-8.
- [149] S. Wu, K. S. Hui, K. N. Hui, *Adv. Sci.*, 5 (2018) 1700491.
- [150] J. Sun, H. W. Lee, M. Pasta, H. Yuan, G. Zheng, Y. Sun, Y. Li, Yi Cui, *Nat. Nanotechnol.*, 10 (2015) 980-985.
- [151] L. Xiao, Y. Cao, J. Xiao, W. Wang, L. Kovarik, Z. Nie, J. Liu, *Chem. Commun.*, 48 (2012) 3321-3323.
- [152] L. Hu, X. Zhu, Y. Du, Y. Li, X. Zhou, J. Bao, *Chem. Mater.*, 27 (2015) 8138-8145.

- [153] M. He, K. Kravchyk, M. Walter, M. V. Kovalenko, *Nano Lett.*, 14 (2014) 1255-1262.
- [154] Y. C. Lu, N. Dimov, S. Okada, T. H. Bui, *Energies*, 11 (2018) 1614.
- [155] H. Xie, X. Tan, E. J. Lubner, B. C. Olsen, W. P. Kalisvaart, K. L. Jungjohann, D. Mitlin, J. M. Buriak, *ACS Energy Lett.*, 3 (2018) 1670-1676.
- [156] L. Ji, W. Zhou, V. Chabot, A. Yu, X. Xiao, *ACS Appl. Mater. Interfaces*, 7 (2015) 24895-24901.
- [157] J. Qin, T. Wang, D. Liu, E. Liu, N. Zhao, C. Shi, F. He, L. Ma, C. He, *Adv. Mater.*, 30 (2018) 1704670.
- [158] S. C. Jung, J. H. Choi, Y. K. Han, *J. Mater. Chem. A*, 6 (2018) 1772-1779.
- [159] J. Qian, Y. Xiong, Y. Cao, X. Ai, H. Yang, *Nano Lett.*, 14 (2014) 1865-1869.
- [160] J. Choi, W. S. Kim, K. H. Kim, S. H. Hong, *J. Mater. Chem. A*, 6 (2018) 17437-17443.
- [161] E. Irisarri, A. Ponrouch, M. R. Palacin, *J. Electrochem. Soc.*, 162 (2015) A2476.
- [162] J. Vetter, P. Novák, M. R. Wagner, C. Veit, K. C. Möller, J. O. Besenhard, M. Winter, M. Wohlfahrt-Mehrens, C. Vogler, A. Hammouche, *J. Power Sources*, 147 (2005) 269-281.
- [163] F. Holtstiege, A. Wilken, M. Winter, T. Placke, *Phys. Chem. Chem. Phys.*, 19 (2017) 25905-25918.
- [164] M. Winter, *Z. Phys. Chem.*, 223 (2009) 1395-1406.
- [165] N. Takenaka, H. Sakai, Y. Suzuki, P. Uppala, M. Nagaoka, *J. Phys. Chem. C*, 119 (2015) 18046-18055.
- [166] M. Wang, Y. Tang, *Adv. Energy Mater.*, 8 (2018) 1703320.
- [167] S. Komaba, W. Murata, T. Ishikawa, N. Yabuuchi, T. Ozeki, T. Nakayama, A. Ogata, K. Gotoh, K. Fujiwara, *Adv. Funct. Mater.*, 21 (2011) 3859-3867.
- [168] M. Á. Muñoz-Márquez, D. Saurel, J. L. Gómez-Cámer, M. Casas-Cabanas, E. Castillo-Martínez, T. Rojo, *Adv. Energy Mater.*, 7 (2017) 1700463.
- [169] R. Mogensen, D. Brandell, R. Younesi, *ACS Energy Lett.*, 1 (2016) 1173-1178.
- [170] K. Xu, *Chem. Rev.*, 114 (2014) 11503-11618.
- [171] B. Philippe, M. Valvo, F. Lindgren, H. Rensmo, K. Edström, *Chem. Mater.*, 26 (2014) 5028-5041.
- [172] F. A. Soto, P. Yan, M. H. Engelhard, A. Marzouk, C. Wang, G. Xu, Z. Chen, K. Amine, J. Liu, V. L. Sprenkle, F. El-Mellouhi, P. B. Balbuena, X. Li, *Adv. Mater.*, 29 (2017) 1606860.

- [173] N. Weadock, N. Varongchayakul, J. Wan, S. Lee, J. Seog, L. Hu, *Nano Energy*, 2 (2013) 713-719.
- [174] L. Y. Kuo, A. Moradabadi, H. F. Huang, B. J. Hwang, P. Kaghazchi, *J. Power Sources*, 341 (2017) 107-113.
- [175] G. G. Amatucci, F. Badway, A. D. Pasquier, T. Zheng, *J. Electrochem. Soc.*, 148 (2001) A930.
- [176] JM Energy Company patents:
- (a) Y. Naoshi, C. Takashi, O. Kazuyoshi, H. Kuniyasu, Lithium-ion capacitor, WO2012063545A1 (2012)
 - (b) T. Makoto, M. Chiaki, Lithium-ion capacitor, JP2009059732A (2009)
- [177] https://en.wikipedia.org/wiki/Prices_of_chemical_elements
- [178] A. Chojnacka, X. Pan, P. Jeżowski, F. Béguin, *Energy Storage Mater.*, 22 (2019) 200-206.
- [179] F. Meng, T. Long, B. Xu, Y. Zhao, Z. Hu, L. Zhang, J. Liu, *Front. Chem.*, 8 (2020) 652.
- [180] A. M. Glushenkov, A. V. Ellis, *Adv. Sustain. Syst.*, 2 (2018) 1800006.
- [181] J. Ding, W. Hu, E. Paek, D. Mitlin, *Chem. Rev.*, 118 (2018) 6457-6498.
- [182] V. Aravindan, M. Ulaganathan, S. Madhavi, *J. Mater. Chem. A*, 4 (2016) 7538-7548.
- [183] H. Wang, C. Zhu, D. Chao, Q. Yan, H. J. Fan, *Adv. Mater.*, 29 (2017) 1702093.
- [184] P. Han, X. Han, J. Yao, L. Zhang, X. Cao, C. Huang, G. Cui, *J. Power Sources*, 297 (2015) 457-463.
- [185] D. Shanmukaraj, K. Kretschmer, T. Sahu, W. Bao, T. Rojo, G. Wang, M. Armand, *ChemSusChem*, 11 (2018) 3286-3291.
- [186] X. Shen, J. Zhao, Y. Li, X. Sun, C. Yang, H. Liu, Y. S. Hu, *ACS Appl. Energy Mater.*, 2 (2019) 7474-7482.
- [187] D. Dewar, A. M. Glushenkov, *Energy Environ. Sci.*, 14 (2021) 1380-1401.
- [188] K. Zou, W. Deng, P. Cai, X. Deng, B. Wang, C. Liu, J. Li, H. Hou, G. Zou, X. Ji, *Adv. Funct. Mater.*, 31 (2020) 2005581.
- [189] G. Singh, B. Acebedo, M. C. Cabanas, D. Shanmukaraj, M. Armand, T. Rojo, *Electrochem. Commun.*, 37 (2013) 61-63.
- [190] J. M. De Ilarduya, L. Otaegui, J. M. L. del Amo, M. Armand, G. Singh, *J. Power Sources*, 337 (2017) 197-203.

- [191] J. M. De Iarduya, L. Otaegui, M. Galcerán, L. Acebo, D. Shanmukaraj, T. Rojo, M. Armand, *Electrochim. Acta*, 321 (2019) 134693.
- [192] X. Yu, A. Manthiram, *Chem. Eur. J.*, 21 (2015) 4233-4237.
- [193] X. Yu, A. Manthiram, *Chem. Mater.*, 28 (2016) 896-905.
- [194] L. M. Bloi, J. Pampel, S. Dörfler, H. Althues, S. Kaskel, *Adv. Energy Mater.*, 10 (2020) 1903245.
- [195] P. Jeżowski, A. Chojnacka, X. Pan, F. Béguin, *Electrochim. Acta*, 375 (2021) 137980.
- [196] P. Jeżowski, O. Crosnier, T. Brousse, *Open Chem.*, 19 (2021) 432-441.
- [197] M. Sathiya, J. Thomas, D. Batuk, V. Pimenta, R. Gopalan, J. M. Tarascon, *Chem. Mater.*, 29 (2017) 5948-5956.
- [198] J. H. Jo, J. U. Choi, Y. J. Park, J. Zhu, H. Yashiro, S. T. Myung, *ACS Appl. Mater. Interfaces*, 11 (2019) 5957-5965.
- [199] J. H. Jo, J. U. Choi, Y. J. Park, J. K. Ko, H. Yashiro, S. T. Myung, *Energy Storage Mater.*, 32 (2020) 281-289.
- [200] K. Park, B. C. Yu, J. B. Goodenough, *Chem. Mater.*, 27 (2015) 6682-6688.
- [201] B. Shen, R. Zhan, C. Dai, Y. Li, L. Hu, Y. Niu, J. Jiang, Q. Wang, M. Xu, *J. Colloid Interface Sci.*, 553 (2019) 524-529.
- [202] D. Shanmukaraj, S. Grugeon, S. Laruelle, G. Douglade, J. M. Tarascon, M. Armand, *Electrochem. Commun.* 12 (2010) 1344-1347.
- [203] D. Aurbach, Y. Gofer, M. Ben-Zion, P. Aped, *J. Electroanal. Chem.*, 339 (1992) 451-471.
- [204] D. Aurbach, Y. Ein-Eli, O. Chusid, Y. Carmeli, M. Babai, H. Yamin, *J. Electrochem. Soc.*, 141 (1994) 603.
- [205] X. Pan, A. Chojnacka, F. Béguin, *Energy Storage Mater.*, 40 (2021) 22-30.
- [206] Y. B. Niu, Y. J. Guo, Y. X. Yin, S. Y. Zhang, T. Wang, P. Wang, S. Xin, Y. G. Guo, *Adv. Mater.*, 32 (2020) 2001419.
- [207] K. Zou, P. Cai, Y. Tian, J. Li, C. Liu, G. Zou, H. Hou, X. Ji, *Small Methods*, 4 (2020) 1900763.
- [208] M. Arnaiz, D. Shanmukaraj, D. Carriazo, D. Bhattacharjya, A. Villaverde, M. Armand, J. Ajuria, *Energy Environ. Sci.*, 13 (2020) 2441-2449.
- [209] Y. Xu, B. Peng, F. M. Mulder, *Adv. Energy Mater.*, 8 (2017) 1701847.

- [210] J. Liu, P. Kopold, C. Wu, P. A. van Aken, J. Maier, Y. Yu, *Energy Environ. Sci.*, 8 (2015) 3531-3538.
- [211] D. Lan, W. Wang, L. Shi, Y. Huang, L. Hu, Q. Li, *J. Mater. Chem. A*, 5 (2017) 5791-5796.
- [212] X. Fan, T. Gao, C. Luo, F. Wang, J. Hu, C. Wang, *Nano Energy*, 38 (2017) 350-357.
- [213] X. Sun, X. Zhang, W. Liu, K. Wang, C. Li, Z. Li, Y. Ma, *Electrochim. Acta*, 235 (2017) 158-166.
- [214] Y. Sun, J. Tang, F. Qin, J. Yuan, K. Zhang, J. Li, D. M. Zhud, L. C. Qin, *J. Mater. Chem. A*, 5 (2017) 13601-13609.
- [215] <https://www.fritsch-international.com/sample-preparation/milling/planetary-mills/details/product/pulverisette-7-premium-line/accessories/>
- [216] D. Weingarth, H. Noh, A. Foelske-Schmitz, A. Wokaun, R. Kötz, *Electrochim. Acta*, 103 (2013) 119-124.
- [217] A. Sadezky, H. Muckenhuber, H. Grothe, R. Niessner, U. Pöschla, *Carbon*, 43 (2005) 1731-1742.
- [218] H. Alptekin, H. Au, A. CS Jensen, E. Olsson, M. Goktas, T. F. Headen, P. Adelhelm, Q. Cai, A. J. Drew, M. M. Titirici, *ACS Appl. Energy Mater.*, 3 (2020) 9918-9927.
- [219] V. Khomenko, E. Raymundo-Piñero, F. Béguin, *J. Power Sources*, 177 (2008) 643-651.

Scientific achievements

1. Publications:

- 1.1 **X. Pan**, A. Chojnacka, P. Jeżowski, F. Béguin, Na₂S Sacrificial Cathodic Material for High Performance Sodium-Ion Capacitors, **Electrochimica Acta** 318 (2019) 471-478. (IF: 6.215)
- 1.2 A. Chojnacka, **X. Pan**, P. Jeżowski, F. Béguin, High performance hybrid sodium-ion capacitor with tin phosphide used as battery-type negative electrode, **Energy Storage Materials** 22 (2019) 200-206. (IF:16.280)
- 1.3 P. Jeżowski, A. Chojnacka, **X. Pan**, F. Béguin, Sodium amide as a “zero dead mass” sacrificial material for the pre-sodiation of the negative electrode in sodium-ion capacitors, **Electrochimica Acta** (2021) 137980. (IF: 6.215)
- 1.4 **X. Pan**, A. Chojnacka, F. Béguin, Advantageous carbon black deposition during the irreversible electrochemical oxidation of Na₂C₄O₄ used as presodiation source for the anode of sodium-ion systems, **Energy Storage Materials** 40 (2021) 22-30. (IF:16.280)
- 1.5 A. Chojnacka, **X. Pan**, F. Béguin, A strategy for designing more durable sodium-ion capacitors with optimized output energy, submitted to **Energy & Environmental Science**. (IF: 30.289)

2. Oral presentations:

- 2.1 A. Chojnacka, P. Jeżowski, **X. Pan**, F. Béguin, Evaluation of advanced hybrid sodium-ion capacitors with sacrificial cathodic materials, Electrochemistry Conference: Finding New Inspiration (BEChem 2018), Tartu, Estonia, 4-7 November 2018
- 2.2 P. Przygocki, P. Ratajczak, **X. Pan**, A. Chojnacka, P. Jeżowski, F. Béguin, Self-consistent methodology to quantitatively analyze the phenomena taking place during operation of both EDL and sodium-ion capacitors, 8th International Conference on CARBON FOR ENERGY STORAGE AND ENVIRONMENT PROTECTION, Alicante, Spain, 20-24 October 2019
- 2.3 F. Béguin, A. Chojnacka, P. Przygocki, P. Jeżowski, **X. Pan**, Advanced Hybrid Metal-Ion Capacitors Based on Sacrificial Cathodic Materials, Third International Conference on Energy Storage Materials, Shenzhen, China, 29 November- 1 December 2019
- 2.4 A. Chojnacka, P. Jeżowski, **X. Pan**, O. Crosnier, P. Poizot, T. Brousse, F. Béguin, From lithium-ion to sodium-ion capacitors using the strategy of sacrificial cathodic materials,

Americas International Meeting on Electrochemistry and Solid State Science AIMES 2018, Cancun, Mexico, 30 September -4 October 2018

- 2.5 A. Chojnacka, **X. Pan**, P. Jeżowski, F. Béguin, Tin phosphide battery-type negative electrode for high-performance Na-ion capacitor, International Symposium on Enhanced Electrochemical Capacitors (ISEECap) 2019, Nantes, France, 6 - 10 May 2019
- 2.6 **X. Pan**, A. Chojnacka, P. Jeżowski, F. Béguin, Na₂S sacrificial material mixed with various types of nanoporous carbons as positive electrode for high performance Na-ion capacitors, 2nd Scientific Workshop of Polish Carbon Society, Poznan, Poland, 27 September 2019

3. Poster presentations:

- 3.1 **X. Pan**, A. Chojnacka, P. Jeżowski, F. Béguin, Na₂S Sacrificial Cathodic Material for High Performance Sodium-Ion Capacitors, 69th Annual Meeting of the International Society of Electrochemistry, Bologna, Italy, 2-7 September 2018
- 3.2 **X. Pan**, A. Chojnacka, P. Jeżowski, F. Béguin, Use of sacrificial Na₂S for the presodiation of HC/Sn₄P₃ negative electrode used in high performance Na-ion capacitors, The 2018 E-MRS Fall Meeting, Warsaw, Poland, 17-20 September 2018
- 3.3 **X. Pan**, A. Chojnacka, P. Jeżowski, F. Béguin, Sacrificial cathodic materials for high performance Na-ion capacitors, International Symposium on Enhanced Electrochemical Capacitors (ISEECap) 2019, Nantes, France, 6-10 May 2019

4. Participation in scientific project:

- 4.1 HYCAP project (research grant EAM TECH/2016-3/17)

Project funded by the Polish Foundation for Science (FNP)

Project leader: Prof. François Béguin

As a stipendee (PhD thesis): 08.11.2017 - 30.06.2021

Abstract

The rapid development of portable electronics put forward higher requirements for energy storage devices, especially in terms of high specific energy and power, as well as long life span and reduced cost. Therefore, the sodium-ion capacitor (NIC) based on the dual-storage mechanism of Na-ion batteries (NIBs) and electrical double-layer capacitors (EDLCs) is a promising device. As a NIC can deliver higher specific energy than an EDLC and higher specific power than a NIB, it is one of the optimum choices for hybrid and electric vehicles. In terms of the future industrialization of NICs, activated carbons (ACs) seem to be the best option for the positive electrode due to their adapted porosity, high availability and low cost. However, several issues related to the NIC optimization are specified in the conclusion of the literature review (chapter I), *e.g.*, i) the development of suitable anodic materials with an optimized presodiation potential limit; ii) the simplification of the NIC technology by applying composite positive electrodes with a sodium source; iii) the balancing of the capacity ratio between the negative and positive electrodes constituting this hybrid system, to maximize its energy output and life span.

Specifically, the commercially available hard carbon anodic hosts are not adapted for cycling NICs at high currents, due to sodium plating. Therefore, this dissertation proposes to adjust the preparation parameters of a battery-type alloy material of high capacity and to optimize the final sodium insertion potential for an application in NICs. Nonetheless, as the anodic host does not contain sodium, the realization of a NIC requires first to insert/intercalate sodium in the host material, and once it is done, to use the as-prepared anode for the construction of the NIC; in other words two separate cells must be constructed, what renders the total process complicated and costly. Thus, as sacrificial sodiated materials have been already proposed to solve the metal deficiency created by the S.E.I. formation in NIBs, herein they were used to simplify the construction of NICs: namely, they are added in the positive EDL electrode and applied to presodiate the negative electrode, leading to the formation of the NIC, which can be then cycled. Finally, as the insertion/deinsertion of sodium in alloys results in considerable volumetric variations which are at the origin of mechanical damages, we propose to maximize the cycle life and specific output energy of NICs by i) mixing the alloy with a hydrothermal hard carbon constituted of spherical particles, which partly adsorb the volume changes during cycling and ii) adjusting the capacity ratio between the positive and negative electrode.

The first chapter of the dissertation is a literature review, which presents EDLCs, NIBs and NICs. Precisely, the basic principles of energy storage and the most commonly applied electrode materials and electrolytes are discussed in detail. In the last part of this chapter, two main premetallation technologies are introduced, including a metallic auxiliary electrode in the MICs and a sacrificial metallic salt in the positive electrode.

The chapter II is focused on demonstrating, for the first time, the possible application of Sn_4P_3 as a promising anodic host for NIC. The optimized conditions of synthesis by ball-milling, *i.e.* by reducing the mixing time to 4 h and adjusting the balls to powder mass ratio to 24, allow the Sn_4P_3 negative electrode to display the lowest irreversible capacity (83 mAh g^{-1} at a low limit potential of 0.1 V vs. Na/Na^+) today reported in the Na-ion literature. It is shown that, if the low limit potential is equal to or higher than 0.1 V vs. Na/Na^+ , the reversible capacity of the Sn_4P_3 electrodes is not deteriorated during galvanostatic cycling. Therefore, the NICs were constructed with a AC positive EDL electrode and a negative electrode presodiated down to 0.1 V vs. Na/Na^+ , and the electrolyte was NaClO_4 in EC:PC. This hybrid system displayed a discharge capacitance retention of 94% after 6,500 galvanostatic cycles at 0.2 A g^{-1} (per total mass of electrodes) in the voltage range from 2.2 V to 3.8 V, with a specific energy of 39 Wh kg^{-1} at 1 kW kg^{-1} . However, the two separate steps necessary to realize the NIC make the fabrication process complicated and costly.

To simplify the construction of the NICs, in chapter III, Na_2S has been used as a sacrificial material for the presodiation of a Sn_4P_3 negative electrode. A stability limit of 4.1 V vs. Na/Na^+ has been determined by the S-method for AC electrodes in the NaClO_4 :EC:PC electrolyte; this value should not be surpassed during the Na_2S oxidation process and operation of the NICs. Hence, sodium was successfully extracted from Na_2S at a potential lower than 3.8 V vs. Na/Na^+ , with an irreversible capacity of 697 mAh g^{-1} , close to the theoretical value of 687 mAh g^{-1} . AC- $\text{Na}_2\text{S}/\text{Sn}_4\text{P}_3$ cells, incorporating Sn_4P_3 as an anodic host and Na_2S in the EDL positive AC electrode were constructed; Na_2S was oxidized to irreversibly extract sodium and transfer it to the Sn_4P_3 host where it was inserted, leading AC/ $\text{Na}_x\text{Sn}_4\text{P}_3$ NICs to be realized. During cycling of such NICs at 0.18 A g^{-1} (per total mass of the electrodes) in the voltage range from 2.0 V to 3.8 V, the best performance was demonstrated for the system incorporating a highly microporous carbon (Maxsorb), with a capacitance retention of 97% after 3,500 cycles and a high specific energy of 48 Wh kg^{-1} at 1 kW kg^{-1} , confirming that the energy metrics of hybrid cells depend strongly on the type of

porous carbon. Though the NICs construction is simplified, the need to process the AC-Na₂S electrodes in the moisture free atmosphere of a glove box represents an obstacle for any industrial development of NICs based on using a sacrificial material.

Therefore, in view of solving this issue, chapter IV introduces the implementation of Na₂C₄O₄ as a sacrificial material, which offers the essential advantage of being stable in air, *i.e.* the manufacturing of electrodes does not require a controlled atmosphere. The irreversibility of sodium extraction was confirmed by CV and galvanostatic charge, with a capacity of 342 mAh g⁻¹, close to the theoretical one of 339 mAh g⁻¹. Interestingly, the gaseous oxidation products of the C₄O₄²⁻ were identified as CO and CO₂ by *operando* electrochemical mass spectrometry, whereas the presence of carbon blended in the electrode (produced by the disproportionation of CO) was confirmed by Raman spectroscopy and nitrogen adsorption/desorption at 77 K. Subsequently, AC-Na₂C₄O₄ composites were applied as positive electrodes together with Sn₄P₃ negative ones to produce NICs by oxidative sodium transfer. The resulting NICs were then cycled at 0.18 A g⁻¹ (per total mass of the electrodes) in the voltage range from 2.0 V to 3.8 V, demonstrating an excellent life span with a capacitance retention of 94% after 11,000 cycles, much higher than for the NICs presented in chapter II, where Sn₄P₃ was sodiated in a separate cell. Such a remarkable life span of these NICs was attributed to the CO₂ oxidation product of the C₄O₄²⁻ anion, which enabled to form a Na₂CO₃ S.E.I. layer passivating very efficiently the anode surface.

The last chapter of the manuscript proposes a strategy to optimize the cycle life, capacitance and specific energy output of NICs, by combining an EDL-type AC positive electrode and a Sn₄P₃-based anode. To partly absorb the volumetric variations of Sn₄P₃ during cycling, and consequently maximize the life span of the negative electrode of NICs, a hydrothermal hard carbon from glucose (HCG) with spherical particles is mixed with Sn₄P₃ by ball milling. In addition, as the low limit potential of sodium in the HCG/Sn₄P₃ electrodes is also expected to strongly influence their stability during cycling, the HCG/Sn₄P₃ electrodes were presodiated at various selected potential values in separate cells. Subsequently, as-prepared Na_x(HCG/Sn₄P₃) electrodes were used to assemble NICs with different values of the capacity ratio, Q₋/Q₊, adjusted by the value of the low sodium insertion potential and/or the mass of the positive AC electrode. The best compromise between the life span (end-of-life criterion reached after 10,200 cycles) and specific energy output (55 Wh kg⁻¹ at 1 kW kg⁻¹)

Strategies for designing high performance sodium-ion capacitors

was found for the NIC with $Q_-/Q_+ = 7.5$ obtained by limiting the presodiation potential of the HCG/Sn₄P₃ electrode to 0.22 V vs. Na/Na⁺.

Streszczenie

Szybki rozwój elektroniki postawił wyższe wymagania dla urządzeń do magazynowania energii, zwłaszcza pod względem wysokiej energii i mocy, a także długiej żywotności i obniżonych kosztów. Z tego względu, kondensator sodowo-jonowy (NIC) oparty na mechanizmie magazynowania energii łączącym akumulatory Na-ion (NIBs) i kondensatory elektrycznej warstwy podwójnej (EDLCs) jest obiecującym urządzeniem. Ponieważ NIC może dostarczać wyższą energię niż EDLC i wyższą moc niż NIB, jest to jeden z optymalnych rozwiązań dla pojazdów hybrydowych i elektrycznych. W kontekście przyszłej industrializacji NIC, węgle aktywne (AC) wydają się być najlepszą opcją dla elektrody dodatniej ze względu na ich dostosowaną porowatość, wysoką dostępność i niski koszt. Jednak zgodnie z wnioskami płynącymi z przeglądu literaturowego (rozdział I) kilka kwestii związanych z optymalizacją NIC jest koniecznych do zrealizowania, np. i) opracowanie odpowiednich materiałów anodowych o zoptymalizowanym potencjale insercji sodu; ii) uproszczenie technologii NIC poprzez zastosowanie kompozytowych elektrod dodatnich zawierających źródło jonów sodu; iii) zrównoważenie współczynnika pojemności między elektrodami ujemnymi i dodatnimi tworzącymi system hybrydowy, w celu zmaksymalizowania jego wydajności energetycznej i żywotności.

Komercyjnie dostępne anody wykonane z twardego węgla nie są przystosowane do pracy w NIC przy wysokich obciążeniach prądowych, ze względu na osadzanie się metalicznego sodu powierzchni anody (*ang. plating*). Dlatego też w niniejszej rozprawie doktorskiej zaproponowano dostosowanie parametrów syntezy materiału anodowego o dużej pojemności i zoptymalizowanie potencjału insercji sodu, tak aby materiał ten mógł być z powodzeniem zastosowany w NIC. Niemniej jednak wykonanie NIC wymaga najpierw dodatkowego procesu insercji/interkalacji sodu w materiale anodowym, a następnie zastosowanie tak przygotowanej anody do budowy NIC; innymi słowy, konieczne jest zbudowanie dwóch oddzielnych ogniw, co sprawia, że proces wytworzenia NIC jest skomplikowany i kosztowny. W związku z tym, że materiały zawierające źródło jonów metalu (*ang. sacrificial materials*) zostały już zaproponowane w literaturze w celu rozwiązania problemów związanych z tworzeniem się S.E.I. w NIBs, w niniejszej pracy materiały te zastosowano w celu uproszczenia konstrukcji NIC, a mianowicie są one dodawane do dodatniej elektrody EDL i stosowane w celu insercji sodu do elektrody ujemnej, co prowadzi do wytworzenia NIC, który może być następnie cyklowany. Ponieważ insercja/deinsercja sodu w stopach skutkuje znacznymi zmianami objętości, które są przyczyną uszkodzeń mechanicznych, w niniejszej

rozprawie doktorskiej zaproponowano maksymalizację energii i żywotności NIC poprzez i) zmieszanie stopu z hydrotermalnym węglem twardym w postaci kulistych cząstek, które częściowo adsorbują zmiany objętości podczas cyklowania ogniwa oraz ii) dostosowanie wskaźnika pojemności między elektrodą dodatnią i ujemną.

Pierwszy rozdział rozprawy stanowi przegląd literatury, w którym przedstawiono EDLCs, NIBs i NICs oraz omówiono podstawowe zasady magazynowania energii wraz z najczęściej stosowanymi materiałami elektrodowymi i elektrolitami. W ostatniej części tego rozdziału przedstawiono dwie główne technologie wprowadzenia metalu w elektrodę ujemną (*ang. premetallation*), w tym przy użyciu metalicznej elektrody pomocniczej w kondensatorach metalowo-jonowych oraz poprzez wprowadzenie soli będącej źródłem jonów metalu jako dodatkowego komponentu w elektrodzie dodatniej.

Rozdział II koncentruje się na zaaplikowaniu Sn_4P_3 jako obiecującego materiału anodowego dla NIC, co zostało zaproponowane po raz pierwszy w literaturze. Zoptymalizowane warunki syntezy metodą mielenia kulowego, tj. skrócenie czasu mieszania do 4 h oraz dostosowanie stosunku masy kul do proszku do 24, pozwoliły na uzyskanie przez elektrodę ujemną Sn_4P_3 najniższej pojemności nieodwracalnej (83 mAh g^{-1} przy potencjale insercji sodu równym $0,1 \text{ V}$ względem Na/Na^+) jaka do tej pory była przedstawiana w literaturze dotyczącej systemów sodowo-jonowych. Wykazano, że jeśli potencjał insercji sodu jest równy lub wyższy niż $0,1 \text{ V}$ względem Na/Na^+ , odwracalna pojemność elektrod Sn_4P_3 nie ulega pogorszeniu podczas cyklowania galwanostaticznego. Dlatego też NIC zostały skonstruowane przy zastosowaniu elektrody dodatniej EDL, elektrody ujemnej po insercji sodu do $0,1 \text{ V}$ względem Na/Na^+ , oraz elektrolitu jakim był NaClO_4 w EC:PC. Ten hybrydowy układ wykazał zachowanie pojemności rozładowania na poziomie 94% po 6500 cyklach galwanostaticznych przy $0,2 \text{ A g}^{-1}$ (na całkowitą masę elektrod) w zakresie napięć od $2,2 \text{ V}$ do $3,8 \text{ V}$, uzyskując energię układu równą 39 Wh kg^{-1} przy 1 kW kg^{-1} (na całkowitą masę elektrod). Jednak dwa oddzielne etapy niezbędne do wykonania NIC sprawiają, że proces produkcji jest skomplikowany i kosztowny.

W celu uproszczenia konstrukcji NIC, w rozdziale III Na_2S został użyty jako materiał do insercji sodu do elektrody ujemnej Sn_4P_3 . Dla elektrod węglowych w elektrolicie NaClO_4 (EC:PC) wyznaczono najpierw granicę stabilności równą $4,1 \text{ V}$ względem Na/Na^+ metodą S; wartość ta nie powinna zostać przekroczona podczas procesu utleniania Na_2S i działania NIC. W związku z tym ekstrakcja sodu z Na_2S została przeprowadzona przy niższym

potencjale niż 3,8 V względem Na/Na⁺, z nieodwracalną pojemnością Na₂S równą 697 mAh g⁻¹, zbliżoną do teoretycznej wartości równej 687 mAh g⁻¹. Następnie skonstruowano ogniwa AC-Na₂S//Sn₄P₃, zawierające Sn₄P₃ jako materiał anodowy i kompozytową elektrodę dodatnią zawierającą źródło jonów sodu w postaci Na₂S, po czym Na₂S poddano utlenieniu, aby nieodwracalnie wyekstrahować sód i przetransferować go do elektrody ujemnej Sn₄P₃, gdzie następuje jego insercja, prowadząc do realizacji AC//Na_xSn₄P₃ NIC. Podczas cyklowania tak przygotowanych NICs przy 0,18 A g⁻¹ (na całkowitą masę elektrod) w zakresie napięć od 2,0 V do 3,8 V, najlepszą wydajność wykazano dla układu zawierającego wysoce mikroporowaty węgiel (Maxsorb) przy zachowaniu pojemności układu na poziomie 97% po 3500 cyklach i wysokiej energii równej 48 Wh kg⁻¹ przy 1 kW kg⁻¹ (na całkowitą masę elektrod), potwierdzając, że energia ogniw hybrydowych silnie zależy od rodzaju porowatego węgla. Pomimo tego, że konstrukcja NIC została uproszczona, potrzeba przygotowywania elektrod AC-Na₂S w wolnej od wilgoci atmosferze w komorze rękawicowej stanowi przeszkodę dla przemysłowego rozwoju NIC w oparciu o zastosowany materiał będący źródłem jonów sodu w elektrodzie dodatniej.

W związku z tym, mając na względzie rozwiązanie tego problemu, rozdział IV wprowadza zastosowanie Na₂C₄O₄ jako materiału będącego źródłem jonów sodu w elektrodzie dodatniej, który ma istotną zaletę jaką jest stabilność w powietrzu, co sprawia, że wytwarzanie elektrod nie wymaga kontrolowanej atmosfery. Nieodwracalność ekstrakcji sodu potwierdzono woltamperometrią cykliczną i galwanostaticznym ładowaniem, wykazując pojemność Na₂C₄O₄ równą 342 mAh g⁻¹, zbliżoną do wartości teoretycznej 339 mAh g⁻¹. Co ciekawe, gazowe produkty utleniania C₄O₄²⁻ zidentyfikowano jako CO i CO₂ metodą *operando* elektrochemicznej spektrometrii masowej, natomiast obecność węgla zmieszanego w elektrodzie (wynikającego z dysproporcjonowania CO) potwierdzono metodą spektroskopii Ramana i adsorpcji/desorpcji azotu przy 77 K. Następnie zastosowano kompozytowe elektrody dodatnie AC-Na₂C₄O₄ wraz z elektrodami ujemnymi Sn₄P₃ w celu wytworzenia NIC poprzez utleniający transfer sodu. Uzyskane NICs były następnie poddawane cyklowaniu przy 0,18 A g⁻¹ (na całkowitą masę elektrod) w zakresie napięcia od 2,0 V do 3,8 V, wykazując doskonałą żywotność z zachowaniem pojemności układu na poziomie 94% po 11 000 cyklach, znacznie wyższym niż dla NIC przedstawionym w rozdziale II, gdzie sód do Sn₄P₃ wprowadzano w oddzielnym ogniwie. Tak dobrą żywotność

tych NIC przypisano produktowi utleniania CO_2 z anionu $\text{C}_4\text{O}_4^{2-}$, który umożliwił utworzenie warstwy Na_2CO_3 S.E.I. bardzo skutecznie pasywującej powierzchnię anody.

Ostatni rozdział manuskryptu przedstawia strategię optymalizacji żywotności, pojemności i energii NIC składającego się z elektrody dodatniej typu EDL i anody opartej na Sn_4P_3 . Aby częściowo zaabsorbować zmiany objętości elektrody Sn_4P_3 podczas cyklowania, a w konsekwencji zmaksymalizować żywotność elektrody ujemnej, hydrotermalny węgiel twardy otrzymany z glukozy (HCG) o kulistym kształcie ziaren zmieszano z Sn_4P_3 przez mielenie kulowe. Ponadto, ponieważ oczekuje się, że niski potencjał insercji sodu w elektrodach HCG/ Sn_4P_3 również silnie wpływa na ich stabilność pracy podczas pracy ogniw, elektrody HCG/ Sn_4P_3 poddano insercji sodu przy różnych wybranych wartościach potencjału w oddzielnych ogniwach. Następnie elektrody $\text{Na}_x(\text{HCG}/\text{Sn}_4\text{P}_3)$ wykorzystano do montażu NIC o różnych wartościach współczynnika pojemności Q^-/Q^+ , ustalonych poprzez dopasowanie potencjału insercji sodu i/lub masy dodatniej elektrody. Najlepszy kompromis między żywotnością (kryterium końca życia osiągnięto po 10200 cyklach), a energią wyrażoną na całkowitą masę elektrod (55 Wh kg^{-1} przy 1 kW kg^{-1}) stwierdzono dla NIC z $Q^-/Q^+ = 7,5$, przy ograniczeniu potencjału insercji sodu elektrody HCG/ Sn_4P_3 do $0,22 \text{ V vs. Na/Na}^+$.